TOWARDS A FRAGMENT APPROACH TO HAEMOZOIN INHIBITING ANTIMALARIALS: EXPLORATION OF COORDINATION AND π-STACKING INTERACTIONS WITH FE(III)PPIX BY SPECTROSCOPY AND SYNTHESIS

University of Cape Town

Department of Chemistry

December 2009

A dissertation submitted to the University of Cape Town in fulfilment for the degree of

Master of Science.

by

David Kuter

SUPERVISORS: Prof. T. J. Egan and Prof. K. Chibale

DECLARATION

Towards a fragment approach to haemozoin inhibiting antimalarials: Exploration of coordination and π-stacking interactions with Fe(III)PPIX by spectroscopy and synthesis

I, David Kuter, hereby declare the following:

1. That the above-titled thesis is my own work, both in concept and execution, apart from the normal guidance of my supervisors;

2. That in cases where others' work has been cited, this has been acknowledged and referenced;

3. That no part of this work has been, is being, or is to be submitted for another degree at this or any other university;

4. That I grant the University of Cape Town free license to reproduce this work, in whole or in part, for the purpose of research.

I hereby present this dissertation in fulfilment for the degree of Master of Science.

David Kuter: _____

Witness: _____

ABSTRACT

Investigation of coordination and π-stacking interactions with ferriprotoporphyrin IX (Fe(III)PPIX) using a fragment approach was undertaken in order to propose and synthesise novel compounds which followed a hypothesised mechanism of action to inhibit β-haematin formation. Coordination of a series of pyridines, imidazoles, amines and phenolates with Fe(III)PPIX, and π-stacking interactions of these compounds with protoporphyrin IX (PPIX) and Fe(III)PPIX were measured in 40% (v/v) aq. DMSO by spectrophotometric titration. The calculated pH independent log association constants for coordination (log K_c) in this solvent system were found to exhibit a linear free energy relationship (LFER) with the pK_a of the ligand donor atom. This relationship was confirmed for observed association constants under non-aqueous conditions (20% (v/v) DMSO in methanol). Calculated log $K_{c,\ calc}$ values under acidic aqueous conditions (pH 4.8) are predicted to be extremely weak. Association arising from π-stacking interactions (log K_s) with PPIX and Fe(III)PPIX was found to strengthen with an increase in the number of π-electrons in the aromatic ring system. It was observed that Fe(III)PPIX has a log K_s which is on average 0.57 log units lower than with PPIX. Association constants of compounds that can coordinate and π-stack were found to be the sum of log $K_{c,\ obs}$ and log K_s. This allows for the prediction of association constants (log K_{calc}) with Fe(III)PPIX for a variety of compounds, provided their pK_a values are known. Using the derived prediction equation, 9-hydroxyfluorene was identified as a scaffold compound with a relatively strong Fe(III)PPIX association (log K_{obs} = 3.64 ± 0.09 at pH 7.4, 40% aq. DMSO). Guanidine, amine and 1,3,5-azaadamantane hydrogen bonding moieties were identified as being suitable for incorporation into the scaffold molecule through a one or two carbon linker at the 9-position of the fluorene ring system to provide five proposed compounds for inhibition of β-haematin (synthetic haemozoin) formation. These five compounds were 9-(2-aminoethyl)-fluoren-9-ol (**A**); 1-[2-(9-hydroxy-fluoren-9-yl)ethyl]guanidine (**B**); 9-(aminomethyl)-fluoren-9-ol (**C**); 1-[(9-hydroxy-fluoren-9-yl)methyl]guanidine (**D**) and 9-(1,3,5-triazatricyclo[3.3.1.13,7]dec-7-ylmethyl)-fluoren-9-ol (**E**). Compounds **A**, **B**, **C** and **D** were successfully synthesised but isolation of **D** was unsuccessful. All attempts to synthesise compound **E** failed at the final step.

Synthesis of compounds **A** – **D** began with a Corey epoxidation of 9-fluorenone, giving the spiro[fluorene-9,2'-oxirane] epoxide which underwent ring opening upon nucleophilic attack by sodium cyanide and subsequent reduction with lithium aluminium hydride produced compound **A**. Compound **B** was obtained as a nitrate salt through guanylation of compound **A** using the guanylating agent 3,5-dimethylpyrazole-1-carboxamidine nitrate (DPCN). Compound **C** was obtained via a Staudinger reduction of 9-(azidomethyl)-fluoren-9-ol, produced from the ring opening of spiro[fluorene-9,2'-oxirane] by sodium azide. Compound **D** was produced by guanylation of compound **C** using DPCN but low yields and large amounts of by-product formation prevented isolation. Compounds **A**, **B**, **C** and 9-hydroxyfluorene were tested for β-haematin inhibition, however, none showed any activity towards preventing formation at 200 equivalents (67 equivalents in the case of compound **C** owing to lack of solubility). This was expected for 9-hydroxyfluorene owing to the lack of a hydrogen bonding moiety as well as for compounds **A** and **C**. Modelling indicated the hydrogen bonding group of compound **A** was directed away from the propionate side chain and compound **C** had too short a linker length to provide favourable hydrogen bonding interactions with the propionate side chain. The lack of inhibition was initially unexpected for compound **B**. Association constants of the synthesised compounds were found to be lower than that of the scaffold compound, indicating that substitution at the 9-position of 9-hydroxyfluorene had a negative effect on Fe(III)PPIX association. It was found using a pK_a prediction program (MOKA) that the substitution at this position probably causes an increase in the predicted pK_a of the hydroxyl moiety which results in a lowered affinity for coordination to Fe(III)PPIX owing to its increased proton competition and thus could account for the lower overall association and failure to inhibit β-haematin formation.

ACKNOWLEDGEMENTS

Completion of this Masters work would never have been possible without the valued support mentors and friends. I feel privileged to have interacted with those listed below.

Professor Tim Egan – I count myself fortunate to have had a supervisor of your calibre. Your interest and enthusiasm towards teaching and sharing knowledge is infective, and I am a richer person for it.

Professor Kelly Chibale – I thank you for your valuable time and continued patience, but most of all I appreciate giving me the opportunity to learn a great deal which I would otherwise have never been exposed to.

Fellow colleagues: **Dr Aman Mahajan, Dr Frederic Douelle, Dr Vincent Zishiri** and **Dr Ebrahim Mohammed** for their valuable insight about the synthetic side of the project as well as friendly banter; **Constant Asher** and **Anh Hoang,** for providing plenty of laughs; **Dr Kanyile Ncokazi** and **Dr Kath de Villiers-Chen,** for invaluable help in the lab and being the glue which holds the group together.

Noel Hendricks and **Pete Roberts** for NMR services. They make a difficult job seem easy.

To my very good friends **Siri Lie Olsen, Dale Taylor, Dyanne Cruickshank, Craig and Caylee Rossouw** for their unfailing support, companionship and humour. I am sincerely gratefully for your friendship.

Finally, to my family. It is without doubt that I would not have accomplished as much as I have without your support, understanding and love.

ABBREVIATIONS

A	observed absorbance
A_0	initial absorbance
A_1	absorbance of intermediate species
A_∞	absorbance of final complex
Ad··Br	transient species
Ad-Ad	bi-adamantane
Ad-Br	7-bromo-adamantane
Ad-H	adamantane
Ad-MgBr	adamantane Grignard reagent
Ad-S	adamantane-solvent by-product
Ar	aromatic group
bs	broad singlet (in ^{1}H NMR)
CP	coordination possible
CQ	chloroquine
$CQ2H^+$	doubly protonated chloroquine
CQH^+	monoprotonated chloroquine
CQR	chloroquine resistant
CQS	chloroquine sensitive
d	doublet (in ^{1}H NMR)
DCM	dichloromethane (methylene chloride)
DMF	dimethylformamide
DMSO	dimethylsulfoxide
DNA	deoxyribonucleic acid
DPCN	3,5-dimethylpyrazole-1-carboxamidine nitrate
EA	elemental analysis
EI	electron ionisation
EQD	epiquinidine
EQN	epiquine
ESI	electron spray ionisation
Et_2O	diethyl ether
EtOAc	ethyl acetate
EtOH	ethanol
FBDD	fragment based drug design
Fe(II)PPIX	ferroprotoporphyrin IX / Haem
Fe(III)PPIX	ferriprotoporphyrin IX / Haematin
FSA	formamidinesulfonic acid
Hb	haemoglobin
Hex	hexane
Hf	halofantrine
HPLC	high-performance liquid chromatography
HRMS	high resolution mass spectrometry
HTS	high throughput screening
IR	infrared
L	free ligand concentration
LAH	lithium aluminium hydride

LFER	linear free energy relationship
log K_c	pH independent coordination association constant
log $K_{c,\ calc}$	calculated coordination association constant
log $K_{c,obs}$	observed coordination association constant
log $K_{c,org}$	observed coordination association constant under organic conditions
log K_{calc}	calculated association constant
log K_s	π-stacking association constant
MeCN	acetonitrile
MeOH	methanol
Mf	mefloquine
$MgSO_4$	magnesium sulfate
MP-8	microperoxidase-8
MS	mass spectrometry
N-Ac-MP-8	N-acetyl-microperoxidase-8
NaOH	sodium hydroxide
ND	not determined
NMR	nuclear magnetic resonance
n_π	number of π-electrons in an aromatic ring system
PfCRT	*Plasmodium falciparum* chloroquine resistant transporter
Pfmdr1	*Plasmodium falciparum* multidrug resistance
PGH-1	P-glycoprotein homologue
PPH_3	triphenylphosphine
PPIX	Protoporphyrin IX
ppm	parts per million
QD	quinidine
QN	quinine
RaNi	Raney Nickel
RBC	red blood cell
RT	room temperature
s	singlet (in ^{1}H NMR)
SEM	standard error of the mean
SEM	scanning electron micrograph
SERCA	Sarco/endoplamsic reticulum Ca^{2+} - ATPase
SiO_2	silica
t	triplet (in ^{1}H NMR)
TEA	triethylamine
TEM	transmission electron micrograph
THF	tetrahydofuran
TLC	thin layer chromatography
TMSCN	trimethylsilyl cyanide
TMSOI	trimethylsulfoxonium iodide
VDW	van der Waals
W2-MEF	mefloquine resistant parasite strain
WB	weak binding

TABLE OF CONTENTS

Declaration		i
Abstract		ii
Acknowledgements		iv
Abbreviations		v
Table of Contents		vii
CHAPTER 1. INTRODUCTION		1
1.1	**Malaria**	2
1.2	**Parasite life cycle**	3
1.3	**Antimalarial drugs**	4
1.4	**Haemoglobin degradation by the parasite**	6
1.5	**Haemozoin formation**	8
1.6	**Inhibition of haemozoin by antimalarials**	10
1.7	**Antimalarial drug resistance**	11
1.7.1	Mechanism of chloroquine resistance.	11
1.7.2	Mechanism of aryl-amino alcohol antimalarial resistance.	13
1.8	**Mechanism of haemozoin inhibition**	14
1.9	**Fragment approach to drug discovery**	18
1.10	**Interactions with Fe(III)PPIX**	21
1.10.1	Coordination interactions.	22
1.10.2	π-Stacking interactions.	24
1.10.3	Hydrogen bonding.	28
1.11	**Aims and objectives**	31
1.11.1	Aims.	31
1.11.2	Objectives.	31
CHAPTER 2. INVESTIGATION OF COORDINATION AND π-STACKING INTERACTIONS WITH Fe(III)PPIX		32
2.1	**Introduction**	33
2.2	**Coordination interactions**	33
2.3	**π-Stacking interactions**	40
2.4	**Coordination and π-stacking combined**	43
2.5	**Conclusions**	47

CHAPTER 3. DESIGN OF NOVEL POTENTIAL β-HAEMATIN INHIBITORS 48

3.1 Introduction 49
3.2 Identification of a scaffold molecule 49
3.3 Incorporation of a hydrogen bond donor moiety 52
3.4 Molecular modelling of proposed inhibitor/Fe(III)PPIX complexes 53
3.4.1 Compounds A to D. 53
3.4.2 Compound E. 55
3.5 Conclusions 57

CHAPTER 4. SYNTHESIS OF PROPOSED β-HAEMATIN INHIBITORS 59

4.1 Introduction 60
4.2 Synthesis of 9-(2-aminoethyl)-fluoren-9-ol, A 60
4.2.1 Synthesis of Spiro[fluorene-9,2'-oxirane], 26. 61
4.2.2 Synthesis of (9-hydroxy-fluoren-9-yl)acetonitrile, 25. 63
4.2.3 Synthesis of 9-(2-aminoethyl)-fluoren-9-ol, A. 64
4.3 Synthesis of 1-[2-(9-hydroxy-fluoren-9-yl)ethyl]guanidine, B 66
4.4 Synthesis of 9-(aminomethyl)-fluoren-9-ol, C 69
4.4.1 Synthesis of 9-[(trimethylsilyl)oxy]-fluorene-9-carbonitrile, 30. 70
4.4.2 Synthesis of 9-(azidomethyl)-fluoren-9-ol, 31. 72
4.4.3 Synthesis of 9-(aminomethyl)-fluoren-9-ol, C. 73
4.5 Attempted synthesis of 1-[(9-hydroxy-fluoren-9-yl)methyl]guanidine, D 75
4.6 Attempted synthesis of 9-(7-methyl-1,3,5-triaza-adamantanyl)-fluoren-9-ol, E 80
4.6.1 Synthesis of 7-nitro-1,3,5-triazaadamantane, 38. 82
4.6.2 Synthesis of 7-amino-1,3,5-triazaadamantane, 37. 84
4.6.3 Synthesis of 7-bromo-1,3,5-triazaadamantane, 36. 86
4.6.4 Attempted Grignard reaction between 7-bromo-1,3,5-triazaadamantane, 36, and spiro[fluorene-9,2'-oxirane], 26. 88
4.7 Conclusions 90

CHAPTER 5. INVESTIGATION OF β-HAEMATIN INHIBITION ACTIVITY BY SYNTHESISED COMPOUNDS 91

5.1 Introduction 92
5.2 β-Haematin inhibition 92

5.3 Fe(III)PPIX association 93

5.4 Conclusions 95

CHAPTER 6. CONCLUSIONS AND FUTURE WORK 96

6.1 Conclusions 97

6.2 Future Work 98

CHAPTER 7. EXPERIMENTAL METHODOLOGIES 99

7.1 Physicochemical methods 100

7.1.1 General. 100

7.1.2 Beers law studies. 100

7.1.3 Spectrophotometric titrations. 100

7.1.4 pK_a determination. 101

7.1.5 Molecular mechanics and dynamics (with simulated annealing) modelling. 102

7.1.6 β-Haematin inhibition. 102

7.2 Synthesis 103

7.2.1 General. 103

7.2.2 4-Quinonline methanol, 22. 104

7.2.3 Spiro[fluorene-9,2'-oxirane], 26. 105

7.2.4 9-Hydroxy-fluorene-9-acetonitrile, 25. 106

7.2.5 9-(2-Aminoethyl)-fluoren-9-ol, A. 107

7.2.6 1-[2-(9-Hydroxy-fluoren-9-yl)ethyl]guanidinium nitrate, B. 108

7.2.7 9-[(Trimethylsilyl)oxy]-fluorene-9-carbonitrile, 30. 109

7.2.8 9-(Azidomethyl)-fluoren-9-ol, 31. 110

7.2.9 9-(Aminomethyl)-fluoren-9-ol, C. 111

7.2.10 Formamidinesulfonic acid, 33. 112

7.2.11 7-Nitro-1,3,5-azaadamantane, 38: Method a. 112

7.2.12 7-Nitro-1,3,5-azaadamantane, 38: Method b. 113

7.2.13 7-Amino-1,3,5-azaadamantane, 37. 113

7.2.14 7-Bromo-1,3,5-azaadamantane, 36. 114

CHAPTER 8. REFERENCES 115

CHAPTER 1.

INTRODUCTION

1.1 Malaria

Malaria has had a long history as a disease, with records of its occurrence dating back to the times of classical Rome.[1] It has been closely associated with marshes and in fact, the name malaria stems from the Italian phrase "mal'aria" meaning "bad air".[2] It has continued to make its presence felt in the modern world with between 350 to 500 million reported clinical cases and over 1 million deaths annually, the majority of which are children under five years of age.[3, 4] Globally, malaria is predominantly encountered in the tropical and subtropical regions (see figure 1.1) with roughly 80% of malaria cases occur in sub-Saharan Africa.[3]

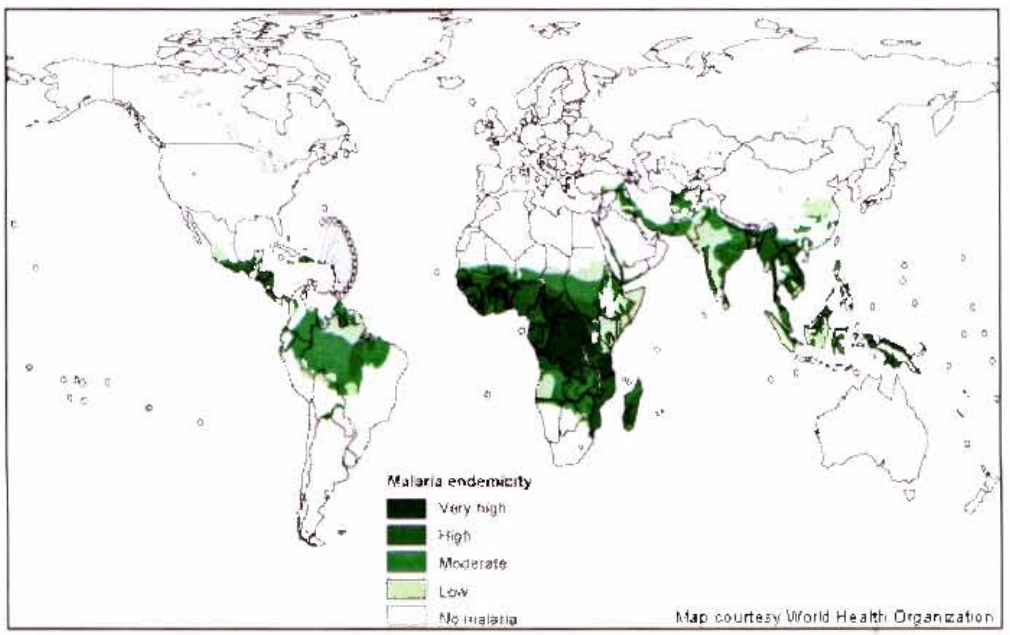

Figure. 1.1. Global distribution of malaria transmission. Reproduced from reference 5.

The spread of the disease is rife in the sub-Saharan African countries where a large majority of the population live in rural areas, allowing for more frequent contact between the human host and the vector mosquito, *Anopheles*.[6]

1.2 Parasite life cycle

Malaria is caused by five species of the parasite *Plasmodium*, with the most dangerous being *P. falciparum* and to a much lesser extent *P. vivax*.[2, 4] *P. malariae* and *P. ovale* are less common than the former two and more recently *P. knowlesi*, the species found to cause malaria in rhesus monkeys, has been discovered in the human population in South East Asia.[7] While all species are found in the tropics and subtropics, *P. vivax* is also able to survive in the vector mosquito at lower temperatures and thus can occur further away in more temperate areas.[6] The parasite has a complex life cycle (illustrated in figure 1.2) consisting of three stages, however, the symptoms of malaria only become apparent in the blood stage.[2, 8]

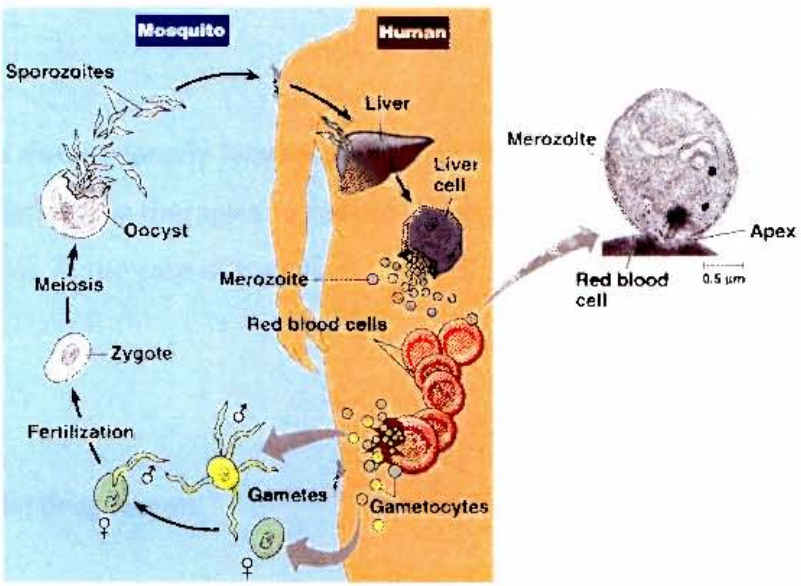

Figure 1.2. Life cycle of the malaria parasite, *Plasmodium*. Figure reproduced from reference 6.

The malaria parasite enters the human host blood stream in the form of sporozoites via the salivary glands of an infected female *Anopheles* mosquito.[2] The sporozoites migrate to the liver where they invade hepatic cells and undergo asexual fission forming a cyst-like structure known as a liver schizont.[2, 6] During this reproductive period, lasting five to twenty five days depending on the species, the host remains free of malaria symptoms.[2] Inside the liver schizont, the sporozoites develop into merozoites which are released into the blood stream when the liver schizont ruptures.[2, 6]

Up until this point, the parasite is said to be in the liver stage. The merozoites then invade red blood cells (RBCs) to begin the blood stage. Once inside the RBC, the parasite utilises the haemoglobin present as an energy source providing for its growth into a trophozoite, before developing into a blood schizont. Once this schizont eventually ruptures, six to twenty four parasites are released and infect further RBCs, beginning another blood cycle.[6] One blood cycle occurs every 48 to 72 hours, depending on the species, and increases the parasite load by roughly 8- to 10- fold in P. *falciparum*.[5, 6] The release of the parasite, toxins and RBC debris caused by the ruptured blood schizonts results in the symptoms of malaria, namely fever and chills, becoming apparent.[2, 6] Certain parasites within the RBCs develop into sexually mature male and female forms termed gametocytes. Once a female *Anopheles* mosquito feeds on an infected human host's blood, the gametocytes undergo sexual reproduction to produce oocysts, which then release sporozoites that migrate to the salivary glands, completing the parasitic life cycle.[2]

The control of this disease largely focuses on control of vector mosquitoes, use of bed nets and the use of antimalarial drug therapies to reduce and eradicate the parasitaemia load in infected persons. Prophylaxis, in the case of travellers is also of importance.[9]

1.3 Antimalarial drug targets

Antimalarial drugs act on the different stages of the parasite life cycle but the majority are active in the blood stage. Drugs acting on this stage can be divided into three broad categories: (i) nucleic acid inhibitors; (iii) oxidative stress inducers/Ca^{2+}ATPase inhibitors and (iii) haem detoxification inhibitors.[10, 11] Table 1.1 summarises the various classes and their modes of action albeit the mechanisms through which some of them assert their antimalarial activity are not well understood.

Table 1.1. Summary of antimalarials and their targets in the blood stage of the malaria parasite.

Pathway	Drug Class	Antimalarial Examples	Mode of Action
Nucleic acid inhibitors	Folate antagonists	Sulfadoxine Pyrimethamine	Inhibition of parasitic enzymes involved in folate metabolism which are responsible for the synthesis of parasitic pyrimidines and are essential for DNA production.[10, 11]
	Naphthoquinones	Atovaquone	Uncouples electron transport in the mitochondrion, causing a collapse in the organellar membrane potential preventing the regeneration of ubiquinone, an electron acceptor for dihydroorotate dehydrogenase which in turn is an essential enzyme for pyrimidine biosynthesis.[11, 12]
Oxidative stress inducers/Ca^{2+}ATPase inhibitors	Endoperoxides	Artemesinin	The mode of action of artemesinin is of debate in the literature. Two main processes have been proposed: **(1)** Inhibition of SERCA (Sarco/Endoplasmic Reticulum Ca^{2+} - ATPase) orthologue protein PfATP6 after activation by Fe(II) through cleavage of the artemesinin endoperoxide bridge.[13] **(2)** Formation of radicals by reaction with Fe(II)PPIX can lead to the alkylation or hydroxylation of biomolecules and thus parasitic death.[10]
Haem detoxification inhibitors	4-Aminoquinolines	Chloroquine Amodiaquine	Inhibition of detoxification of haem, produced as a by product of haemoglobin degradation, leads to parasitic lipid peroxidation and thus death. [14-16]
	Aryl-amino quinolines	Quinine Halofantrine Mefloquine	Various modes of action have been proposed, including that of inhibition of haem detoxification. Disruption of essential metabolite membrane trafficking has also been proposed for mefloquine.[17-19]

Of the three broad categories, antimalarial compounds that are active through inhibition of haem detoxification are of particular interest owing to the fact that some of the most commonly used and most effective antimalarial drugs fall in this class.

1.4 Haemoglobin degradation by the parasite

During the blood stage of the malaria parasite life cycle (see section 1.2), in order for the parasite to be able to survive in the harsh conditions of the RBC, it needs to degrade the oxygen carrying protein haemoglobin (Hb) into peptides essential for nutrition.[20] Once *P. falciparum*, in the meroziote stage, has invaded the red blood cell, it engulfs a large quantity of haemoglobin in a process termed the "Big Gulp" by Elliott *et al.*[21] This produces a haemoglobin containing vacuole which has been proposed to form the acidic digestive vacuole of the parasite.[21] In the trophozoite stage, 60 to 70% of the haemoglobin present in the RBC is said to be ingested through transportation by endocytotic vesicles, created from the parasitic plasma membrane, to the acidic digestive vacuole.[22-24] Studies estimate the pH of this digestive vacuole to be approx. 4.8 – 5.4.[25, 26] Once in the digestive vacuole, degradation of the haemoglobin into peptides is facilitated by proteolytic enzymes which include the (i) aspartic proteases plasmepsin I, II and IV and histo-aspartic protease; (ii) cysteine proteases falcipain 1, 2 and 3; and (iii) zinc metalloprotease facilysin.[27-30] Further degradation of the peptides into amino acids is accomplished by hydrolysis which takes place in the parasitic cytosol (summarised in figure 1.3).[31]

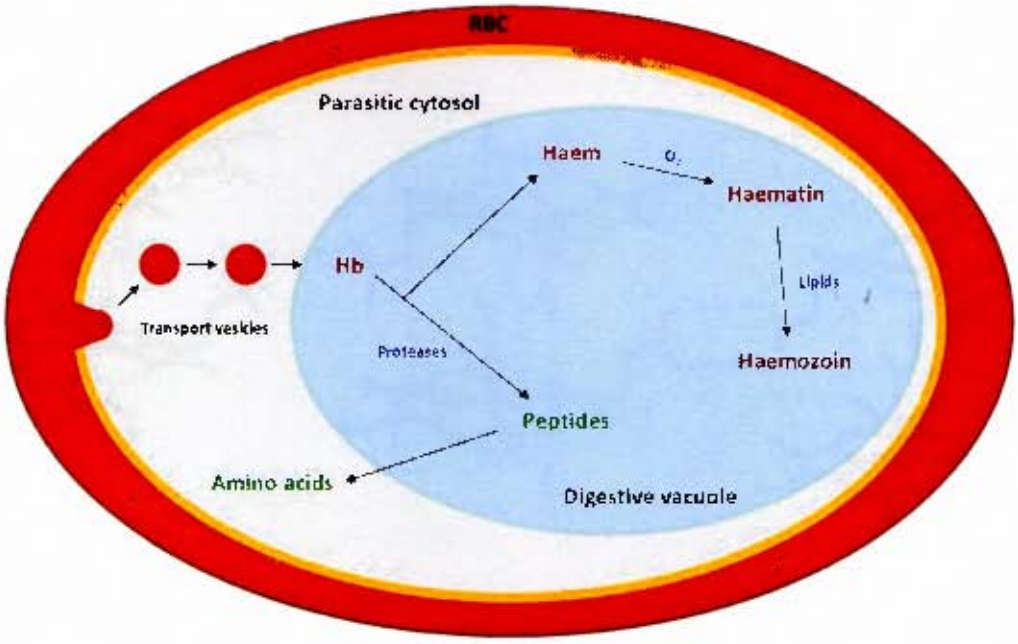

Figure 1.3. Process of haemoglobin (Hb) degradation and subsequent detoxification of Fe(III)PPIX (haematin) by the malaria parasite (grey) inside the red blood cell (RBC). Figure adapted from reference 31.

As a consequence of haemoglobin degradation, a large amount of haem (ferroprotoporphyrin IX, Fe(II)PPIX) is released as a by-product which is rapidly and irreversibly oxidised to haematin (hydroxo/aqua-ferriprotoporphyrin IX, HO$^-$/H_2O-Fe(III)PPIX), the structure of which (excluding the axial HO$^-$/H_2O ligand) is illustrated in figure 1.4a.[32] Fe(III)PPIX present in such large quantities is toxic to the parasite, making a natural detoxification process necessary.[33] This process involves the dimerisation of Fe(III)PPIX whereby one propionate of each monomer coordinates to the iron centre of the other. The second propionic acid group of each Fe(III)PPIX hydrogen bonds to a neighbouring dimer to form highly insoluble crystals known as haemozoin (see figure 1.4b for structure).[34] It has been shown that at least 95% of haem is detoxified though this pathway.[22]

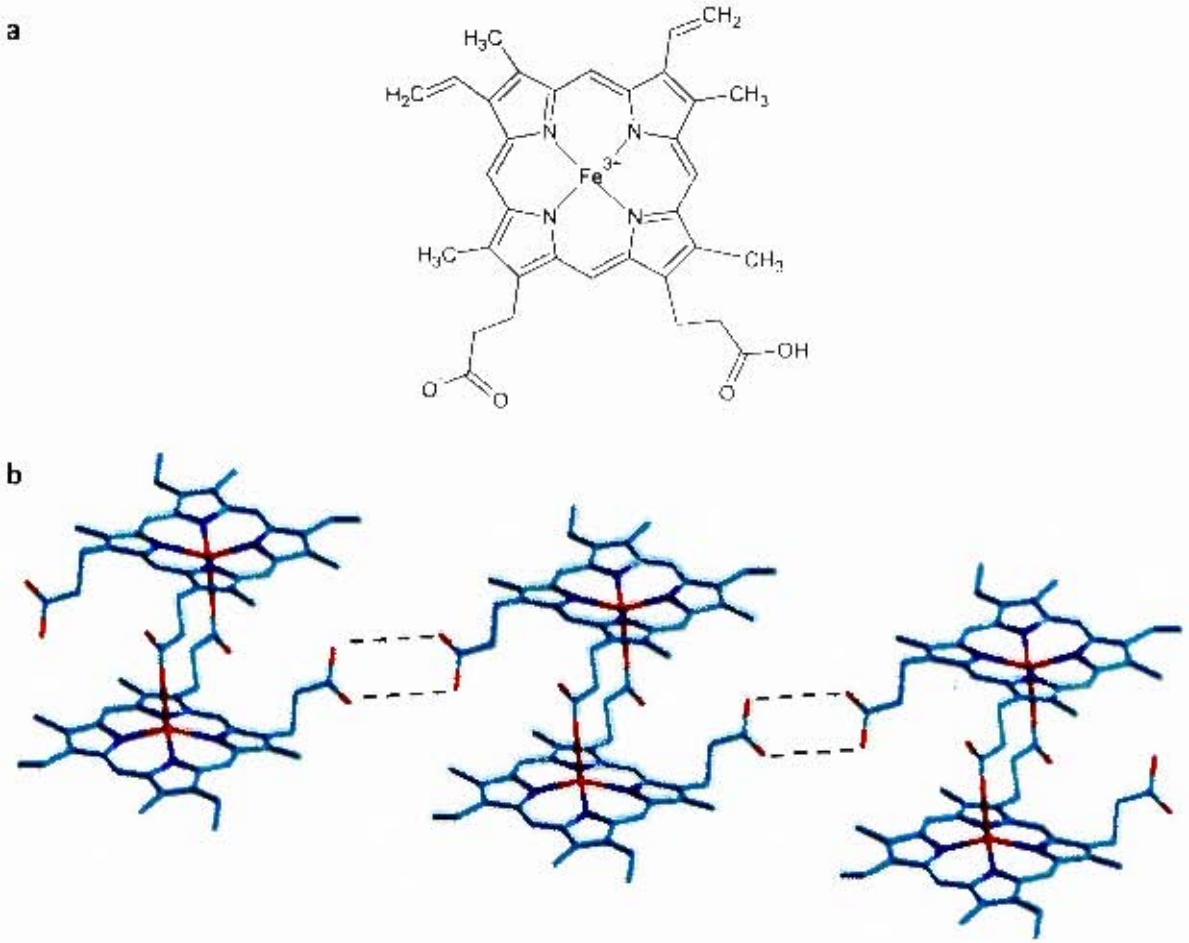

Figure 1.4. (a) The structure of ferriprotoporphyrin IX, Fe(III)PPIX, excluding the axial HO$^-$/H_2O ligand for clarity. (b) The structure of haemozoin consists of a Fe(III)PPIX dimer where the propionate side chain is coordinated to the iron centre of the other. Hydrogen bonding (dashed lines) occurs between the free propionates of neighbouring dimers. Figure adapted from reference 34.

1.5 Haemozoin formation

There has been much controversy in the literature over the mechanism by which haemozoin forms with many authors such as Sullivan and co workers[35] initially suggesting the involvement of histidine-rich protein II. On the other hand, Dorn *et al.*[36] showed that formation could be governed by an autocatalytic process, while a further mechanism was proposed by Bendrat *et al.*[37] where formation was observed to involve lipids. Recent evidence seems to lend support to the idea of lipid involvement in haemozoin formation with Coppens and Vielemayer[38] having observed haemozoin crystals encapsulated in lipid droplets within the acidic digestive vacuole and later by Pisciotta *et al.*[39] who demonstrated that haemozoin occurs within neutral lipid nanospheres (see figure 1.5). A similar discovery was made by Oliveria and co-workers[40] in the helminth worm, *Schistosoma mansoni*, and while this parasite is not a relative of *Plasmodium*, the finding supports the possibility that haemozoin formation occurs universally in close contact with lipids.

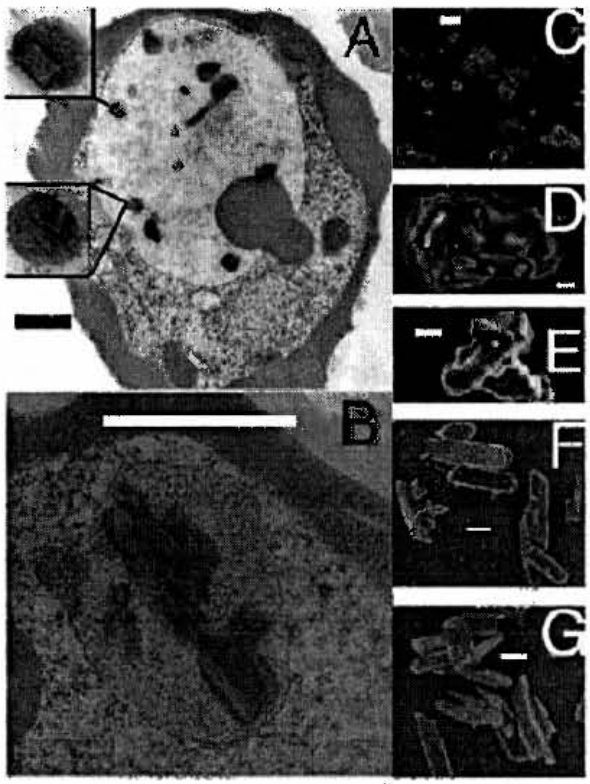

Figure 1.5. Transmission electron micrograph (TEM) images of early stage and mature (A and B) *P. falciparum* trophozoites. **Insets.** Haemozoin encapsulated in lipid nanospheres. Scanning electron micrograph (SEM) images of isolated haemozoin coated by lipids (C to E) and delipidated (F and G). Figure reproduced from reference 39.

Additional support for this formation process has also been described by Egan *et al.*[41] where the formation of synthetic haemozoin, known as β-haematin, occurs very efficiently at lipid/water interfaces under physiological conditions. The identification of the spontaneous formation of a π-π Fe(III)PPIX dimer species in aqueous solution by de Villiers *et al.*[42] using UV-vis spectroscopy and NMR spectrometry as well as computational investigations by Egan *et al.*[43] indicating spontaneous formation of a haemozoin dimer precursor from the π-π dimer also strongly support the validity of this proposed mechanism of formation (see figure 1.6).

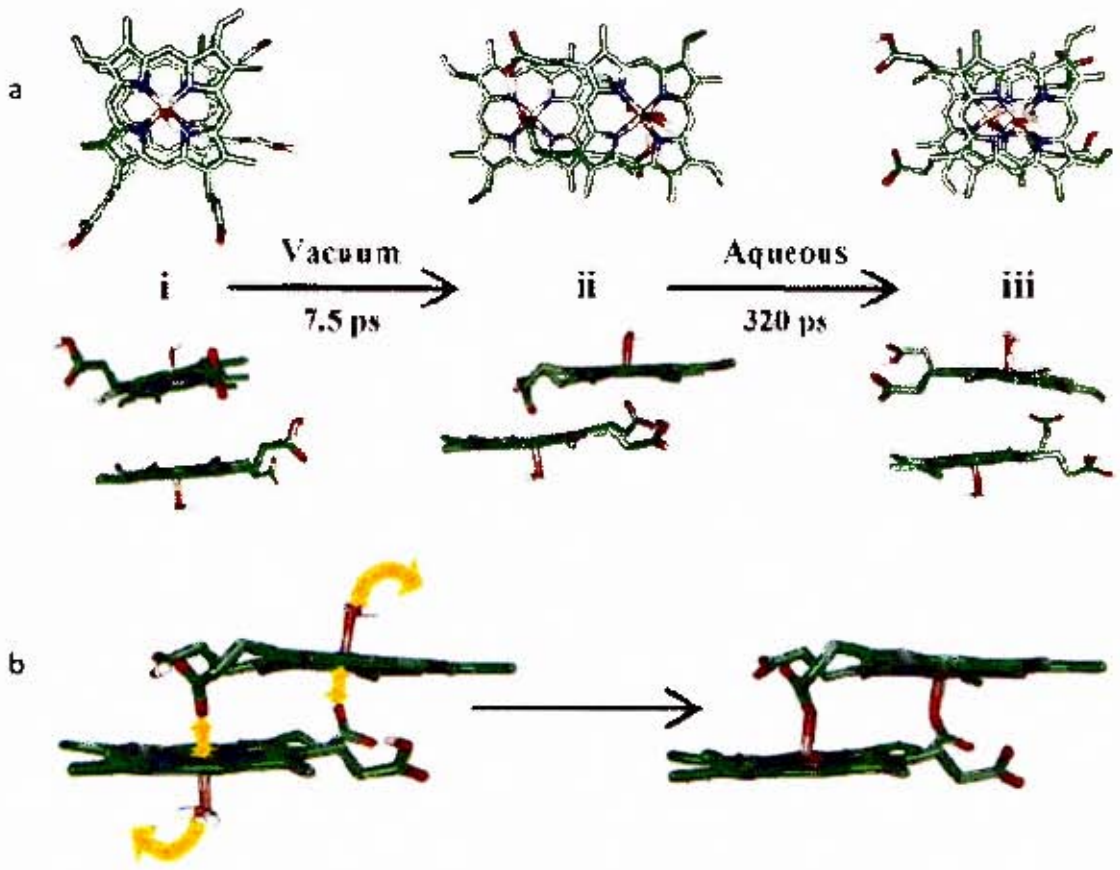

Figure 1.6. (**a**) Spontaneous conversion of the π π dimer of Fe(III)PPIX in vacuum (i) to a haemozoin precursor dimer (ii). In aqueous solution this precursor reverts to a π π dimer, indicating that formation of the precursor is unlikely in an aqueous environment. (**b**) Formation of haemozoin from the precursor dimer where coordination to the iron centre of Fe(III)PPIX results in the release of the axial water ligands. Reproduced from reference 41.

1.6 Inhibition of haemozoin by antimalarials

As mentioned in section 1.3, several classes of drugs are reported to act against haemozoin formation, with the family of quinoline derivatives and related compounds the most important. The reason for the importance is the potent antimalarial activity and widespread clinical use of members of this family including such drugs as chloroquine (CQ), mefloquine (Mf) and halofantrine (Hf, structures shown in figure 1.7). The ability of chloroquine and related compounds to inhibit β-haematin formation has been previously reported and these β-haematin activities correlate with their corresponding *in vivo* activity, lending support to their proposed mechanism of action.[43, 44]

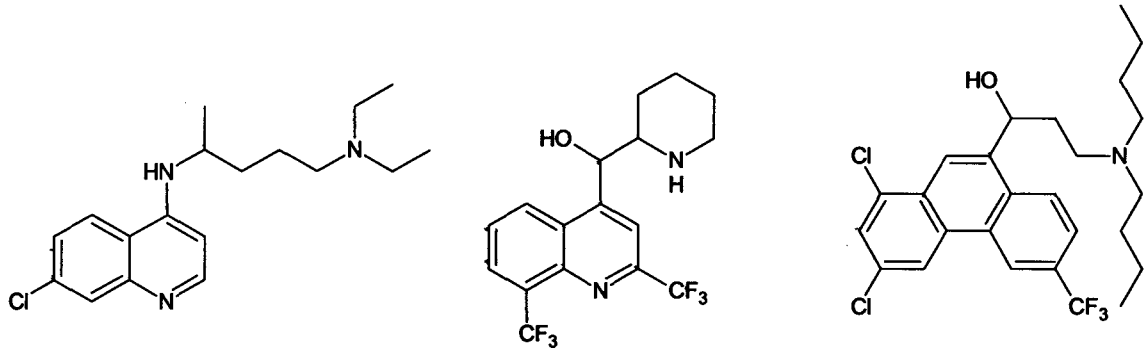

CQ Mf Hf

Figure 1.7. Structures of antimalarials chloroquine (CQ), mefloquine (Mf) and halofantrine (Hf).

Chloroquine has been referred to as one of the most successful antimalarials ever developed because of its effectiveness, safety and low cost.[45] Following the appearance of chloroquine resistant parasites, it has been necessary to turn to a variety of drugs of similar structure, such as mefloquine and halofantrine, to combat malaria. More recently, artemisinin combination therapy has been the treatment of choice, but this also invariably involves a quinoline or related compound such as mefloquine, amodiaquine or lumefantrine.[46, 47] In addition to the emergence of resistant parasitic strains, the mechanism of action by which chloroquine and related drugs assert their antimalarial activity is not fully understood.

1.7 Antimalarial drug resistance

Resistance to antimalarial drugs, especially chloroquine, have been the attributed as the main cause in the rising morbidity and mortality rates for malaria.[48] While the use of artemesinin combination therapy has helped alleviate this disease to some extent, there have been reports of sporadic decreased sensitivity to this treatment and evidence seems to suggest resistant strains are emerging.[49-51] In order to propose novel antimalarial compounds which are effective against both sensitive and resistant strains, knowledge of how parasites become resistant to antimalarial drugs is of importance.

1.7.1 Mechanism of chloroquine resistance.

It has long been known that resistance to chloroquine by parasites is not a result of an alteration of the original target but is rather a reduced ability to reach this target as observed by drug accumulation in the parasitic digestive vacuole which is lower in chloroquine resistant (CQR) parasites than in chloroquine sensitive (CQS) ones.[52, 53] Because chloroquine is a weak base which accumulates in the digestive vacuole via pH trapping, it was initially proposed that increases in the vacuolar pH would result in decreased accumulation.[54] Subsequent studies have shown this not to be the case as measurements of vacuolar pH in chloroquine sensitive and resistant strains have been found to be similar.[23] One of the more favoured explanations for this lack of accumulation has been proposed to be caused by a mutated membrane transport protein (PfCRT, *Plasmodium falciparum* chloroquine resistant transporter) which causes an increase in chloroquine efflux from the digestive vacuole resulting in decreased intravacuolar concentrations that are unable to inhibit haemozoin formation.[55, 56] Wild-type PfCRT is found in the membrane of the digestive vacuole and is a member of the so called drug metabolite transporter family of proteins. However, its normal function is unknown.[55] The proposed mechanism of chloroquine efflux is through transport of chloroquine out of the digestive vacuole, which is further supported by the fact that chloroquine resistance is reversible by verapamil, a known membrane transport inhibitor.[57] Only very recently did Martin *et al.*[58] directly show transport of chloroquine across a membrane by mutant PfCRT, using a *Xenopus laevis* oocyte model system.

It has been found that the key mutation in PfCRT for chloroquine resistance is that of lysine (K) 76 to threonine (T). This mutation by itself is not enough to convey resistance and so various other mutations (differing from strain to strain) seemingly are also required, probably to maintain activity of the protein.[59] The K76T mutation results in the PfCRT transporter losing a positive charge which is believed to allow for the transport of chloroquine in its protonated state, where previously this would not have been possible because of cation-cation repulsion (see figure 1.8).[60]

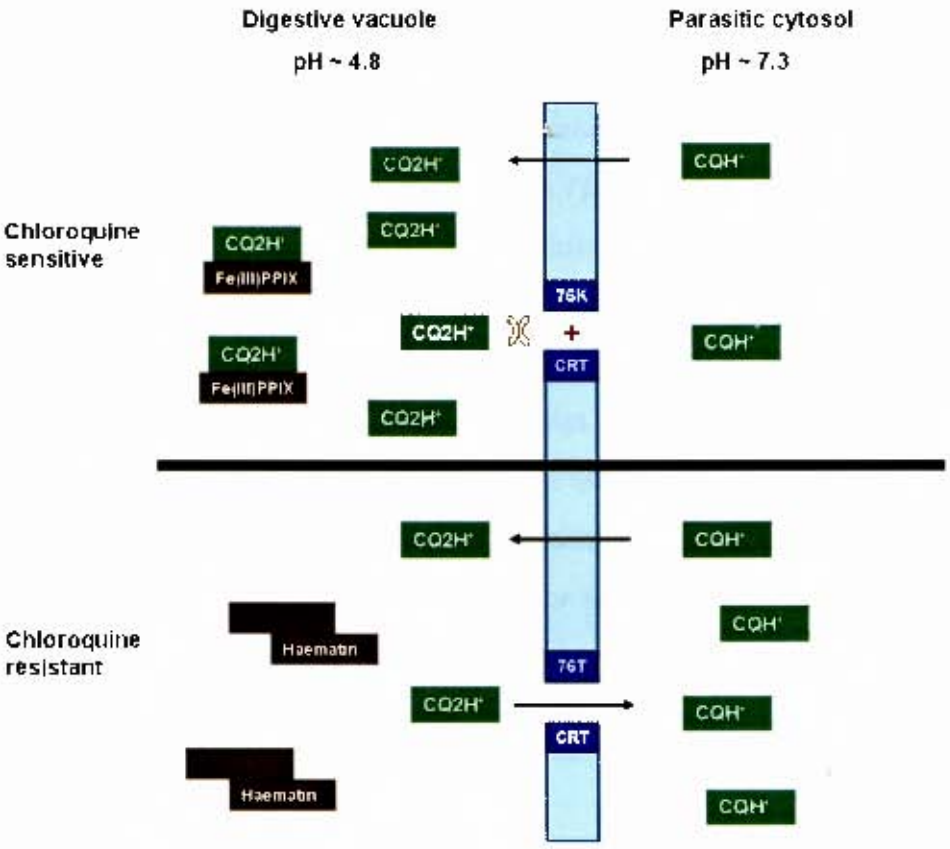

Figure 1.8. Chloroquine is monoprotonated (CQH^+) under parasitic cytosol conditions and becomes doubly protonated ($CQ2H^+$) when crossing the pH gradient into the digestive vacuole. In chloroquine sensitive parasites, chloroquine accumulates as the cation-cation repulsions between $CQ2H^+$ and the positively charged lysine (K) in position 76 on the Chloroquine Resistant Transport (CRT) protein prevents efflux. Chloroquine concentrations allow for inhibition of the Fe(III)PPIX detoxification process. In chloroquine resistant parasites, mutation of the positive lysine in CRT to neutral threonine (T), allows for the transportation of chloroquine out of the digestive vacuole and Fe(III)PPIX detoxification to haemozoin can occur.[56] Figure adapted from reference 56.

1.7.2 Mechanism of aryl-amino alcohol antimalarial resistance.

The mechanism by which parasites exhibit resistance to aryl-amino alcohol antimalarial drugs is not well understood. It is believed that the membrane transport protein PGH-1 (P-glycoprotein homologue), coded by the gene *Pfmdr1* (*Plasmodium falciparum* multidrug resistance), is involved. Studies have shown that some laboratory mefloquine resistant parasites (e.g. W2-MEF) have an increased copy number of *Pfmdr1* and/or an over-expression of PGH-1 which has also been shown to cause a decreased sensitivity to halofantrine and quinine antimalarials.[61, 62] This amplification of the PGH-1 protein has thus been suggested as a cause of resistance. Further evidence to support this has been found where increased chloroquine resistance in W2-MEF resulted in de-amplification of PGH-1 and subsequent increased sensitivity to quinine, mefloquine and halofantrine.[63] There is evidence that contradicts this proposed resistance mechanism with some field studies reporting strains with no amplification of PGH-1 that are mefloquine resistant, which suggests additional mechanisms that may mediate resistance.[64, 65] There have also been reports that some mutations in *Pfmdr1* may cause resistance to quinine and that there is some interaction of quinine and quinidine with PfCRT.[66, 67]

While there are many theories as to the mechanisms of resistance to chloroquine and related compounds, it is clear that there is still much that is not well understood. To add to this is the fact that there is a lack of chemical diversity between many antimalarials and cross-resistance has begun to develop.[68] There is thus a great need for the development of novel antimalarial drugs of differing structural classes. However, in order to be able to propose compounds of a new class as potential antimalarial drugs, understanding the mechanism of action of known antimalarials is important.

1.8 Mechanisms of haemozoin inhibition

The mechanism of action of haemozoin inhibiting antimalarial drugs is, unfortunately, not well understood. Literature has suggested two main possible modes of action. The first is a mechanism proposed for haemozoin inhibition by Buller *et al.*[59] and involves the interaction of an inhibiting compound with the fastest growing faces of the haemozoin crystal (001 and 00-1). These faces are orientated in such a way that corrugated grooves are formed from which the propionic acid and aromatic surface of the Fe(III)PPIX units are exposed (see figure 1.9a). It is with these protruding moieties that haemozoin inhibiting antimalarial drugs are thought to interact. As an example, chloroquine (CQ) is shown modelled in the groove of the haemozoin crystal and four possible intermolecular interactions were identified as a (i) *porphyrin*-COO ··· *CQ*-R_3NH^+ salt bridge; (ii) *porphyrin*-CH_3 ··· *CQ*-Cl contact; (iii) *porphyrin*-C=CH ··· *CQ*-$N_{quinoline}$ contact and (iv) *porphyrin*-C=C (π-cloud) ··· *CQ*-R_2NH contact (illustrated in figure 1.9b).[69] This model is not without criticism because CQ was modelled in its singly protonated state. Under the acidic digestive vacuole conditions where CQ is thought to accumulate and interact with the haemozoin, the doubly protonated form is the major species. However, with the discovery of lipid involvement in haemozoin formation, the monoprotonated species may well be present in a lipid environment and thus this is a plausible mechanism.

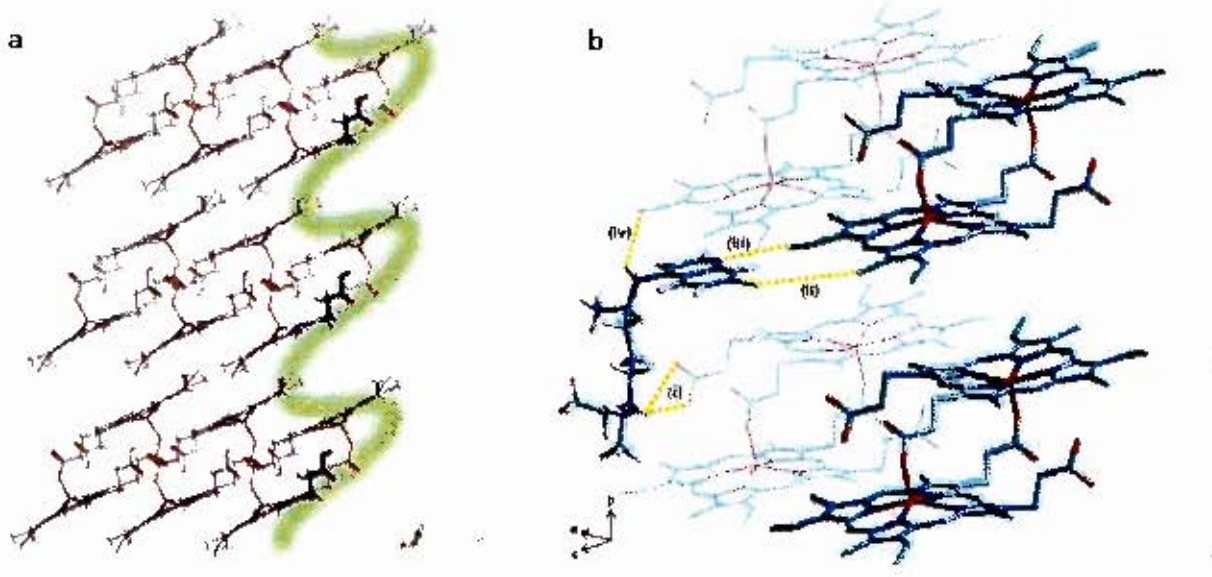

Figure 1.9. (**a**) Model of β-haematin, viewed along the *a* axis, showing corrugated grooves where haemozoin inhibiting antimalarial drugs are thought to adsorb. (**b**) Chloroquine is thought to associate in the β-haematin groove through four interactions. Lengths of interactions are (i) 2.7 Å, (ii) 3.0 Å, (iii) 2.4 Å and (iv) 2.7 Å. Figures reproduced from reference 69.

The second proposed mechanism of action involves the association of quinoline haemozoin inhibiting antimalarials through electronic interactions (such as π-stacking) with free Fe(III)PPIX.[70, 71] In the case of arylmethanol antimalarials such as quinine and quinidine, it has been proposed that in addition to π-stacking, coordination to the iron centre of Fe(III)PPIX, through the alkoxide, occurs.[72-74] However, owing to the inactivity of the epimers of quinine and quinidine, additional interactions other than coordination and π-stacking were obviously present.[75] Up until recently, these proposed interactions were only supported by UV-vis and NMR spectrometric evidence. More convincing evidence in support of this theory was obtained when the first crystal structure of an antimalarial drug-Fe(III)PPIX complex, that of halofantrine, was elucidated (see figure 1.10).[76] The crystal structure showed halofantrine coordinated to the iron centre of Fe(III)PPIX through its benzyl alcohol moiety and favourable distances were observed for π-stacking interactions between the phenanthrene and porphyrin ring systems. In addition, an intermolecular hydrogen bond between the tertiary amine of halofantrine and the propionate side chain of a neighbouring complex was also observed.

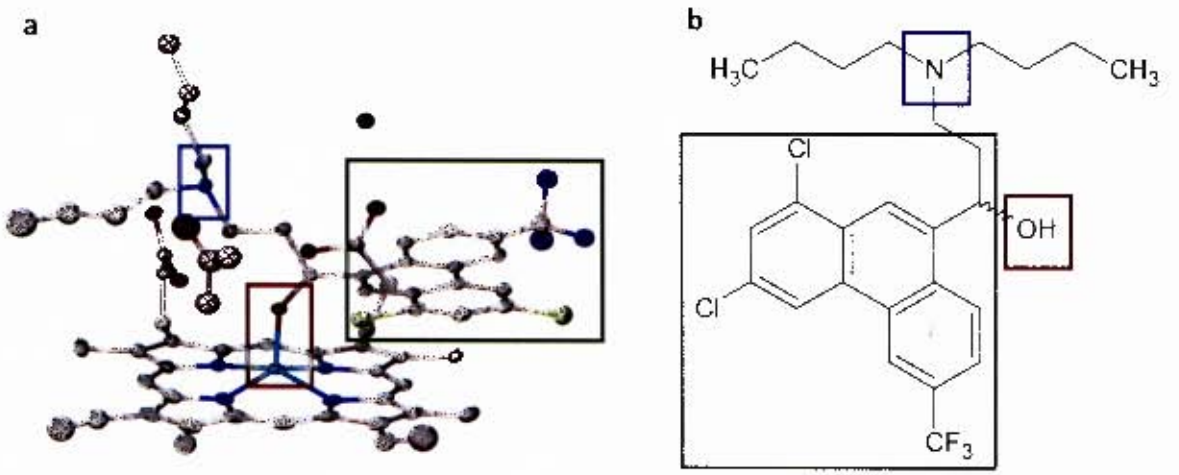

Figure 1.10. (a) Crystal structure of the haem halofantrine complex. Figure reproduced from reference 76. (b) Structure of halofantrine. Highlighted areas indicate key interactions with Fe(III)PPIX as being coordination (red), π-stacking (green) and hydrogen bonding (blue).

Because of the structural similarities of the antimalarials quinine (QN) and quinidine (QD) as well as its epimers epiquinine (EQN) and epiquinidine (EQD) to halofantrine (see figure 1.11), it was proposed that these compounds associate with Fe(III)PPIX through similar interactions. Of the four, QD is known as the most active antimalarial compound, with QN showing slightly less activity and the epimers EQN and EQD showing almost no activity.[76] Association constants (log K_{obs}) of the four compounds with Fe(III)PPIX (see table 1.2) do not show the same trend as the biological activities (as determined by the 50% inhibitory concentration or IC_{50}), indicating that an additional interaction must play a role.[76]

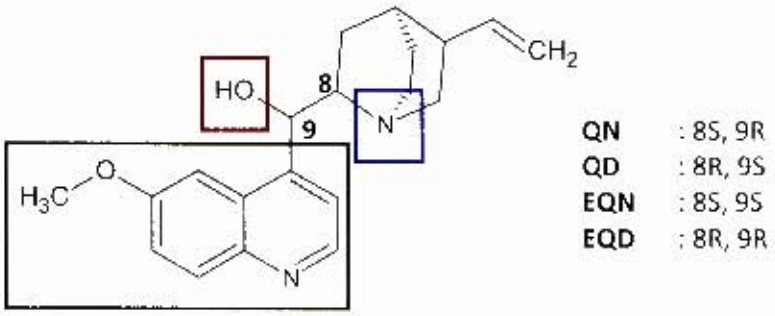

Figure 1.11. Structure of quinine and its epimers. Shaded regions show the structural similarities to halofantrine and thus these compounds are thought to follow the same mechanism of action with Fe(III)PPIX through coordination (red), π-stacking (green) and hydrogen bonding (blue) interactions.

Table 1.2: Association constants and IC_{50} for quinoline antimalarials. Reproduced from reference 76.

Compound	Log K_{obs}	IC_{50} (nM)[a]	β-Haematin Inhibition (%)
QN	4.10	29.3	84 ± 1
QD	5.02	13.4	85 ± 9
EQN	4.04	3471	2 ± 13
EQD	4.37	2700	12 ± 12

[a] Against *P. falciparum*, D6 strain.

The hypothesis that this additional interaction is an intramolecular hydrogen bond between the haem propionate and the quinuclidine nitrogen of the drug was proposed by de Villiers *et al.*[76] and is supported by computational results reported by the same authors. The findings showed that in order for the EQN and EQD complexes to form such an intramolecular hydrogen bond, they have to adopt unfavourable high energy conformations, while the QN and QD complexes can easily form the hydrogen bond, owing to the lower energy of the conformations needed. A plot of the IC_{50} of each drug versus the difference in energies between the strained conformation needed for intramolecular hydrogen bonding and minimum energy conformations of each of the haem-drug complexes (ΔE), shows a linear relationship (see figure 1.12). This linear relationship suggests that the ability to form the intramolecular hydrogen bond determines the antimalarial activities of each compound.

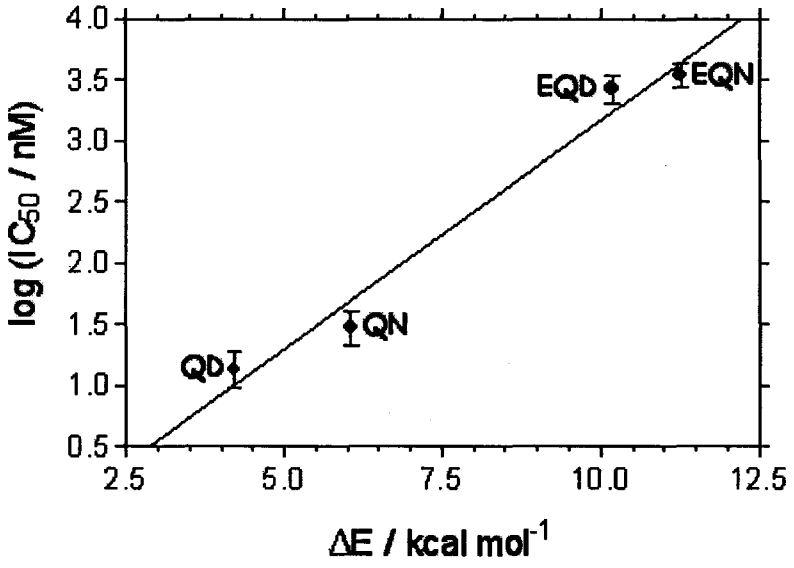

Figure 1.12. Graph of the IC_{50} of quinine (QN) and its epimers versus the difference in energies (ΔE) between strained and minimum energy conformations of the haem-drug complex. Figure reproduced from reference 76.

Thus the proposed mechanism of action for halofantrine and related antimalarials in the inhibition of haemozoin formation involves firstly anchoring the molecule to haematin through coordination to the iron centre and π-stacking with the protoporphyrin ring system. This then allows for hydrogen bonding interactions with the propionate side chain to occur resulting in the inhibition of haemozoin formation.

In light of this new information, the rational design of novel antimalarial drugs can for the first time be proposed based on a similar mode of interaction with Fe(III)PPIX. Uncovering compounds with novel scaffolds that possess the potential to have strong interactions with Fe(III)PPIX is possible through the use of fragment based drug design as well as by gaining better understanding of the relationships of coordination, π-stacking and hydrogen bonding with Fe(III)PPIX.

1.9 Fragment approach to drug discovery

In the quest to identify novel hit compounds, fragment based drug design (FBDD) has become a popular alternative to techniques such as high throughput screening (HTS). This move towards FBDD is a result of the increased efficiency of this technique.[77] While the use of HTS has produced many important hit compounds, the technique generally suffers from a low hit rate, meaning a large body of compounds (typically in the millions) need be searched in order to identify a small quantity of compounds of interest.[78, 79] The FBDD approach is able to alleviate this HTS problem somewhat by screening lower molecular weight compounds (typically 150 to 200 g/mol), termed fragments, as by decreasing molecular weight of compounds results in an exponential decrease in the number of different molecules possible with the same molecular weight.[80] This results in smaller compound libraries needing to be screened, with the libraries themselves often containing compounds that can be either commercially available or require minimal synthetic modification. As a consequence, reported hit rates from FBDD approaches are typically higher than those obtained through HTS.[78] An added benefit to the use of FBDD is that it provides for a more rational approach to drug discovery and can lend itself to a better understanding of the target by providing some structural information.[80]

FBDD uses small molecules to probe the binding affinity to a target, but because of the small molecular size of the fragment, it is unlikely that the molecule will contain all the moieties required to produce strong target binding and so individual binding affinity is generally low (see figure 1.13a to c).[80] One approach of FBDD is to identify fragments that bind to different sites on a target and combine them into a single compound using linkers to give a compound that has enhanced binding affinity (see figure 1.13d).[78] In fact, this approach can lead to the development of stronger binding compounds than those identified by HTS, as in many cases the HTS identified molecule contains moieties which may not provide optimal interactions with the target site (see figure 1.13e).[78]

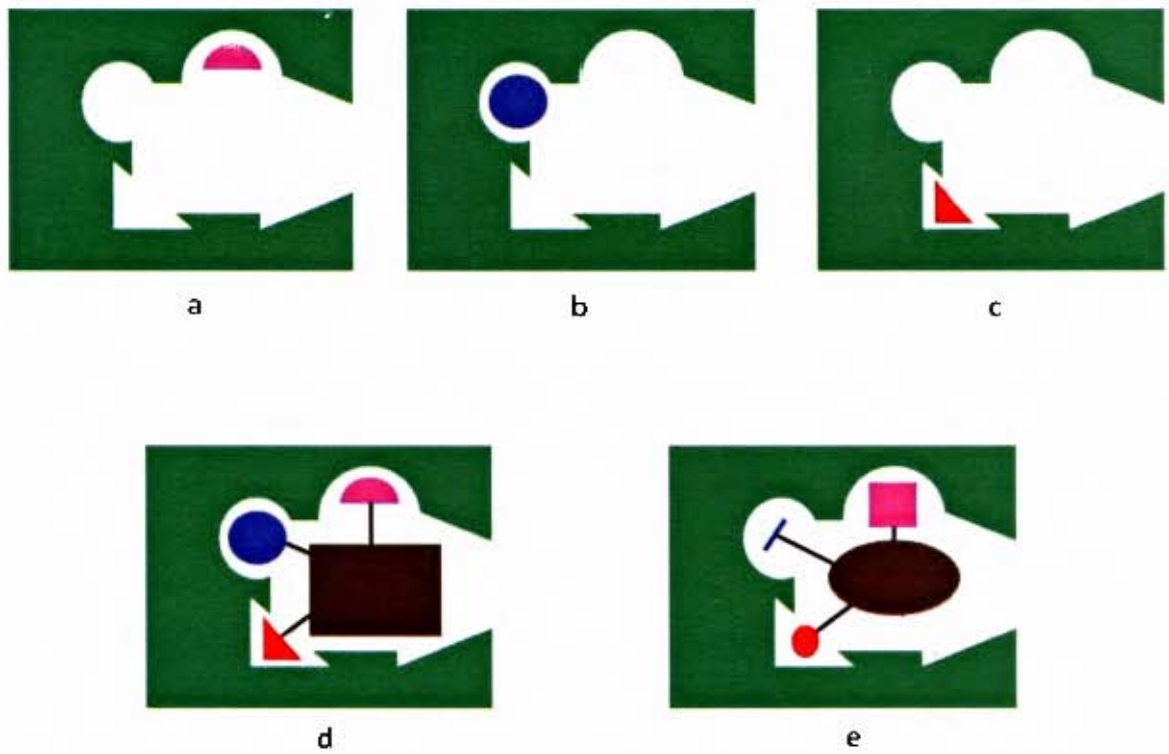

Figure 1.13. Small compounds, identified through the use of fragment based drug design, exhibit weak target binding (a to c). Combining individual fragments into a single molecule (d) can result in a hit compound with strong target binding which may provide even stronger interactions than compounds identified through high throughput screening methods (e) that have not been optimised. Figure adapted from reference 78.

FBDD relies on a variety of computational, biochemical and biophysical experimental techniques to obtain information about strength and structure of binding fragments.[77, 80] Computational methods are a useful tool in FBDD, where interactions of fragments can be modelled to identify potential hit fragments, while biochemical assays can provide information on binding strength. Biophysical techniques such as x-ray crystallography and NMR spectrometry are routinely employed to provide physical evidence of the structure of fragment binding. Unfortunately, very few of these techniques can be directly employed to identify fragment compounds in the case of Fe(III)PPIX.

At present there are several β-haematin (synthetic haemozoin) inhibition assays (see references 81 to 83 for examples), including a HTS assay developed by Ncokazi and Egan.[44] Using a fragment approach with these assays would be futile as almost all fragments would have less than the three required features (iron coordinator, aromatic π-stacker and hydrogen bond donor) of aryl methanols for β-haematin inhibition and thus the assay would likely simply give negative results. NMR techniques cannot be used because of the paramagnetic nature of iron which causes line broadening and x-ray crystallography is seemingly very difficult for this target as seen by the fact that there is only one reported drug-haematin crystal structure. While a computational approach can theoretically be employed for Fe(III)PPIX, the nature of this compound does not make for definitive results and so is not very effective. To elaborate, because of the planar structure of Fe(III)PPIX there are few steric and electronic interactions that can constrain a compound into specific conformations, thus interaction between fragments and Fe(III)PPIX results in very flexible structures and can lead to multiple possible conformations.

The most useful technique that can be employed for FBDD with Fe(III)PPIX is that of spectrophotometric titration. This method is able to provide binding affinities (in the form of association constants) as well as binding stoichiometries.

The UV-visible spectrum of free Fe(III)PPIX in its monomeric form is generally subject to hypochromism in its Soret peak (see figure 1.14) when compounds, such as chloroquine, are titrated into the solution. This effect has been attributed to the interaction between the transition dipole moments of the $\pi \rightarrow \pi^*$ electronic transition of Fe(III)PPIX and the π-electron cloud of the quinoline which are in close proximity.[84]

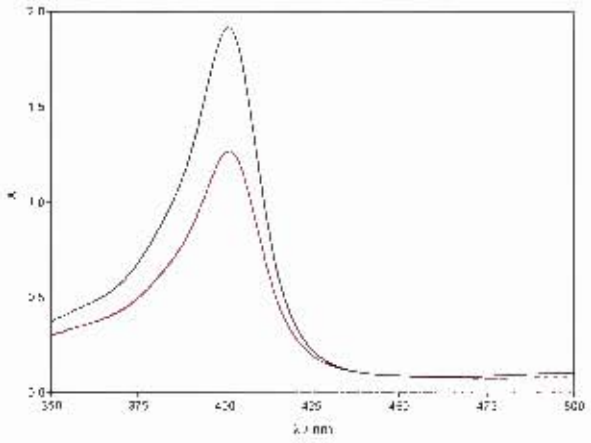

Figure 1.14. UV visible spectrum of free monomeric Fe(III)PPIX (black line) showing hypochromism of the Soret peak upon addition of quinoline, resulting in the presence of quinoline:Fe(III)PPIX complexes (red line).

Utilising spectrophotometric titrations and small compounds possessing interaction specific groups (for coordination, etc.), greater insights into the relationships of interactions with Fe(III)PPIX can be obtained, and it may be possible to combine these fragments to form new β-haematin inhibitors as potential starting points to novel antimalarials.

1.10 Interactions with Fe(III)PPIX

The three key interactions of coordination, π-stacking and hydrogen bonding form the basis of the proposed mechanism of action of halofantrine and related antimalarial compounds. While there exists an extensive body of literature on hydrogen bonding interactions with carboxylic acid receptors, there are no reported systematic investigations into relationships of coordination and π-stacking interactions with Fe(III)PPIX. Some insight can be gained from studies of these interactions with similar porphyrin and metalloporphyrin complexes.

1.10.1 Coordination interactions.

Investigation of the coordinating ability of various nitrogen donor ligands (imidazoles, pyridines and amines) with the haem octapeptide microperoxidase-8 (MP-8) by Pratt and co-workers[85-88] and N-acetyl microperoxidase-8 (N-AcMP-8) by Marques *et al.*[89] have previously been reported. These metalloporphyrins, see figure 1.15a, have been known to serve as model systems for haem proteins but also provide a monomeric derivative of Fe(III)PPIX in aqueous solution and thus are able to provide some insight into the coordination interactions with free Fe(III)PPIX. Both Marques and Pratt reported that under aqueous conditions, coordination to the iron centre of the metalloporphyrins was dependant on the pK_a and hence basicity of the donor ligand.

In these studies, four distinct families of compounds were identified. Imidazoles produced the strongest association constants, amines were found to be separated into two groups (I and II), with class I amines having the weakest associations, while class II amines shared a similar binding strengths to pyridines (see figure 1.15b).

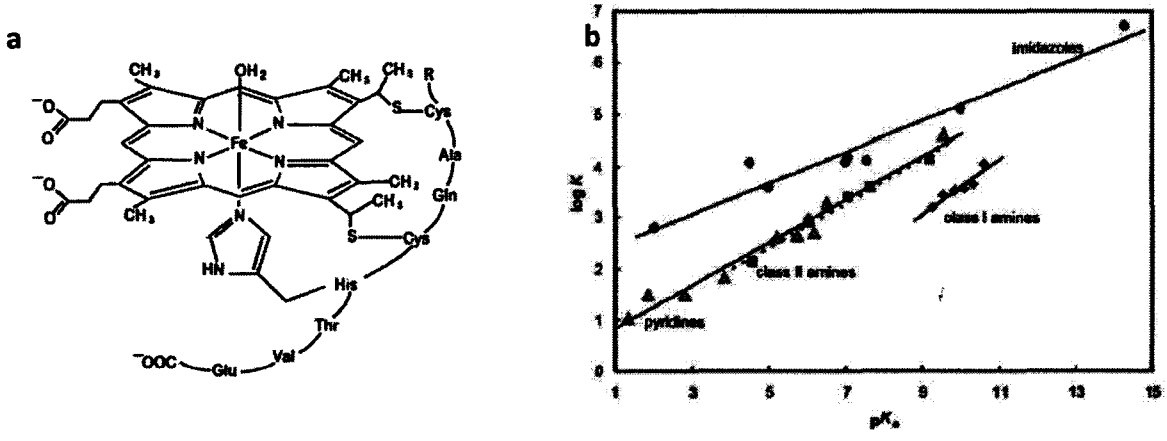

Figure 1.15. (a) Molecular structure of microperoxidase-8 (MP-8) and N-acetyl-microperoxidase-8 (N-Ac-MP-8) when R = NH_3^+ and $NHCOCH_3$, respectively. (b) Linear free energy relationships between associating ability and pK_a of the coordinating ligand. Figures reproduced from reference 89.

Marques *et al.*[89] attributed the formation of these separate families to the increase in electron density on the metal centre provided by the coordinated imidazole moiety of histidine. The imidazole coordinates through its σ-orbital and backbonding occurs between the metal d-orbitals and the empty π*-orbitals of the nitrogen ligand. Strong σ-donors, such as imidazole, cause a polarisation of the t_{2g} metal orbitals which results in an unsymmetric distribution of electron density that accumulates *trans* to the coordinated ligand. These electron rich orbitals provide stronger backbonding interactions, and thus greater association interactions, with a second incoming ligand should it have access to empty π*-orbitals (see figure 1.16).[90]

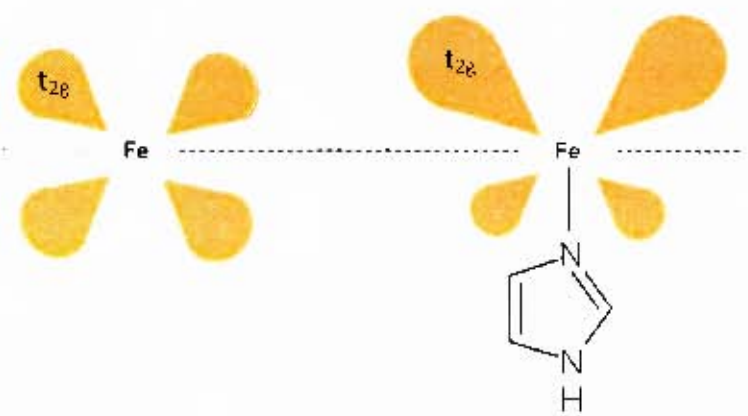

Figure 1.16. Schematic showing the unsymmetric accumulation of electron density in the t_{2g} orbitals upon coordination by the strong σ-donor imidazole. The greater electron density *trans* to imidazole results in stronger coordination of a second incoming ligand, provided it is a π-acceptor, as stronger backbonding interactions are possible. Figure adapted from reference 90.

As the sp^2 nitrogen containing imidazole and pyridine ligands have access to these orbitals, they form stronger association constants. However, sp^3 amine ligands do not have π*-orbitals and thus are not able to partake in backbonding interactions with the metal, which accounts for the separation of class I amines from imidazole and pyridine families. While class II amines are also not able to partake in π-backbonding, the greater strength of association with N-Ac-MP-8 was attributed to the ability of these compounds to hydrogen bond with the propionate side chains when bound. Further separation between the imidazole and pyridine families is attributed to better orbital overlap by imidazoles as compared to pyridines.[89]

1.10.2 π-Stacking interactions.

While many models have been previously proposed to describe π-stacking interactions, the most widely accepted description is that reported by Hunter and Sanders.[91] This model describes the π-stacking interaction as the sum of various attractive and repulsive non-covalent forces between two aromatic compounds (summarised in figure 1.17). The largest attractive contribution to π-stacking is described by van der Waals (VDW) interactions which include dipole-dipole (electrostatic) interactions (figure 1.17a); dipole-induced dipole interactions (figure 1.17b) and induced dipole-induced dipole (London) interactions (figure 1.17c). In theory, attractive charge transfer effects also have the potential to influence interactions but the energetics of these forces are generally regarded as negligible. Solvophobic effects (figure 1.17d) in the form of desolvation and polarising effect of aromatic interactions are also important, with polar solvents providing more favourable π-stacking interactions. The largest unfavourable contribution to π-stacking is Pauli repulsion (figure 1.17e) which becomes significant when electron clouds begin to overlap. It is this term which has a significant effect on the geometry of π-stacked molecules.[91, 92]

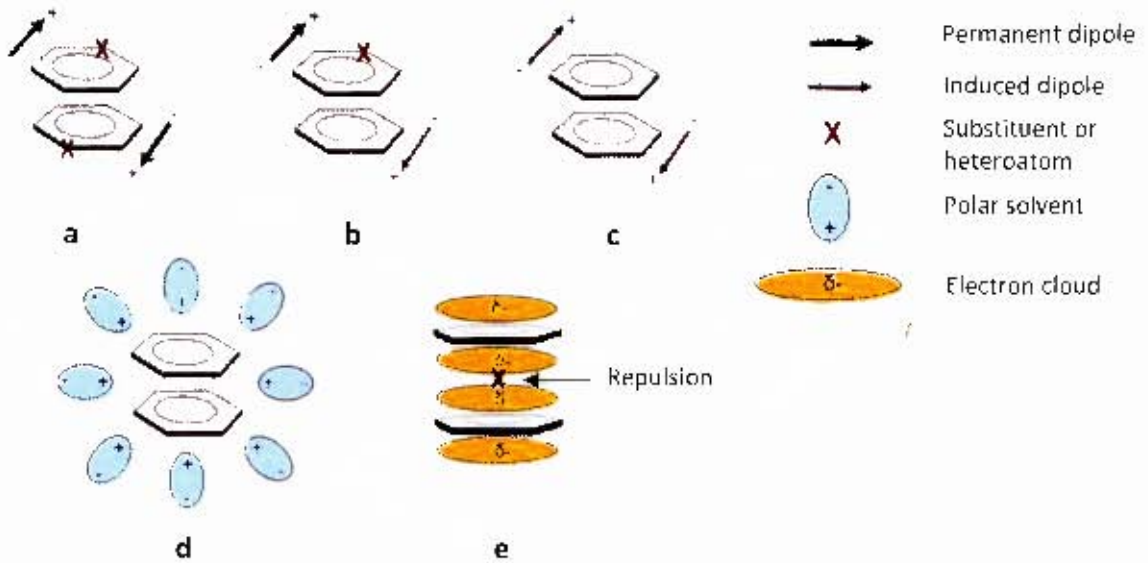

Figure 1.17. Non-covalent forces responsible for aromatic π-stacking interactions. (**a**) dipole dipole interactions; (**b**) dipole-induced dipole interactions; (**c**) induced dipole-induced dipole interactions; (**d**) solvophobic effects; (e) Pauli repulsion. Figure adapted from reference 93.

Through experimental methods it was found that π-stacked aromatic molecules favour either an edge-to-face (T-shaped) or offset stacked geometry.[93] Molecular modelling by Hunter and Sanders[91], using their description of π-stacking, could account for the experimentally determined π-stacking orientations when the aromatic ring system was based on a charge distribution model (see figure 1.18). This model treats the electronegative nature of the π-electron cloud as being slightly negative but since the ring system is neutral, the σ framework is thus considered as slightly positive, giving rise to a quadrupole. It is the π-σ attraction that forms the basis of the π-stacking interaction, although geometry is largely governed by the ability to overcome π-π repulsions (Pauli repulsion). The T-shaped (figure 1.18a) and offset stacked (figure 1.18b) geometries are favoured over other geometries, such as face-to-face (figure 1.18c), owing to the minimal π-π repulsion effects experienced.[92]

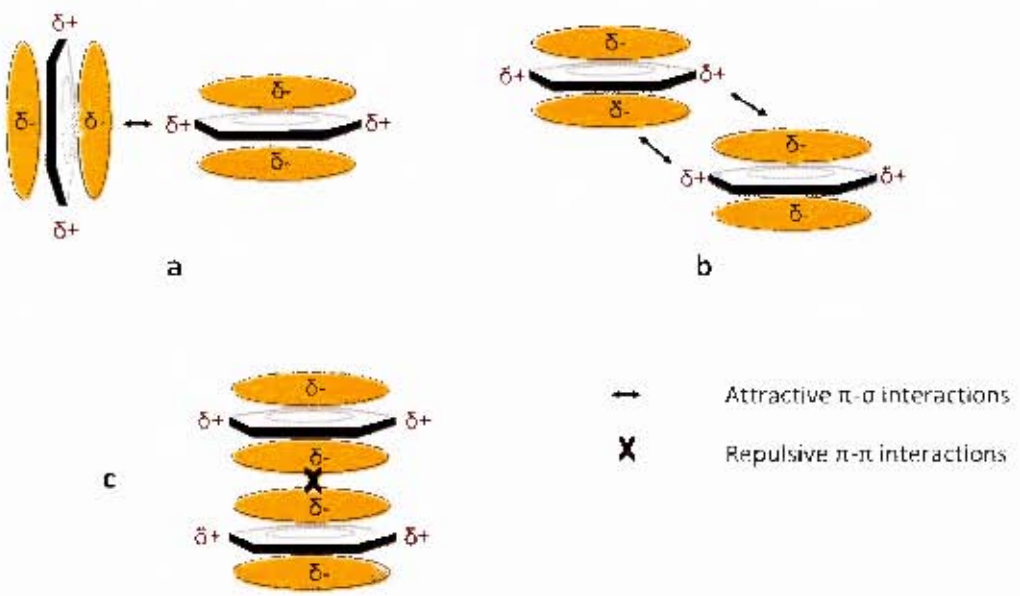

Figure 1.18. Geometries of π-stacking aromatic ring systems. (**a**) Edge-to-face (T-shaped) and (**b**) offset stacked geometries are favoured over (**c**) the face-to-face geometry owing to reduced repulsion. Figure adapted from reference 93.

Because of the significant effect of repulsive π-π interactions on the strength and geometry of π-stacking interactions, Hunter and Sanders[91] theorised that since incorporation of substituents or heteroatoms onto the π-stacking ring systems affect electron densities of the π-cloud (and thus π-π repulsion), they would affect π-stacking interactions. For non-polarised systems (no heteroatom present), substituents which are electron donating would destabilise π-stacking interactions by increasing electron density in the π-electron cloud and causing greater π-π repulsions (see figure 1.19a). Conversely, substituents that are electron withdrawing would decrease π-π repulsive effects, thus favouring π-stacking interactions (see figure 1.19b). Incorporation of heteroatoms into the ring system causes polarisation of the molecule and results in additional atom-atom and atom-πσ electrostatic effects. In the case of highly polarised molecules, it was calculated that atom-atom interactions are dominant and while atom-πσ interactions also have some significance, π-σ interactions become of least importance. The overall effect of the presence of a heteroatom in a ring system was theorised to provide better π-stacking interactions as heteroatoms reduce electron density in the ring.[92]

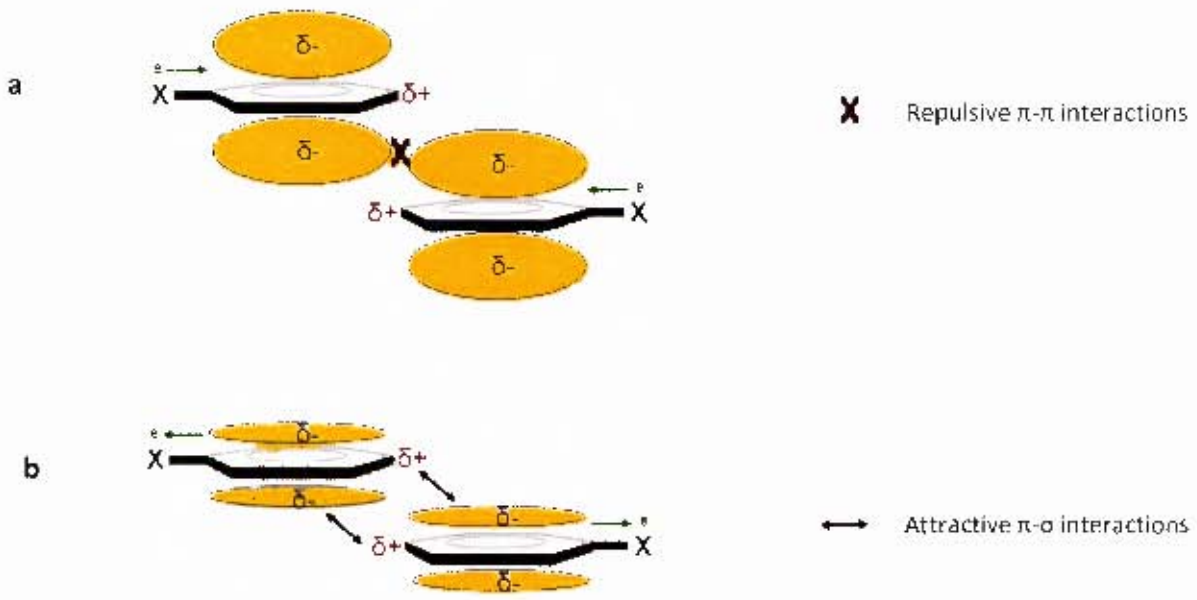

Figure 1.19. Effects proposed by Hunter and Sanders[91] on π-stacking interactions by introducing aromatic substituents. (**a**) Introduction of electron donating groups increase π-electron density and π-π repulsion, thus would disrupt π-stacking interactions. (**b**) Introduction of electron withdrawing groups decrease electron density and π-π repulsion, thus would favour π-stacking interactions. Figure adapted from reference 93.

Since the description of the π-stacking interaction by Hunter and Sanders[91], there have been few reported investigations which quantitatively describe such interactions. Fortunately, work by Schneider *et al.*[94, 95] has provided one of the few detailed investigations of quantitative π-stacking interactions with porphyrin ring systems under aqueous conditions and is of particular interest owing to the structural similarities between Fe(III)PPIX and the water soluble porphyrins used. The investigation of π-stacking interactions involved the measurement of association constants of various aromatic ring systems (0 to 14 π-electrons in size) with porphyrins. The reported findings showed a remarkably simple linear free energy dependence of associating ability (ΔG) on ring size in the form of number of π-electrons, where an increase in ring size resulted in an increase in strength of association with the porphyrin (see figure 1.20a). In addition, it was found that a decrease in solvent polarity (accomplished by increasing methanol content in water) had a detrimental effect on π-stacking interactions between phenanthrene and a water soluble porphyrin (see figure 1.20b). This confirms the solvent effects theorised by Hunter and Sanders.[91]

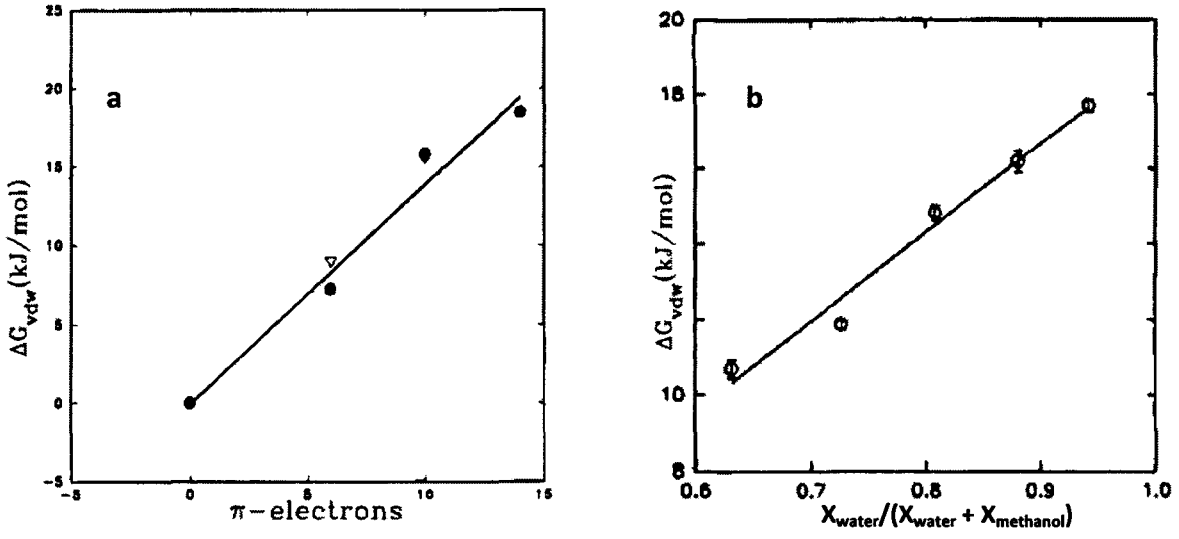

Figure 1.20. (a) Linear free energy relationship reported by Schneider and Wang[94] which indicates a stronger π-stacking ability with an increase in the number of aromatic π-electrons. (b) π-Stacking association between phenanthrene and a water soluble porphyrin decreases as solvent polarity is decreased. Figures reproduced from reference 94.

Investigation on the effect of substituents on π-stacking interactions is somewhat less clear cut, with authors such as Kim *et al.*[96] providing evidence suggesting such effects are negligible, while studies by Liu and Schneider[95] revealed the opposite. Findings by Liu and Schneider suggested substituents, other than alkyl groups, do affect the strength of π-stacking association but they were never able to correlate these effects with a physical property such as Hammett constants (values describing electron withdrawing ability). Interestingly, heteroatom effects were also found to be negligible.[95] From the results of these and many other authors it is obvious that the effects of aromatic ring substituents have a more complicated role than that proposed by Hunter and Sanders.[91]

1.10.3 Hydrogen bonding.

Hydrogen bonding remains one of the most important intermolecular interactions and affects a diverse range of areas from molecular recognition and aggregation to various inorganic and biological systems. The hydrogen bond is defined as a local bond of the form X – H ··· A, where X – H acts as a proton donor to A, is electrostatic in nature and has pronounced directionality.[97, 98] Because of the wide-reaching importance of this fundamental interaction, large bodies of work have been devoted to the investigation and understanding of the hydrogen bond.

With the proposal of a hydrogen bond interaction with the propionate side chain of Fe(III)PPIX, the hydrogen bonding interactions of carboxylic acid groups with various proton donor moieties is of particular interest and a review by Fitzmaurice *et al.*[99] titled 'Synthetic receptors for carboxylic acids and carboxylates' provided useful insights into the selection of potential hydrogen bonding moieties. The review specifically highlighted the use of nitrogen containing (i) ammonium, (ii) guanidinium, (iii) urea, (iv) thiourea, (v) amidopyridine and (vi) amide moieties as receptors for carboxylate anions. While all the above mentioned moieties are able to form at least one hydrogen bond with a carboxylate anion or carboxylic acid, classes (i) and (ii) have an additional electrostatic interaction which provides for stronger interactions with carboxylates. This interaction is known as a salt bridge and is the attractive force experienced between the delocalised positive charge, produced by the protonated state of the nitrogen, and the delocalised negative charge of the carboxylate anion.[99]

Ammonium salts (i) provide the simplest hydrogen bonding interaction between a protonated amine and carboxylate anion. Individually, these interactions are not particularly strong and so are generally utilised as polyamines (such as investigated by Kimura *et al.*[100], see figure 1.21a) or are used in conjunction with other stronger hydrogen bonding moieties to give added stabilisation. Single hydrogen bonding moieties have also been investigated, with Barboiu *et al.*[101] reporting the carboxylate binding of various amino acids through the use of a single ammonium moiety (see figure 1.21b).

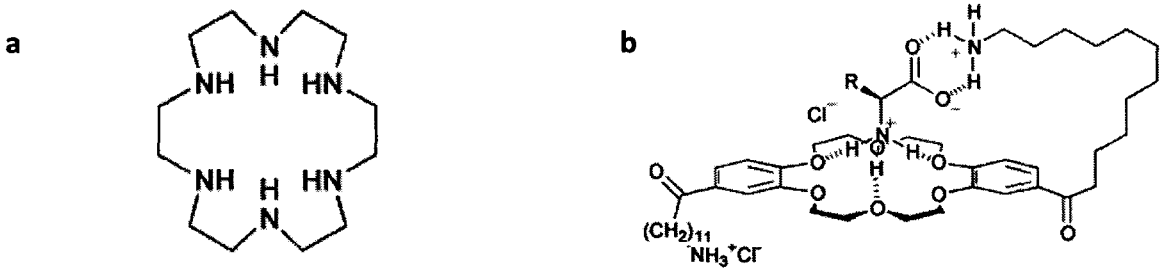

Figure 1.21. Examples of multiple (**a**) and (**b**) single ammonium hydrogen bonding groups used to bind carboxylate anions.[100, 101] Figures reproduced from reference 99.

Guanidinium salts (ii) have the ability to form strong bidentate hydrogen bonded interactions with carboxylate anions (see figure 1.22a) and with their high inherent pK_a values (ca. 13.5[99]) the majority of species present in solution is in the protonated form meaning a greater percentage can partake in salt bridge interactions. It is these two characteristics that account for the strong hydrogen bonding interactions observed between guanidines and carboxylates. The binding ability of these moieties with carboxylates has been extensively investigated and is exemplified by the work of Schmuck[102] where strong binding of N-Ac-α-amino acid carboxylates using guanidine moieties in combination with pyrrole and amide groups were observed (see figure 1.22b). An interesting subclass of guanidinium salts mentioned by Fitzmaurice *et al.*[99] is that of amidinium salts. These moieties provide a similar hydrogen bonding motif as guanidinium salts, but are less basic in nature. Diamidine compounds (see figure 1.22c) reported by Mayence *et al.*[103] have shown good antimalarial activity and were found to inhibit β-haematin formation. Whether this activity is caused by the amidinium moieties hydrogen bonding to the propionate side chain of Fe(III)PPIX or not is uncertain. Nevertheless the incorporation of these moieties in an active anti-malarial drug is promising.

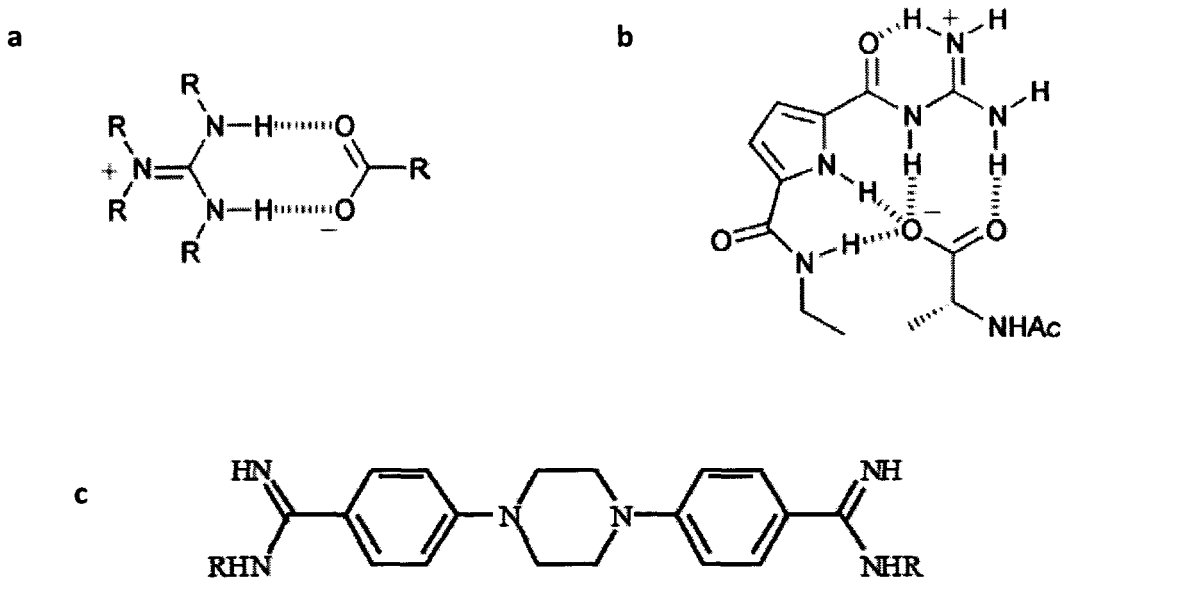

Figure 1.22. (a) Hydrogen bonding motif between guanidinium and carboxylate moieties. (b) Example by Schmuck[102] in the use of guanidines as receptors for carboxylate binding. Pyrrole and amide moieties are used to supplement the hydrogen bonding interaction.[99] Figures reproduced from reference 99. (c) Diamidine compounds reported by Mayence *et al.*[103] have shown the ability to inhibit β-haematin formation. Figure reproduced from reference 103.

The remaining moieties (iii to vi) described by Fitzmaurice *et al.*[99] are less interesting owing to their inability to form salt bridge interactions and thus they provide weaker overall interactions. Moieties (iii) and (iv) are known to have moderate hydrogen bonding strengths with carboxylate anions, but these still do not provide strengths comparable to guanidinium moieties without modifying the electron withdrawing ability of neighbouring groups. Because of the low pK_a values for moieties (v) and (vi), these groups are generally utilised as hydrogen bond donors for carboxylic acids, particularly in non-polar environments.

Owing to the nature of Fe(III)PPIX at digestive vacuole pH where one of the propionic acids is almost always deprotonated,[104] there exists the potential for salt bridge interactions in addition to hydrogen bonding interactions and thus ammonium and guanidinium moieties were of particular interest in this study.

1.11 Aims and objectives

1.11.1 Aims.

The overall aim of this project was to produce compounds using a rational fragment design approach in an attempt to inhibit β-haematin formation and thus confirm the hypothesised mechanism of action. This was envisaged to be achieved through two steps by:

1. Investigating the relationships of coordination and π-stacking interactions with Fe(III)PPIX.

2. Exploiting these relationships such as to propose and synthesise novel compounds which would have a strong possibility of inhibiting β-haematin formation.

1.11.2 Objectives.

The specific objectives required to attain the proposed aims were to:

1. Spectrophotometrically obtain association constants for various coordinating ligands with Fe(III)PPIX and relate them to a physical property of the ligands such as pK_a.

2. Spectrophotometrically obtain association constants for various aromatic ring systems with Fe(III)PPIX and PPIX and relate them to a physical property such as number of π-electrons.

3. Identify small molecules that maximise coordination and π-stacking interactions to be used as scaffold compounds.

4. Incorporate a hydrogen bonding moiety onto the scaffold and use molecular modelling techniques to propose compounds with the potential to inhibit β-haematin formation.

5. Synthesise the proposed compounds and test for β-haematin inhibition ability.

CHAPTER 2.

INVESTIGATION OF COORDINATION AND π-STACKING INTERACTIONS WITH FE(III)PPIX

2.1 Introduction

To date, no detailed investigations of factors governing coordination and π-stacking interactions with Fe(III)PPIX have been reported and thus interactions of this nature are not well understood. By attempting to uncover the underlying relationships of these interactions, the information obtained would be extremely useful in the design of template compounds which could anchor the molecule to Fe(III)PPIX and provide a scaffold to which hydrogen bonding groups may be incorporated, hence conforming to the proposed model required for inhibition of β-haematin formation.

2.2 Coordination interactions

Owing to the complex nature of Fe(III)PPIX speciation,[104] experimental conditions in the present study were limited to a 40% (v/v) aqueous DMSO solvent system at pH 7.4 in order to obtain a monomeric Fe(III)PPIX species.[75] This pH constraint meant that protonation competition had to be explicitly taken into account for donor ligands that have a pK_a higher than 7.4. Equation 1 was employed to calculate the pH independent association constant for coordination with Fe(III)PPIX (log K_c) from the observed association constant at pH 7.4 (log $K_{c,obs}$).

$$\log K_c = \log K_{c,obs} + \mathrm{Log}[1 + 10^{(pKa-pH)}] \qquad (1)$$

Utilising this technique and correcting for protonation, association constants for a variety of pyridine, imidazole, amine and phenolate donor ligands with Fe(III)PPIX were determined. Typical spectra obtained are provided in figure 2.1.

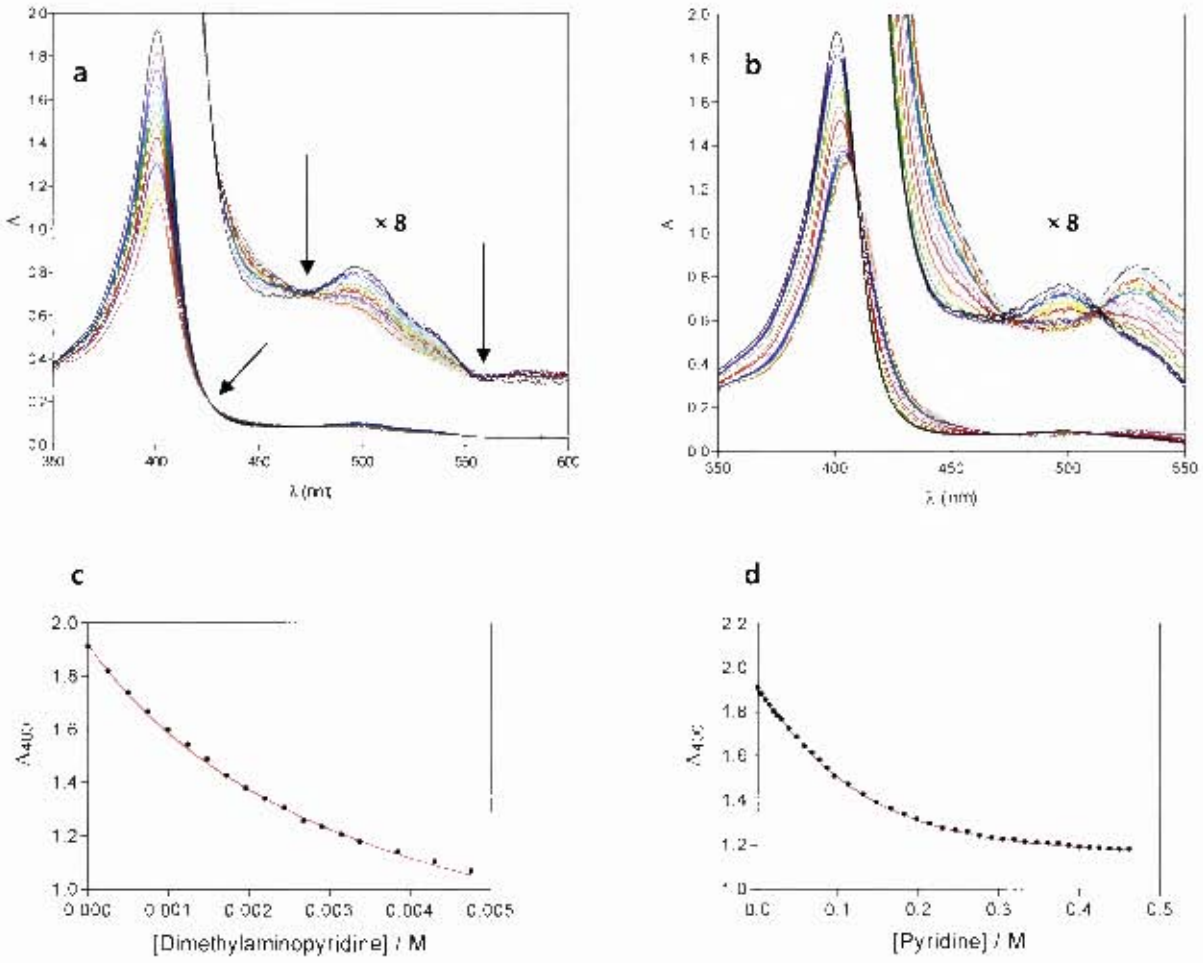

Figure 2.1. Typical spectroscopic changes obtained upon addition to Fe(III)PPIX (dilution corrected) of ligands forming a 1:1 (**a**) and 2:1 (**b**) complex. **Insets.** Expansion of Q band regions with arrows indicating isosbestic points in (**a**) but not (**b**). (**c**) Non-linear least squares fit (red line) of the data (black circles), obtained from (**a**), to equations 2 and 3 (see chapter 7), respectively. (**d**) Non-linear least squares fit (red line) of the data (black circles), obtained from (**b**), to equations 2 and 3 (see chapter 7), respectively.

Analysing the data obtained from the spectrophotometric titrations, it was found that the majority of the compounds tested formed 1:1 ligand:Fe(III)PPIX complexes. In these cases, changes in the absorbance spectra were found to be confined to the intensity of bands with no shifts occurring. The most prominent change identified was hypochromism of the Soret peak (see figure 2.1a).

However, some pyridine and imidazole ligands (compounds **6**, **8**, **10** and **13**, see table 2.1) were found to form to a 2:1 complex which resulted in the formation of a low spin iron centre which was spectroscopically characterised by both hypochromism and a shift of the Soret peak to a longer wavelength, illustrated in figure 2.1b, as well as increasing intensity and shifts in the Q band region. Formation of the 2:1 complex of imidazole with Fe(III)PPIX was found to be a stepwise process with clear evidence of deviation from the cooperative model which is most clearly observed at low and high concentrations (figure 2.2). The observation of such a 5-coordinate intermediate species is uncommon with imidazoles. Many authors report a cooperative mechanism with haemin under various aqueous and non-aqueous environments[105-109], however, these findings are in agreement with those of Marques *et al.*[110] where a similar stepwise process was discovered with imidazole for haematohaemin.

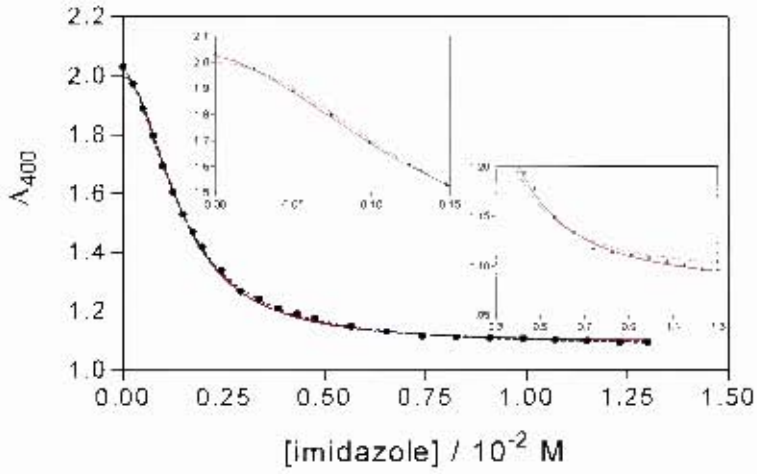

Figure 2.2. Non-linear least squares fits of experimental data (black circles) obtained from spectrophotometric titration of imidazole. Data were fitted to 2:1 stepwise (solid red line) and cooperative (dashed blue line) models using equations 3 and 4 (see chapter 7), respectively. **Insets**. Pronounced deviation is shown for the cooperative, but not stepwise model at low and high concentrations of imidazole.

Plotting log K_c of the coordinating ligands against their corresponding pK_a, values summarised in table 2.1, resulted in a single linear free energy relationship (LFER), shown in figure 2.3. These findings suggest that under conditions devoid of proton competition, such as in a lipid or organic environment, coordination to the iron centre of Fe(III)PPIX is based solely on the basicity of the donor ligand. The LFER between pK_a and coordination strength with Fe(III)PPIX in 40% aqueous DMSO is described by equation 5.

$$\log K_c = 0.71(6) \times pK_a - 2.6(5) \qquad (5)$$

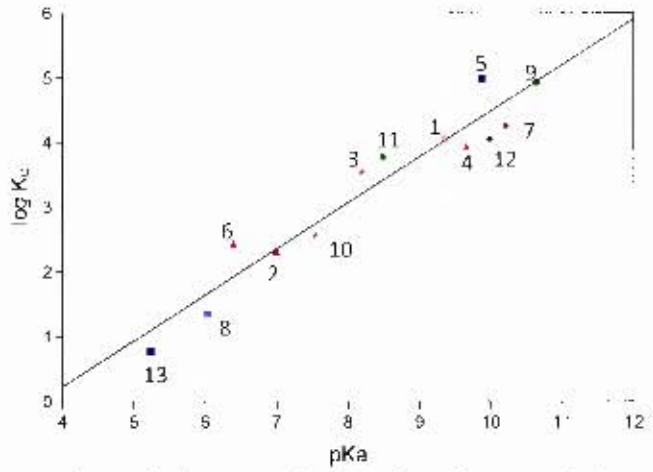

Figure 2.3. Linear free energy relationship between the pH independent association constant (log K_c) and pK_a of nitrogen and oxygen donor ligands. This relationship is described by log K_c = 0.71(6)×pK_a − 2.6(5) with r^2 = 0.93.

In order to confirm the hypothesis of coordination under pH independent conditions, association constants of those ligands, which are free bases, were then determined with Fe(III)PPIX in an organic solvent system. The solvent system consisting of 20% (v/v) DMSO in methanol was chosen, and from Beer-Lambert law studies, it was found that monomeric Fe(III)PPIX species were obtained at concentrations of up to at least 1.5×10^{-5} M (figure 2.4a). Association constants of nitrogen donor ligands were then determined in the organic solvent system (log $K_{c,org}$), values summarised in table 2.1, where similar spectroscopic changes as described for the 40% (v/v) aqueous DMSO solvent system were observed. Observed association constants obtained in the organic solvent system (log $K_{c,org}$) were then compared to the corresponding ligand basicity and a LFER was obtained which is similar to that in aqueous DMSO (see figure 2.4b). This result confirms that in the absence of proton competition, log K_c of ligands with Fe(III)PPIX is indeed directly proportional to the basicity of the donor ligand and demonstrates that the LFER observed in figure 2.3 is not an artefact of corrections made to log $K_{c,obs}$, by equation 1, to account for proton competition.

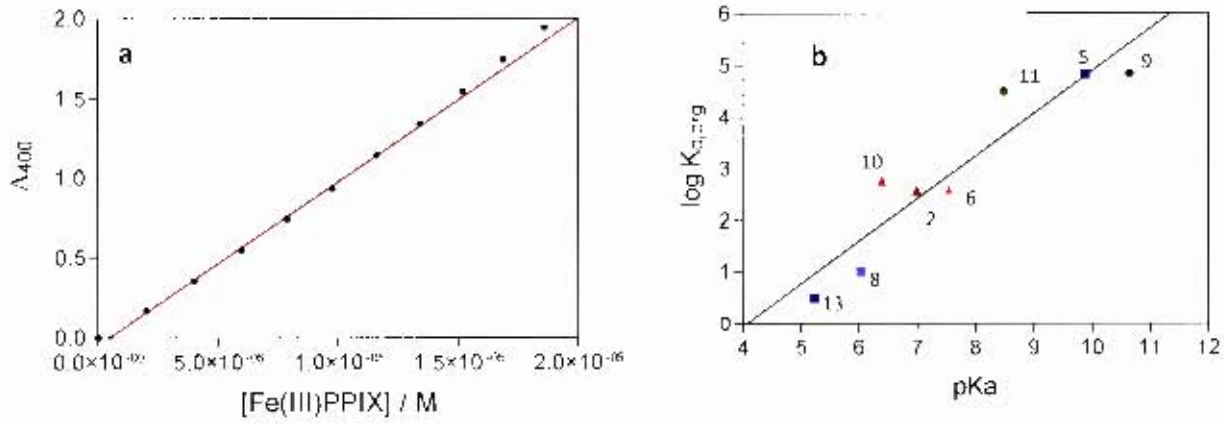

Figure 2.4. (a) Beer-Lambert law plot of Fe(III)PPIX in a 20% (v/v) DMSO in methanol solvent system. Extinction coefficient was found to be 102 400 $M^{-1} cm^{-1}$. (b) Linear free energy relationship between association constants obtained in 20% (v/v) DMSO in methanol (log $K_{c,org}$) and pK_a of N-donor ligands (see table 2.1 for compounds). This relationship is described by log $K_{c,org}$ = 0.8(1)×pK_a - 3(1) with r^2 = 0.87.

Table 2.1. Observed and pH independent association constants as well as pK_a values of nitrogen and oxygen donor ligands used in the determination of coordination association constants with Fe(III)PPIX.

No.	Compound	pK_a	log $K_{c,obs}$	log K_c	log $K_{c,org}$
1	1 naphthanol	9.34 [a]	2.12 ± 0.02	4.08	ND
2	2-phenylimidazole	6.39 [a]	2.41 ± 0.01	2.45	2.78 ± 0.02
3	3,5-dichlorophenol	8.19 [a]	2.63 ± 0.03	3.53	ND
4	3-methoxyphenol	9.65 [a]	1.63 ± 0.02	3.94	ND
5	4-dimethylaminopyridine	9.87 [a]	2.45 ± 0.01	4.99	4.83 ± 0.05
6	4(5)-methylimidazole	7.54 [a]	2.18 ± 0.10	2.59	2.61 ± 0.03
			3.16 ± 0.10	3.57	2.45 ± 0.03
7	4-methoxyphenol	10.21 [a]	1.39 ± 0.03	4.27	ND
8	4-methylpyridine	6.03 [a]	1.34 ± 0.08	1.36	1.01 ± 0.03
			1.25 ± 0.06	1.27	WB
9	butylamine	10.64 [a]	1.63 ± 0.01	4.94	4.84 ± 0.07
10	imidazole	6.99 [a]	2.17 ± 0.05	2.34	2.59 ± 0.01
			3.51 ± 0.06	3.68	2.56 ± 0.03
11	morpholine	8.49 [a]	2.59 ± 0.08	3.78	4.14 ± 0.06
12	phenol	9.98 [a]	1.42 ± 0.05	4.06	ND
13	pyridine	4.81 [a]	0.77 ± 0.05	0.78	0.51 ± 0.04
			0.82 ± 0.02	0.82	WB

[a] Reference 111
[a] Reference 112
ND Not Determined
WB Weak Binding, second association constant could not be determined

The observation of a LFER under aqueous conditions is similar to results obtained by Pratt and co-workers[85-88] with MP-8 and Marques *et al.*[89] with N-Ac-MP-8, except that those authors obtained four separate LFERs for amines, pyridines and imidazoles. As detailed in section 1.10.1 the formation of the four separate families was attributed to the π-backbonding effect caused by the coordinated histidine ligand and hydrogen bonding ability of the ligands. It is likely that the absence of this histidine ligand in free Fe(III)PPIX, which is five coordinate, leads to the single linear relationship seen here, obtained since no analogous effect on π-backbonding is possible.

This explanation is further justified by the association constants obtained in this study for imidazole and 4(5)-methylimidazole where the formation of the six coordinate species of Fe(III)PPIX was found to be more favourable than formation of the five coordinate species, as indicated by the significantly larger second association constant obtained with these ligands. By contrast, with pyridine, the second association constant is only a little larger than the first. Interestingly, this π-backbonding effect appears lessened in the organic solvent system as the second association constant obtained for imidazole derivatives (compounds **6** and **10**) in 20% (v/v) DMSO in methanol is similar in magnitude to the first. This effect is also observed for the pyridine derivatives (compounds **8** and **13**) where a second association constant could not be determined, presumably since it is much weaker than the first. A similar effect of decreased second association constant was observed by Marques *et al.*[110] with pyridine and imidazole in coordination investigations with haematohaemin in a methanol solvent system.

As an aside, the association constant of 1-acetylimidazole with MP-8 and N-AcMP-8 was found by both Pratt and Marques *et al.*[85-89] to have a greater than expected value based on the compound's pK_a. However, in our hands, it was found through proton NMR that in an aqueous environment the acetyl group undergoes rapid hydrolysis to give imidazole and acetic acid. This process accounts for the greater than expected association constant obtained for 1-acetylimidazole, which is, in fact, the same value as that obtained for imidazole.

While the findings obtained for coordination to Fe(III)PPIX are similar to the results of Pratt *et al.*[85, 88] and Marques *et al.*[89], the ability to quantify these interactions with Fe(III)PPIX is of significance as by combining the equations 1 and 5, equation 6 was derived which is able to predict the observed coordination constant (log $K_{c,\,calc}$) at any desired pH, provided the pK_a of the ligand donor atom is known.

$$\log K_{c,\,calc} = 0.71(6) \times pK_a - 2.6(5) - \log[1+10^{(pKa\,-\,pH)}] \qquad (6)$$

From equation 8, it possible to predict observed association constants for compounds with a range of pK_a values under the acidic conditions known to occur in the digestive vacuole of the malaria parasite. The measured vacuolar pH of 4.8 - 5.4 has been previously reported.[23, 24] Figure 2.5 shows the curve obtained when the predicted log $K_{c,\,calc}$ values (calculated from eq. 6 at pH 4.8) are plotted against pK_a. A compound with a pK_a value of 5.15 is identified as the optimum under these conditions. At this optimum a very low association constant is expected, less than 0.6 log units, indicating that coordination under these conditions is weak and would probably be out-competed by other interactions such as π-stacking in the aqueous medium.

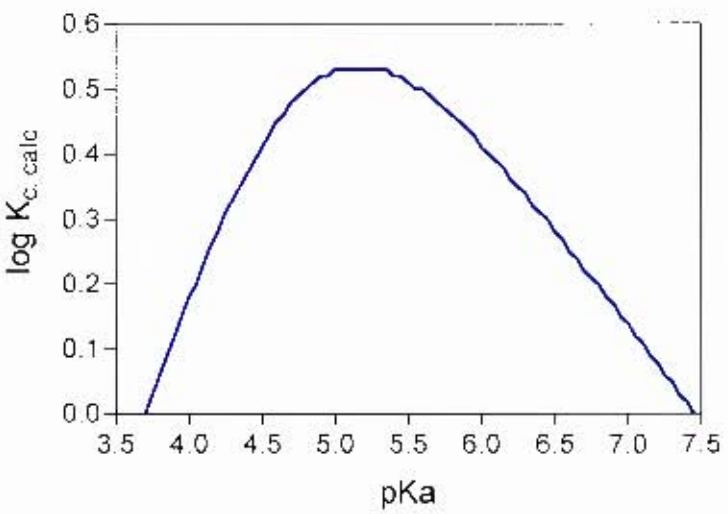

Figure 2.5. Curve of predicted coordination association constants (log $K_{c,\,calc}$, obtained using equation 6) verses pK_a under acidic (pH 4.8) aqueous conditions similar to the digestive vacuole of the malaria parasite. Strongest coordination interactions are produced by a pK_a value of 5.15 but they are still rather weak (< 0.6 log units).

2.3 π-Stacking interactions

Quantitative studies of π-stacking interactions in aqueous solution with porphyrins are few, with Schneider *et al.*[94, 95] providing one of the few detailed investigations. In the present study, spectrophotometric titrations were employed to determine the association constants arising from π-stacking interactions between simple aromatic compounds and the porphyrin ring system. Because of the hydrophobic nature of many aromatic compounds, substituents such as carboxylic acids and alcohols are required to aid solubility under aqueous experimental conditions. Unfortunately, because of these moieties, π-stacking investigations with Fe(III)PPIX proved more challenging than the coordination investigations because of the possibility of coordination to the iron centre by the various solubilising aromatic substituents. Thus in order to obtain association constants resulting only from π-stacking interactions, iron free PPIX was used as a model system for Fe(III)PPIX. Beers law studies under the same aqueous DMSO conditions as used in coordination investigations indicated that the monomeric PPIX species exists below concentrations of approximately 5×10^{-6} M, with deviation from linearity at higher concentrations indicative of aggregation (see figure 2.6).

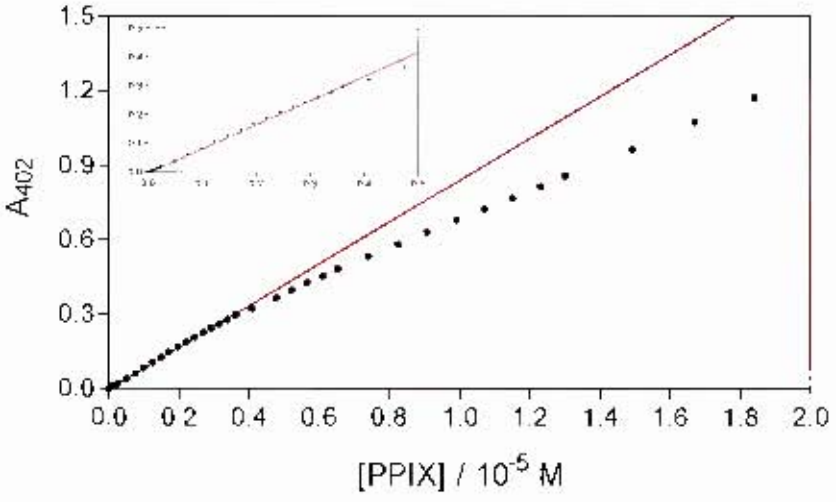

Figure 2.6. Beers law plot for PPIX in 40% (v/v) aqueous DMSO at pH 7.4. Extinction coefficient was found to be 84 290 $M^{-1}cm^{-1}$. **Inset.** Expanded region where concentrations of PPIX lead to a monomeric species.

Association constants arising from π-stacking interactions (log K_s) with PPIX were determined for a range of aromatic compounds (typical spectra obtained shown in figure 2.7) with ring size limited to 14 or fewer π-electrons because of interference in the visual absorption region by the larger ring systems which are chromophores. Fortunately, association constants with Fe(III)PPIX for a few of the compounds (**1**, **14**, **16**, **20** and **21**, see table 2.2) could be measured because steric hindrance prevents coordination from occurring. All compounds tested obeyed a 1:1 association model, summarised in table 2.2, and an average decrease in π-stacking with Fe(III)PPIX of 0.57 log units, relative to PPIX, was found.

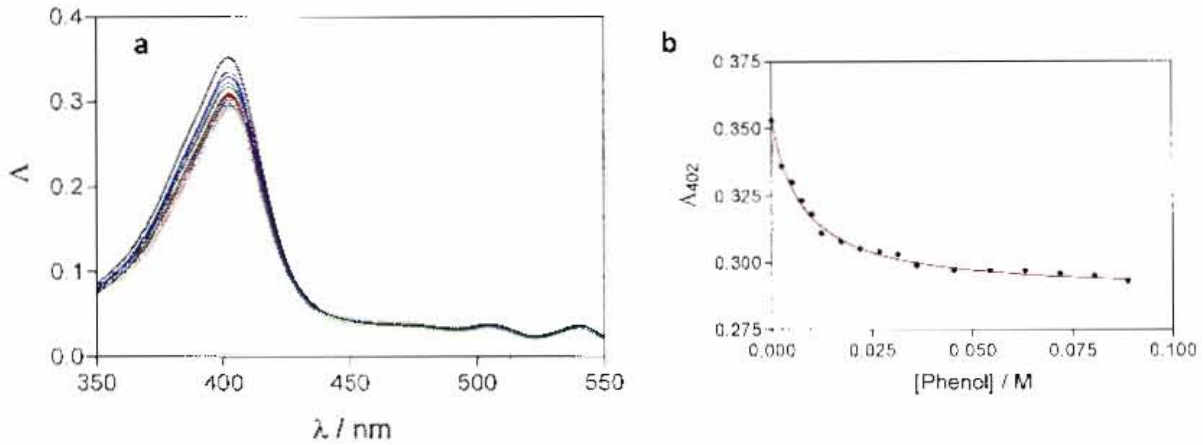

Figure 2.7. (a) Typical spectroscopic changes (dilution corrected) obtained with ligands forming a 1:1 complex with PPIX. (**b**) Non-linear least squares fit (red line) of the data obtained from (a) (black circles), fitted to a 1:1 association model using equation 2.

Plotting log K_s with PPIX against the number of π-electrons of the corresponding aromatic compounds produced a LFER, shown in figure 2.8. This suggests that an increase in the number of π-electrons in the ring system results in an increase in π-stacking association with PPIX. Data scatter above and below the best fit line are attributed to substituent effects of the aromatic ring systems which could have a positive or negative effect on π-stacking interactions. Unfortunately, attempts at unravelling substituent effects from the small data set obtained failed and further experimentation is required to understand and quantify their effect on π-stacking with PPIX.

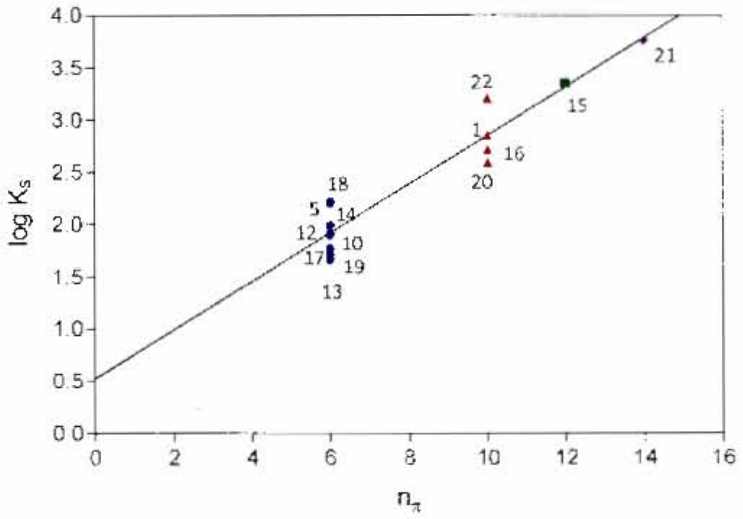

Figure 2.8. Linear free energy relationship between π-stacking association (log K_s) and the corresponding number of π-electrons (n_π) of the aromatic compound. This relationship is described by log K_s = 0.23(2)×n_π + 0.55(18) with r^2 = 0.91.

Table 2.2. Association constants determined for π-stacking interactions with PPIX and Fe(III)PPIX.

No.	Compound	π-electrons	log K_s PPIX	log K_s Fe(III)PPIX
1	1-naphthanol	10	2.86 ± 0.03	2.12 ± 0.04
5	4-dimethylamino pyridine	6	2.21 ± 0.02	CP
10	imidazole	6	1.91 ± 0.04	CP
12	phenol	6	1.99 ± 0.14	CP
13	pyridine	6	1.66 ± 0.14	CP
14	2,6-lutidine	6	2.17 ± 0.09	1.71 ± 0.07
15	9-aminofluorene	12	3.36 ± 0.04	CP
16	benzimidazole	10	2.72 ± 0.04	2.30 ± 0.02
17	benzoic acid	6	1.90 ± 0.10	CP
18	benzyl alcohol	6	2.22 ± 0.08	CP
19	benzyl amine	6	1.77 ± 0.03	CP
20	quinoline	10	2.60 ± 0.07	1.97 ± 0.02
21	5-methyl-1,10-phenanthroline	14	3.76 ± 0.05	3.15 ± 0.05
22	4-quinoline methanol	10	3.22 ± 0.08	CP

CP Coordination Possible.

The findings obtained for π-stacking interactions with Fe(III)PPIX and PPIX are in agreement with the trends obtained by Schneider *et al.*[94, 95] for other water soluble porphyrins. The observed decrease in π-stacking association with Fe(III)PPIX as compared to PPIX is not unexpected for a metalloporphyrin, since Schneider and Wang[94] observed a similar effect with zinc porphyrins. This decrease was attributed to distortions in the porphyrin ring system as a result of the presence of a metal centre. However, there exists a possible additional explanation for this observed decrease that is based purely on the availability of association sites. PPIX has two possible faces with which aromatic π-stacking interactions can occur. Owing to the coordinated axial water ligand, a 5-coordinate species of Fe(III)PPIX is produced[75] which thus has only one sterically unhindered face that allows interactions with π-stacking molecules. This statistical decrease in association sites would account for log 2 (0.30 log units) of the observed deficit. The remaining 0.27 log unit decrease can be attributed to the doming of the metalloporphyrin ring system.

Once again, while this observed trend was not entirely unexpected based on literature precedent, the quantification of this interaction with PPIX is important. By incorporating the observed decrease in π-stacking strength with Fe(III)PPIX into the equation describing π-stacking with PPIX, equation 7 was derived which is able to predict the π-stacking association constants (log K_s) of simple aromatic compounds with Fe(III)PPIX, where n_π is the number of π-electrons in the aromatic ring system.

$$\log K_s = 0.23(2) \times n_\pi - 0.0(2) \qquad (7)$$

2.4 Coordination and π-stacking combined

With LFER equations that describe coordination (eq. 6) and π-stacking (eq. 7) of compounds with Fe(III)PPIX, it remained to be seen whether compounds that can both coordinate and π-stack simultaneously would simply exhibit an additive effect of log K_c and log K_s on the overall log K. Association constants of compounds that could partake in both interactions with Fe(III)PPIX were determined and compared with the individual contributions of coordination and π-stacking calculated from equations 6 and 7.

It was found that compounds containing a benzylic alcohol donor ligand have similar observed association constants to the combined association constants predicted by equations 6 and 7, and so by combining equations 6 and 7, a general equation, 8, was obtained which is able to predict the association constants of any such compound with Fe(III)PPIX.

$$\log K_{calc} = \alpha \times \{0.71(6) \times pK_a - \log[1 + 10^{(pKa - pH)}] - 2.6(5)\} + \beta \times \{0.23(2) \times n_\pi - 0.0(2)\} \quad (8)$$

$$\alpha = 1 \text{ or } 0 \text{ and } \beta = 1 \text{ or } 0$$

Where $\alpha = 1$ if the ligand coordinates or 0 if it does not and $\beta = 1$ if the ligand π-stacks and 0 if does not.

In order to ascertain the accuracy of equation 8, the observed association constants for all compounds tested with Fe(III)PPIX ($\log K_{obs}$) were compared to the predicted association constants calculated from equation 8 ($\log K_{calc}$). The results obtained, tabulated in table 2.3 and shown in figure 2.9, indicate that accuracy of equation 8 is reasonably good given the limitations of this approach, producing an average error between predicted and actual association constant of ± 0.27 log units.

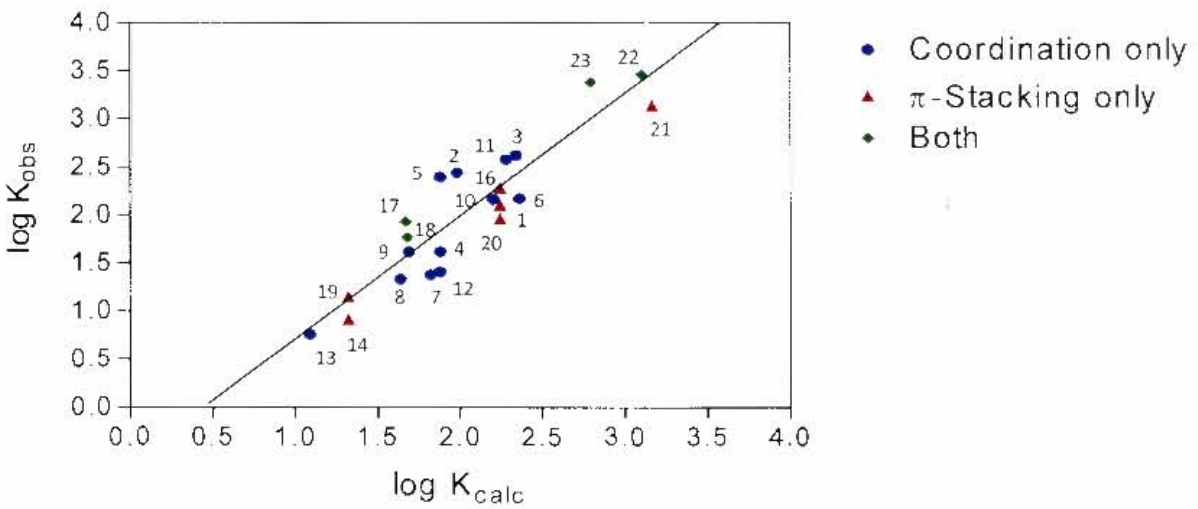

Figure 2.9. Comparison between observed association constants with Fe(III)PPIX obtained through experiment ($\log K_{obs}$) and from prediction using equation 8 ($\log K_{calc}$). Average error between values is ± 0.27 log units, $r^2 = 0.87$.

Table 2.3. Observed and predicted association constants of all compounds tested.

No	Compound	pK_a	log K_{obs}	log K_{calc}	Interaction
1	1-naphthanol	9.34 [a]	2.12 ± 0.02	2.24	π-stacking
2	2-phenylimidazole	6.39 [a]	2.41 ± 0.01	1.88	Coordination
3	3,5-dichlorophenol	8.19 [a]	2.63 ± 0.03	2.34	Coordination
4	3-methoxyphenol	9.65 [a]	1.63 ± 0.02	1.88	Coordination
5	4-dimethylaminopyridine	9.55 [b]	2.45 ± 0.01	1.98	Coordination
6	4(5)-methylimidazole	7.54 [a]	2.18 ± 0.10	2.36	Coordination
7	4-methoxyphenol	10.21 [a]	1.39 ± 0.03	1.82	Coordination
8	4-methylpyridine	6.03 [a]	1.34 ± 0.08	1.64	Coordination
9	butylamine	10.64 [a]	1.63 ± 0.01	1.69	Coordination
10	imidazole	6.99 [a]	2.17 ± 0.05	2.20	Coordination
11	morpholine	8.49 [a]	2.59 ± 0.08	2.28	Coordination
12	phenol	9.98 [a]	1.42 ± 0.05	1.88	Coordination
13	pyridine	5.23 [a]	0.77 ± 0.05	1.09	Coordination
14	2,6-lutidine	6.72 [a]	0.93 ± 0.02	1.32	π-stacking
15	9-aminofluorene	8.22 [c]	2.38 ± 0.02	2.28 or 2.70	Inconclusive [d]
16	benzimidazole	5.46 [a]	2.30 ± 0.01	2.24	π-stacking
17	benzoic acid	4.20 [a]	1.78 ± 0.03	1.68	Both
18	benzyl alcohol	15.05 [e]	1.94 ± 0.09	1.67	Both
19	benzyl amine	9.55 [a]	1.17 ± 0.01	1.32	π-stacking
20	quinoline	4.81 [a]	1.97 ± 0.01	2.24	π-stacking
21	5-methyl-1,10-phenanthroline	5.17 [a]	3.15 ± 0.03	3.16	π-stacking
22	4-quinoline methanol	13.38 [c]	3.47 ± 0.10	3.10	Both
23	1-naphthlene methanol	14.39 [c]	3.39 ± 0.05	2.79	Both

[a] Reference 111
[b] Reference 112
[c] Experimentally determined (see chapter 7)
[d] Predicted coordination (2.28) and π-stacking (2.70) values are too similar to provide an exclusive interaction. This compound has thus been ommited from correlation (figure 2.9).
[e] Predicted using MOKA (reference 113)

The LFER equation (eq. 8) obtained from investigation of coordination and π-stacking interactions with Fe(III)PPIX was shown to be moderately accurate in calculating predicted association constants of small molecules with Fe(III)PPIX. However, the observed association constants of compounds containing amine donor ligands as well as an aromatic moiety (compound **19**) did not conform to the expected values for coordination and π-stacking, with only π-stacking interactions with Fe(III)PPIX observed. It was surmised that this is a result of a steric difference between the O-donor and N-donor ligands.

As illustrated in figure 2.10, in order for π-stacking interactions to occur once bound, the aromatic ring system of a compound must be parallel to the protoporphyrin ring system of Fe(III)PPIX. In the case of nitrogen donor ligands, this results in the formation of a sterically unfavourable semi-eclipsed conformation and is suspected to rearrange to form the more favourable anti-periplanar conformation which is thus unable to π-stack while coordinated. The observed coordination association constant obtained for these types of amine compounds was similar to the predicted contribution from π-stacking interactions, indicating that the coordinated conformation with the aromatic ring system in the anti-periplanar position is the less favourable interaction. A similar result was obtained from 9-aminofluorene, **15**, where the magnitude of the observed association constant implied that only one interaction was occurring. Unfortunately, it was unclear as to which interaction this was because the magnitudes of the predicted values for coordination and π-stacking contributions are similar. In the case of oxygen donor ligands, conformational changes do not occur owing to greater steric freedom of this class of compound.

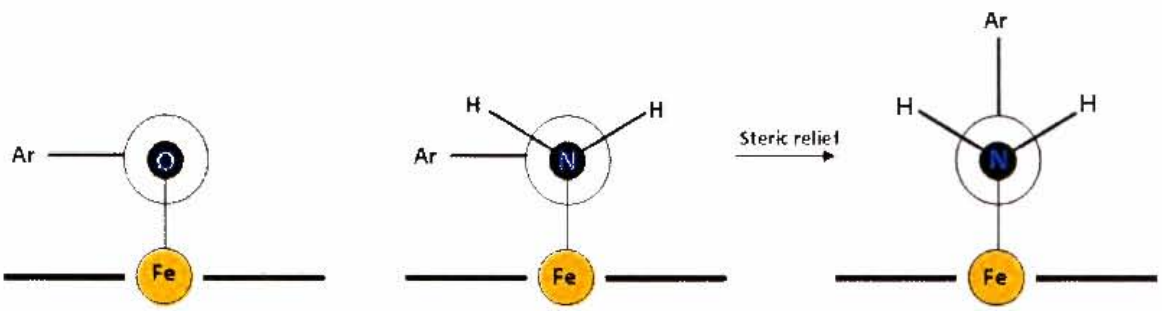

Figure 2.10. Newman projections along the C – O and C – N bonds of compounds that contain a coordinating (O and N) group, bound to Fe(III)PPIX, as well as an aromatic π-stacking (Ar) group. Unfavourable steric conformations of the bound nitrogen donor ligands could result in the formation of an anti-periplanar geometry, thus preventing π-stacking and coordination interactions from simultaneously occurring.

Finally, association constants of 4-aminoquinoline compounds with Fe(III)PPIX also cannot be accurately predicted based on the assumption that the only interaction occurring is that of π-stacking. Predicted log K_{obs} values for π-stacking with Fe(III)PPIX are in the region of 2.30 log units lower than the experimental association constants, indicating that there must be additional interactions with Fe(III)PPIX occurring. Possible interactions that have not been taken into account could be favourable charge-charge interactions between the protonated quinoline nitrogen and deprotonated propionate side chains of Fe(III)PPIX. Schneider and Wang [94] have found that such electrostatic interactions have a contribution of about 0.9 log units for singly charged molecules. Further investigation is required in order to better understand and quantify the effects of these additional interactions.

2.5 Conclusions

The coordination of pyridines, imidazoles, quinolines and phenolates with Fe(III)PPIX was found to be directly proportional to the basicity of the donor ligand. The single LFER relationship obtained between pK_a and coordinating ability allows for prediction of other compounds provided the pK_a is known. π-Stacking interactions of aromatic compounds containing 6, 10, 12 and 14 π-electron ring systems with PPIX and Fe(III)PPIX were found to increase with an increase in the number of π-electrons. Substituents seemingly made small contributions to π-stacking interactions but substituent constants could not be extracted. A decrease in π-stacking ability with Fe(III)PPIX relative to PPIX was also observed. A LFER equation describing π-stacking interactions with Fe(III)PPIX was derived which enabled prediction of this interaction for other aromatic compounds. Predicted coordination and π-stacking association constants of compounds containing moieties that could accommodate both these interactions were found to be additive and these findings led to the derivation of a LFER equation that can predict the associating ability of almost any small molecule with Fe(III)PPIX. Care needs be taken with regard to steric conformations as compounds such as benzylamine, **19**, were found to be unable to both coordinate and π-stack. In addition, there are other interactions with Fe(III)PPIX that seemingly play an important role as the 4-aminoquinoline class of compounds have a markedly stronger observed interaction than predicted. Unfortunately, these interactions are as yet not well understood and require further investigation.

CHAPTER 3.

DESIGN OF NOVEL POTENTIAL β-HAEMATIN INHIBITORS

3.1 Introduction

With the development of equation 8 (see section 2.5), moderately accurate estimates of association constants of simple molecules with Fe(III)PPIX are possible. This provided a platform for the identification of potential scaffold molecules that have a strong association with Fe(III)PPIX which could be further developed into potential β-haematin formation inhibitors through the incorporation of a hydrogen bonding moiety. Utilising molecular modeling techniques, identification of favourable hydrogen bonded conformations with Fe(III)PPIX would allow for further refinement and potentially provide compounds with a higher probability of inhibiting β-haematin formation.

3.1 Identification of a scaffold molecule

In order to identify potential template compounds, a threshold association value needed to be established such that only compounds with an association constant value equal to or greater than the threshold would be considered. This threshold value would have to be the association constant obtained with Fe(III)PPIX for the parent structure of a known β-haematin inhibitor which was thought to follow the proposed mechanism of action through coordination, π-stacking and hydrogen bonding. As previously reported,[76] antimalarials and β-haematin inhibitors, quinine and quinidine (figure 3.1a), are thought to follow the hypothesised mechanism of action and thus the parent structure 4-quinoline methanol, **22**, (see figure 3.1b) was selected to provide the threshold association value.

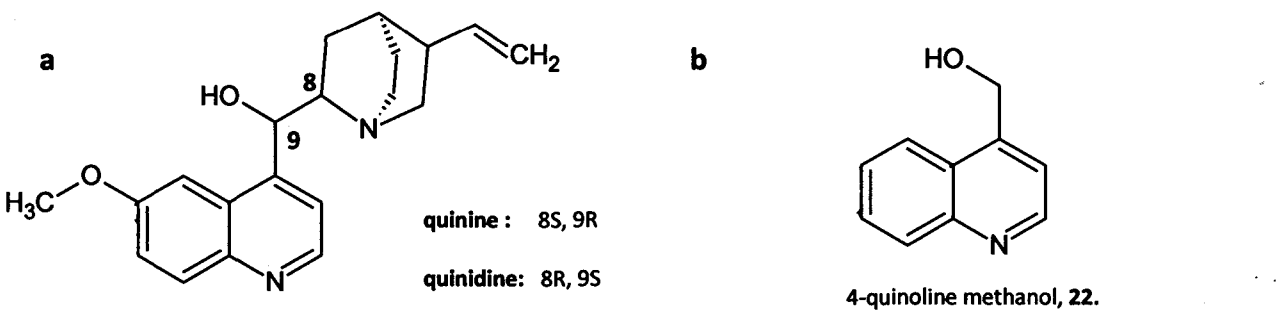

Figure 3.1. (a) Active β-haematin inhibitors quinine and quinidine, contain coordination (hydroxyl), π-stacking (quinoline ring) and hydrogen bonding (tertiary amine) moieties that support the hypothesised mechanism of action. (**b**) Parent structure of quinine and quinidine, 4-quinoline methanol, was chosen to provide the threshold association value.

Unfortunately, compound **22** is not available commercially but it was obtainable by synthetic means through a simple, one step reduction reaction of the commercially available starting material, 4-quinoline carboxaldehyde, **24**. Reaction conditions are detailed in scheme 3.1.

Scheme 3.1

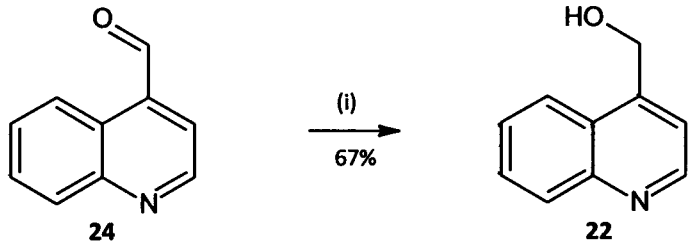

24 **22**

(i) $NaBH_4$, EtOH, RT, 1.5 h.

The reaction proceeded, using the procedure reported by Hörtner *et al.*[114], under mild conditions to give the required product, **22**, in a moderate yield (67%) which was characterised using infrared (IR), NMR and mass spectrometry (see chapter 7 for synthetic details). The association constant with Fe(III)PPIX was determined as described in chapter 2 and the measured value found to be 3.47 ± 0.10 log units, which was set as the threshold association value. This observed value was slightly higher than the predicted value of 3.10 ± 0.25 but is not statistically different.

Various simple compounds were then screened as potential scaffold molecules using the following criteria. Suitable compounds preferably should: (1) contain a benzyl alcohol moiety; (2) contain at least a 10 π-electron aromatic ring system; (3) have a rigid structure to ensure preorganisation; (4) have a predicted association constant greater than or equal to 3.47 log units; (5) be commercially available for measurement of association constant; (6) produce no isomers upon modification; (7) have a commercially available precursor which is inexpensive and (8) be a novel antimalarial scaffold.

The most suitable molecule identified as a potential scaffold was 9-hydroxyfluorene which met all the imposed criteria. This commercially available molecule contains a benzyl alcohol moiety and a 12 π-electron aromatic ring system which have a connectivity that produces a rigid structure. In fact, molecular modelling indicated that the rigid structure provided optimal π-stacking interactions once coordinated to the iron centre of Fe(III)PPIX, as illustrated in figure 3.2, and thus provide a preorganisational feature that may increase association interactions. In addition, owing to the molecular symmetry of this compound, substitution at the 9 position of the ring system would give rise to favourable achrial products that could be synthesised from the inexpensive synthetic precursor, 9-fluorenone.

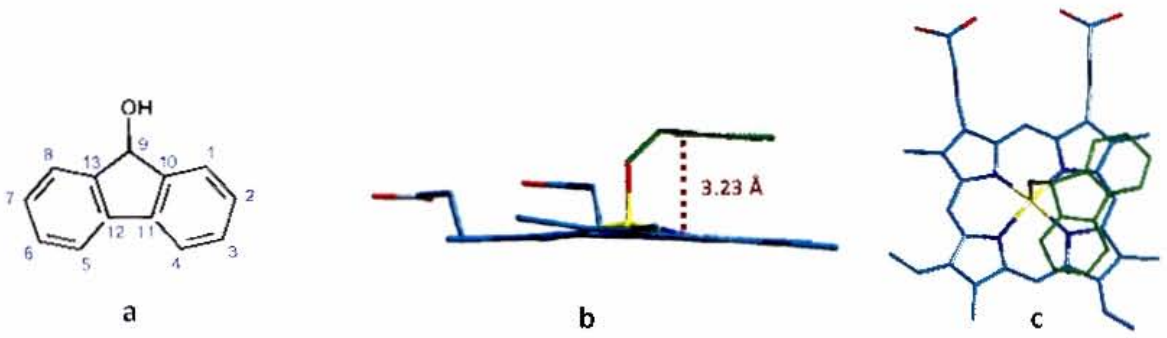

Figure 3.2. Molecular structure of template compound 9-hydroxyfluorene (**a**) and lowest energy conformations of template compound (green) bound to Fe(III)PPIX (**b** and **c**). Conformations indicate favourable π-stacking interactions are possible between fluorene and PPIX ring systems with a measured interplanar distance of 3.23 Å. For clarity, hydrogens have not been shown.

The predicted association constant of 9-hydroxyfluorene was calculated as 3.33 ± 0.27 using equation 8. While this is slightly smaller than the threshold value, it was still considered owing to the larger error in the predicted pK_a value for the hydroxyl moiety (14.33 ± 0.52, predicted using MOKA software[113]) which held the possibility for a slightly stronger association constant that would be closer to the threshold value. Since 9-hydroxyfluorene is commercially available, the observed association constant was able to be determined and found to be 3.64 ± 0.09 log units, which is greater than the threshold value.

It is because of these important properties of 9-hydroxyfluroene as well as the fact that this compound is not a known antimalarial class that 9-hydroxyfluorene was selected as the as the scaffold molecule for this study.

3.3 Incorporation of a hydrogen bond donor moiety

With the template molecule chosen to act as the anchor moiety of the proposed inhibitor, hydrogen bonding groups were incorporated into the structure. As detailed in section 1.10.3, there are a variety of hydrogen bonding groups that provide favourable interactions with carboxylic acids and carboxylate anions, with guanidine moieties being one of the strongest owing to the ability to form bidentate hydrogen bonds and the stabilising presence of a salt bridge. It was for these reasons that the guanidine moiety was selected as the hydrogen bonding feature. In order to provide a comparison with the stronger guanidine group, a primary amine moiety was also included as a hydrogen bond donor.

The incorporation of this amine group required no additional synthesis, as formation of the guanidine moiety required a primary amine as an intermediate compound (see chapter 5 for further details on synthesis). In addition a 1,3,5-azaadamantane moiety was also proposed as a possible hydrogen bond donor because the cage-like structure provided a preorganisation feature, similar to that of quinine and quinidine antimalarials, which was thought to possibly play a significant role in the proposed mechanism of action.

Attachment of the hydrogen bonding moieties to the anchor template molecule, 9-hydroxyfluorene, required a carbon spacer and molecular modelling identified favourable hydrogen bonding interactions of the guanidine moiety and azaadamantane moiety were when the alkyl linker was one or two carbons in length. Thus, compounds **A** to **E** were proposed for investigation (see figure 3.3).

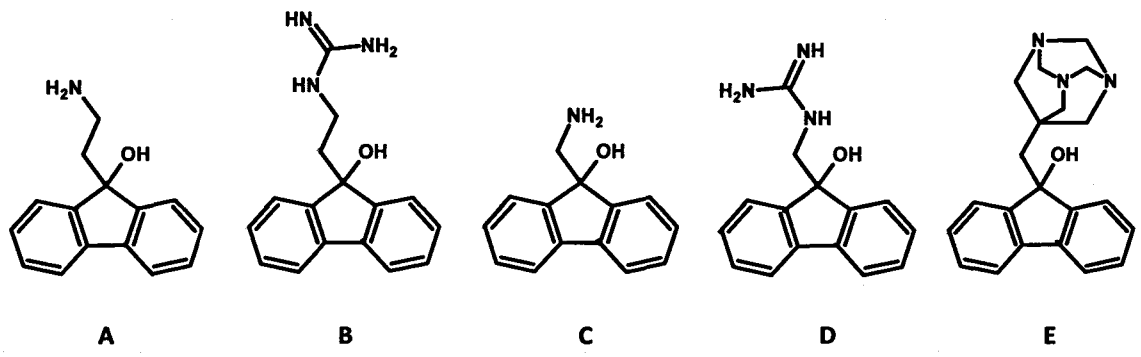

A **B** **C** **D** **E**

Figure 3.3. Proposed β-haematin inhibitors, **A** to **E**.

3.4 Molecular modelling of proposed inhibitor/Fe(III)PPIX complexes

Molecular mechanics and dynamics (with simulated annealing) modelling of the proposed compounds bound to the iron centre of Fe(III)PPIX provided an additional method with which to determine the feasibility of these compounds as potential β-haematin inhibitors. While this technique is not able to directly compare energies between complexes, the modelling provides an insight into the conformations of the bound compounds and allows for the identification of favourable and unfavourable conformations of the complexes. Should these lowest energy conformations have the possibility of an intramolecular hydrogen bond interaction with the propionate side chain, the energy of the hydrogen bonded conformation could then be compared to the lowest energy conformation and insight into whether the possibility exists for a favourable hydrogen bonded interaction could be obtained.

Unfortunately, this technique cannot provide conclusive results because the modelling was performed in vacuum and effects of hydration were not taken into account. This is a significant drawback as interactions between Fe(III)PPIX and proposed compounds are thought to occur, in part, in the aqueous digestive vacuole of the parasite. However, the results obtained from modelling are still of interest as these interactions are also believed to occur in lipid nanospheres within the digestive vacuole.[39] Because of the absence of water, this lipid environment is likely to resemble the vacuum model more closely and thus the results obtained may have some validity for this situation. In addition, the modelling does indicate the feasibility of proposed compounds forming the required interactions.

3.4.1 Compounds A to D.

Proposed compounds **A** to **D** were bonded to the iron centre of Fe(III)PPIX and lowest energy conformations for the complex were obtained. All compounds were observed to have favourable π-stacking interactions with the porphyrin ring system, and in particular, favoured the α carbons of the pyrrole rings of the porphyrin system. Conformations of all compounds are displayed in figure 3.4.

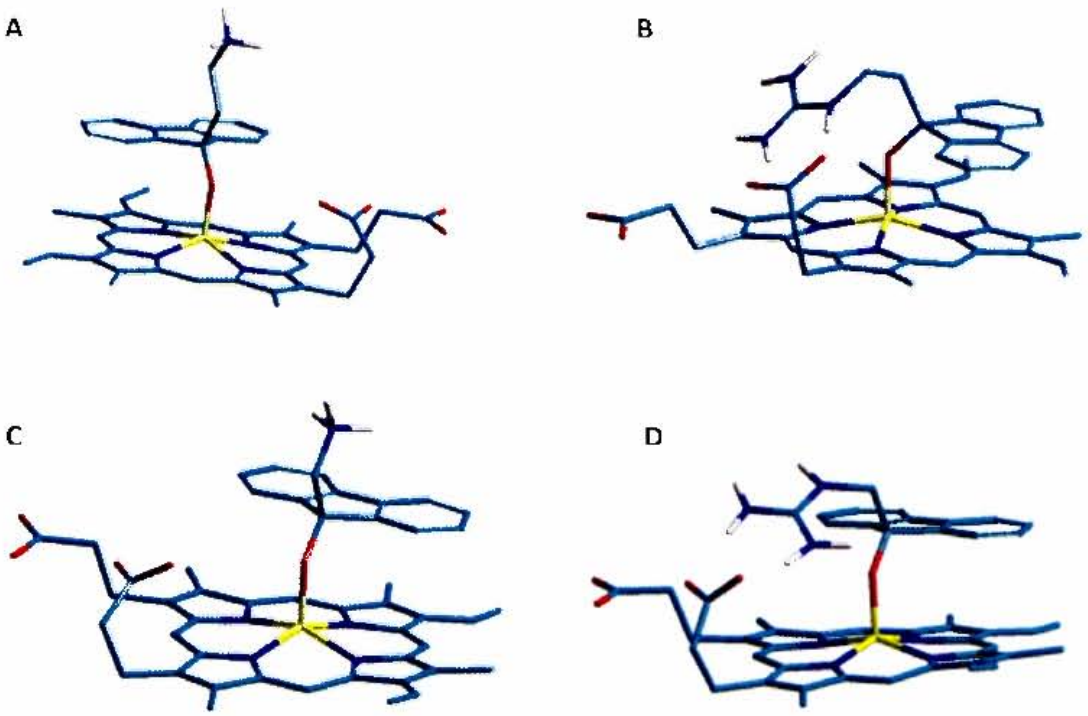

Figure 3.4. Molecular modelling of compounds **A** to **D** indicating the more favourable hydrogen bond conformations of the guanidine derivatives, **B** and **D**. For clarity, all hydrogens except those of the hydrogen bond donors have not been shown.

Guanidine derivatives, **B** and **D**, displayed conformations which provided for favourable hydrogen bonding interactions, with small energy differences of 3.75 and 3.90 kJ/mol, respectively, between the hydrogen bonded and lowest energy conformations. The low energy requirement for the formation of a hydrogen bonded conformation indicated that these compounds were good candidates for β-haematin inhibition. While the lowest energy conformation of the complex allowed for favourable hydrogen bonding interactions to occur, the flexibility of the alkyl linker provides for other conformations, similar in energy, which do not provide for hydrogen bonding interactions as easily and thus a lack of preorganisation was observed.

Amine precursor **A** was found to have a lowest energy conformation where the hydrogen bonding moiety directed away from the propionate side chain. Forcing a hydrogen bonded interaction resulted in a large increase in energy, 8.04 kJ/mol relative to the lowest energy conformations, and a significant distortion of the protoporphyrin ring was also observed. This suggested that compound **A** was not a good potential candidate for β-haematin inhibition, but would provide for an interesting comparison with compounds **B** and **D**.

The amine precursor **C** was found to adopt a similar conformation to that observed with compound **A** but the length of the hydrogen bonding linker did not allow for distances conducive for hydrogen bonding interactions. This compound was retained as a proposed negative control.

3.4.2 Compound E.

Molecular modelling of the azaadamantane derivative, compound **E**, was performed as for compounds **A** to **D**. In this case, the added rigidity of the structure allowed for the calculation of an energy map of the complex. Rotating torsion angles ϕ and ψ, see figure 3.5a, and recording the conformational strain energy of the complex after each rotation, favourable and unfavourable energy regions could be identified (see figure 3.5b). Comparing the torsion angles of the hydrogen bonded conformation to the energy map of the complex indicated that this compound was seemingly preorganised to partake in hydrogen bonding interactions with the propionate side chain once bound, as the torsion angles of the hydrogen bonded conformation were very close to the torsion angles of the lowest energy conformation of the complex. Thus the preorganisation of this compound was thought to provide an interesting comparison to the strength of the guanidine hydrogen bonding moiety.

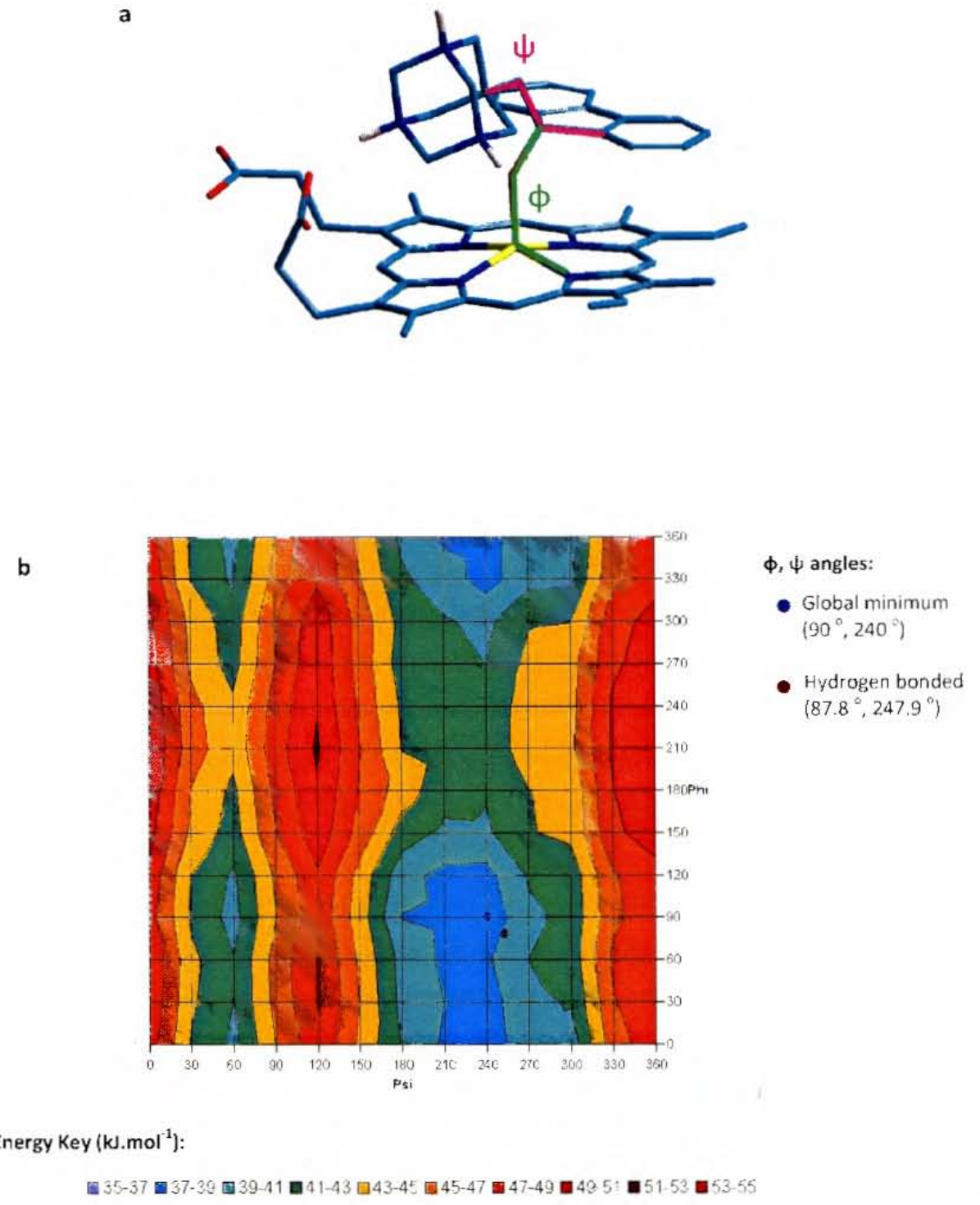

Figure 3.5. (a) Hydrogen bonded conformation of compound **E** bound to Fe(III)PPIX. Torsion angles ϕ and ψ used to calculate an energy map of the complex are shown in green and pink, respectively. All hydrogens apart from those of the hydrogen bonding groups have been removed for clarity. (**b**) Energy map of the compound **E** : Fe(III)PPIX complex, light blue areas indicate low energy conformations while red areas indicate high energy conformations. The diagram indicates that the torsion angles of the global energy minimum (dark blue circle) and of the hydrogen bonded conformation (dark red circle) are similar.

3.5 Conclusions

Using equation 8, derived in section 2.4, association constants for a range of molecules that could both coordinate and π-stack were predicted. The association constant of 4-quinoline methanol, the parent structure of the antimalarials quinine and quinidine, was chosen as a threshold value and the compound was synthesised. Predicted association constants, obtained from equation 8, that were greater than or equal to the threshold minimum (measured as 3.47 ± 0.10) were then only considered. The commercially available compound 9-hydroxyfluorene was chosen as the template molecule as the predicted association constant (3.33 ± 0.25) and experimental value (3.64 ± 0.09) obtained were similar to that of the threshold minimum.

The guanidine moiety was selected as the hydrogen bonding group and a one and two carbon linker was selected to attach it to the template molecule at the 9-position of the fluorene ring. Synthetic precursors to guanidines are amine moieties which were also considered as proposed compounds in order to compare the strength of hydrogen bond interaction. An additional azaadamantane moiety was also proposed as a potential target molecule because of the rigidity of this class of compound, which was thought to have a similar preorganisation feature as quinine and quinidine. In total, five compounds (**A** to **E**) were proposed.

Molecular mechanics and dynamics (with simulated annealing) modelling was performed on the proposed inhibitor/Fe(III)PPIX complexes in order to identify favourable conformations that may support hydrogen bonding interactions with the propionate side chain. It was found that the guanidine derivatives (**B** and **D**) could form favourable hydrogen bonded conformations in vacuum but because of the flexibility of the linkers, preorganisation was unlikely. Amine precursor **A** was found to have a conformation where the hydrogen bonding group was directed away from the propionate side chain and required a large increase in energy to form a hydrogen bonded conformation under vacuum conditions. Compound **C** was unable to form a hydrogen bond with the propionate because of the shorter linker length but was retained as a negative control.

Azaadamantane derivative **E** was found to have a lowest energy conformation that allowed for hydrogen bonding interactions. In addition, because of the rigidity of the complex, an energy map of the complex could be determined and it was found that this compound is preorganised to hydrogen bond as the hydrogen bonded conformation is very similar to the lowest energy conformation. Thus compound **E** was retained to compare this possible preorganisation feature with the strength of the hydrogen bond in the guanidine derivatives.

CHAPTER 4.

SYNTHESIS OF PROPOSED β-HAEMATIN INHIBITORS

4.1 Introduction

By investigating coordination and π-stacking interactions with Fe(III)PPIX (see chapter 2), five compounds (**A** to **E**) were proposed (see chapter 3) based on a 9-hydroxyfluorene scaffold. The details of their attempted synthesis and isolation are presented below.

4.2 Synthesis of 9-(2-aminoethyl)-fluoren-9-ol, A

The retrosynthetic pathway developed for the synthesis of compound **A** is shown in scheme 4.1.

Scheme 4.1:

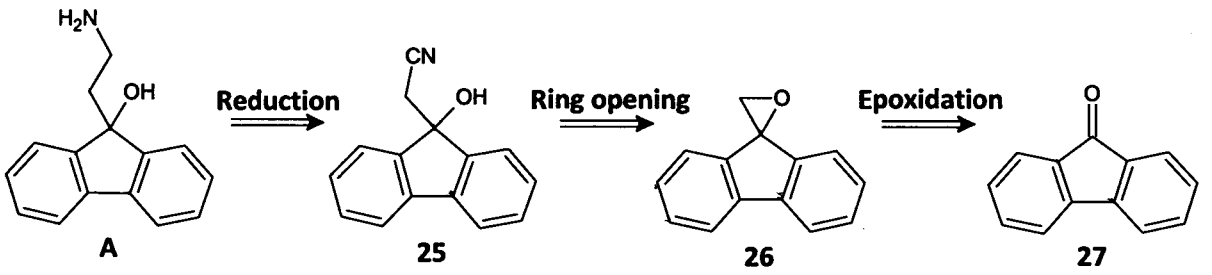

The synthesis of compound **A** was envisaged to be achieved through the reduction of the nitrile, **25**, which in turn could be obtained from the nucleophilic attack of cyanide at the least substituted carbon of epoxide **26** in a ring opening step. Because of steric hindrance, formation of the regioisomer of compound **25**, 9-(hydroxymethyl)-fluorene-9-carbonitrile, was deemed unlikely as this would require attack by the cyanide nucleophile at the more sterically unfavourable quaternary carbon of the epoxide. Finally, synthesis of epoxide **26** was envisaged to occur via the Corey epoxidation[115] of the commercially available 9-fluorenone, **27**.

Compound **A** was successfully synthesised from the starting material **27** based on the retrosynthetic scheme detailed above. Reaction conditions for the formation of compound **A** are summarised in scheme 4.2, while details of the synthesis of intermediates are described further on.

Scheme 4.2:

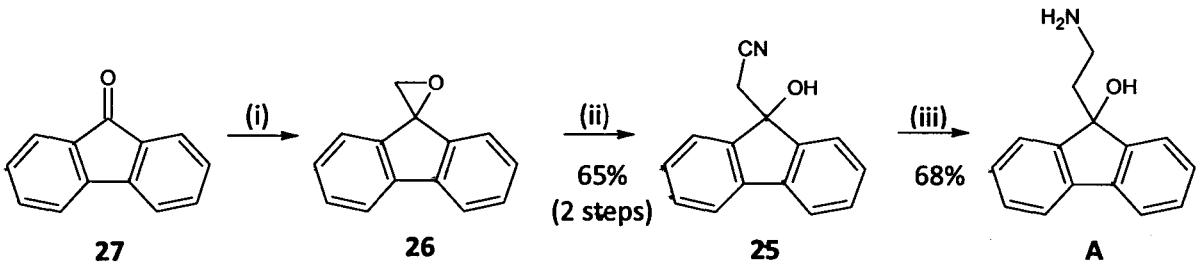

(i) *1.* NaH, TMSOI, DMSO, N_2 atm, 25 °C, 30 min. *2.* 9-Fluorenone, 25 °C, 1.5 h.
(ii) NaCN, NH_4Cl, MeOH/H_2O (8:1), 25 °C, 14 h. (iii) LAH, Et_2O, 0 °C to 25 °C, N_2 atm, 20 h.

4.2.1 Synthesis of Spiro[fluorene-9,2'-oxirane], 26.

A Corey epoxidation of 9-fluorenone, **27**, was required to form the target spiro epoxide, **26**. The reaction involves the conversion of trimethylsulfoxonium iodide (TMSOI) to the corresponding methylene intermediate **28**, through proton abstraction by sodium hydride on one of the TMSOI methyl groups. This intermediate is activated towards nucleophilic attack on the carbonyl group of compound **27** to form **26** with dimethylsulfoxide (DMSO) and sodium iodide produced as side products (see scheme 4.3 for proposed mechanism).

Scheme 4.3:

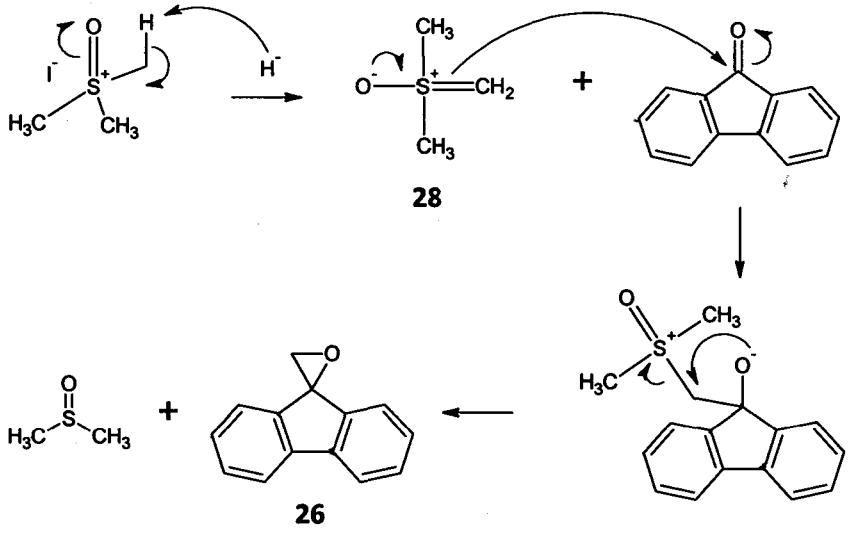

The reaction was carried out under mild conditions, following a procedure of a similar reaction[116], yielding a product identified by NMR spectrometry as compound **26**. Appearance of peaks in the ^{1}H spectrum at 3.71 ppm and ^{13}C spectrum at 54.9 ppm were the key identifiers of compound **26** as they were the peaks assigned to the methylene group (position 2' in figure 4.1) of the epoxide.

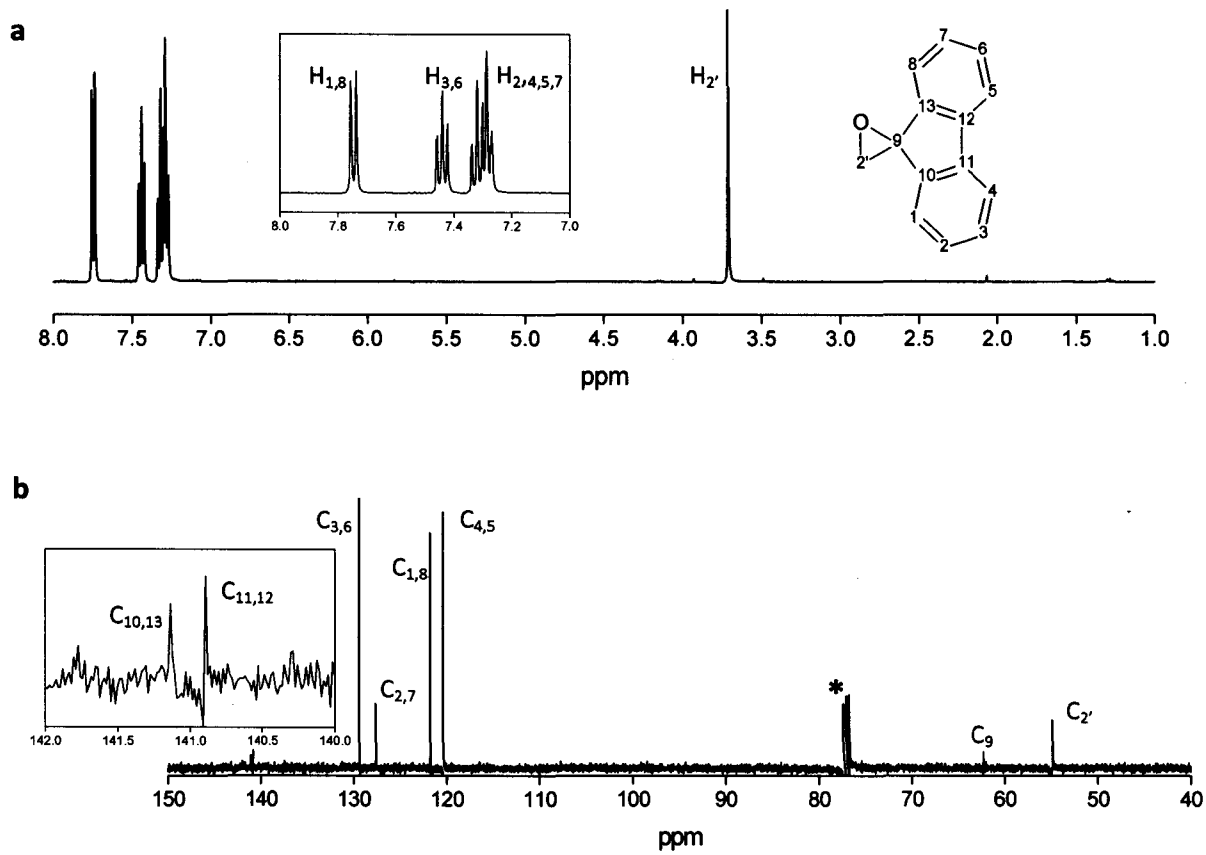

Figure 4.1. (**a**) ^{1}H NMR spectrum of compound **26** with characteristic methylene peak occurring at 3.71 ppm. **Inset.** Expanded aromatic region. (**b**) ^{13}C NMR spectrum of compound **26** showing the indicative methylene peak at 54.9 ppm. **Inset.** Expanded region showing quaternary carbons 10, 11, 12 and 13. Asterisk denotes $CDCl_3$ solvent peaks.

Yields obtained for the formation of compound **26** were satisfactory (63%) and the product obtained was deemed pure enough for use in subsequent steps. It should be noted that this compound was not stable over time and increasing the reaction temperature to 40 °C resulted in a large amount of by-product formation. Thus subsequent reactions with this compound had to be carried out at lower temperatures (25 °C or below) in order to limit by-product formation.

4.2.2 Synthesis of (9-hydroxy-fluoren-9-yl)acetonitrile, ***25****.*

The nitrile **25** was synthesised from a crude mixture of the spiro epoxide **26**, using the mild conditions reported by Chini *et al.*[117], to give the required product in moderate yields (65% over 2 steps), with the identity of the product confirmed using infrared (IR), NMR and mass spectrometry. The IR spectrum revealed a characteristic peak corresponding to the nitrile moiety at 2257 cm^{-1}, while shifts of the methylene peaks in both the ^{1}H and ^{13}C NMR spectrum as well as the appearance of the quaternary carbon (C_9 in figure 4.2) of the nitrile moiety indicated successful target product formation (see figure 4.2 for NMR shifts).

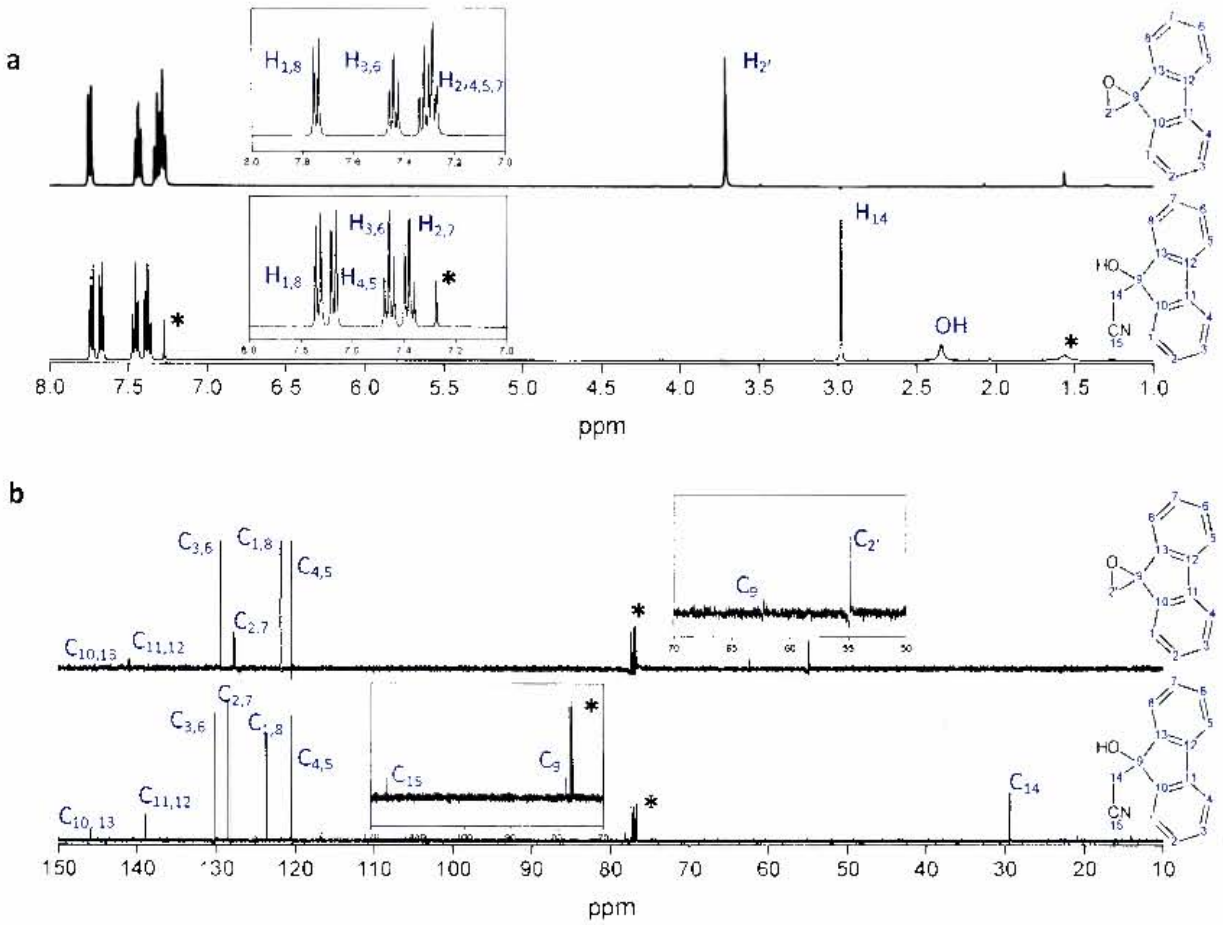

Figure 4.2: (**a**) ^{1}H NMR spectra of compound **26** (top) and compound **25** (bottom) comparing shifts in methylene and aromatic peaks. **Insets.** Expanded aromatic region. **Inset.** Expansion showing quaternary and methylene carbons 2' and 15. (**b**) ^{13}C NMR spectra of compound **26** (top) and compound **25** (bottom) showing shifts in methylene peaks. **Insets.** Expansion showing quaternary and methylene carbons 9 and 15. Asterisk denotes $CDCl_3$ and water solvent peaks.

4.2.3 Synthesis of 9-(2-aminoethyl)-fluoren-9-ol, A.

The synthesis of amine **A** required the reduction of the nitrile **25**, which was achieved using lithium aluminium hydride (LAH). The reaction proceeded as detailed earlier in scheme 4.2 and produced a large variety of unwanted by-products. The temperature was lowered and kept at 0 °C in an attempt to reduce the formation of these side products. However, lowering the temperature resulted in no reaction occurring. Increasing the temperature slowly from 0 °C, keeping it below 10 °C, did not lessen the extent of by-product formation and so the reaction was left overnight to stir at 25 °C. Nevertheless, even with the by-product formation, yields obtained were satisfactory (68%) and so no further attempt at decreasing the side product formation was attempted. Instead it was purified using column chromatography.

The product obtained was confirmed as compound **A** by comparing the ^{1}H and ^{13}C NMR spectra of the starting material and product, shown in figure 4.3. The disappearance in the proton spectrum of the singlet peak at 2.98 ppm (ascribed as H-14 of compound **A**) and appearance of two triplet peaks at 2.03 and 2.68 ppm (ascribed as H-14 and H-15 in compound **B**) were indicative of the formation of the two carbon chain. Both these methylene carbons were seen in the ^{13}C spectrum at 38.0 and 44.0 ppm. In addition, the IR spectrum showed the disappearance of the nitrile peak observed at 2257 cm^{-1} in the starting material and mass spectrometry confirmed the formation of compound **A**.

With the successful synthesis of **A**, synthesis of compound **B** could be attempted utilising compound **A** as the starting material.

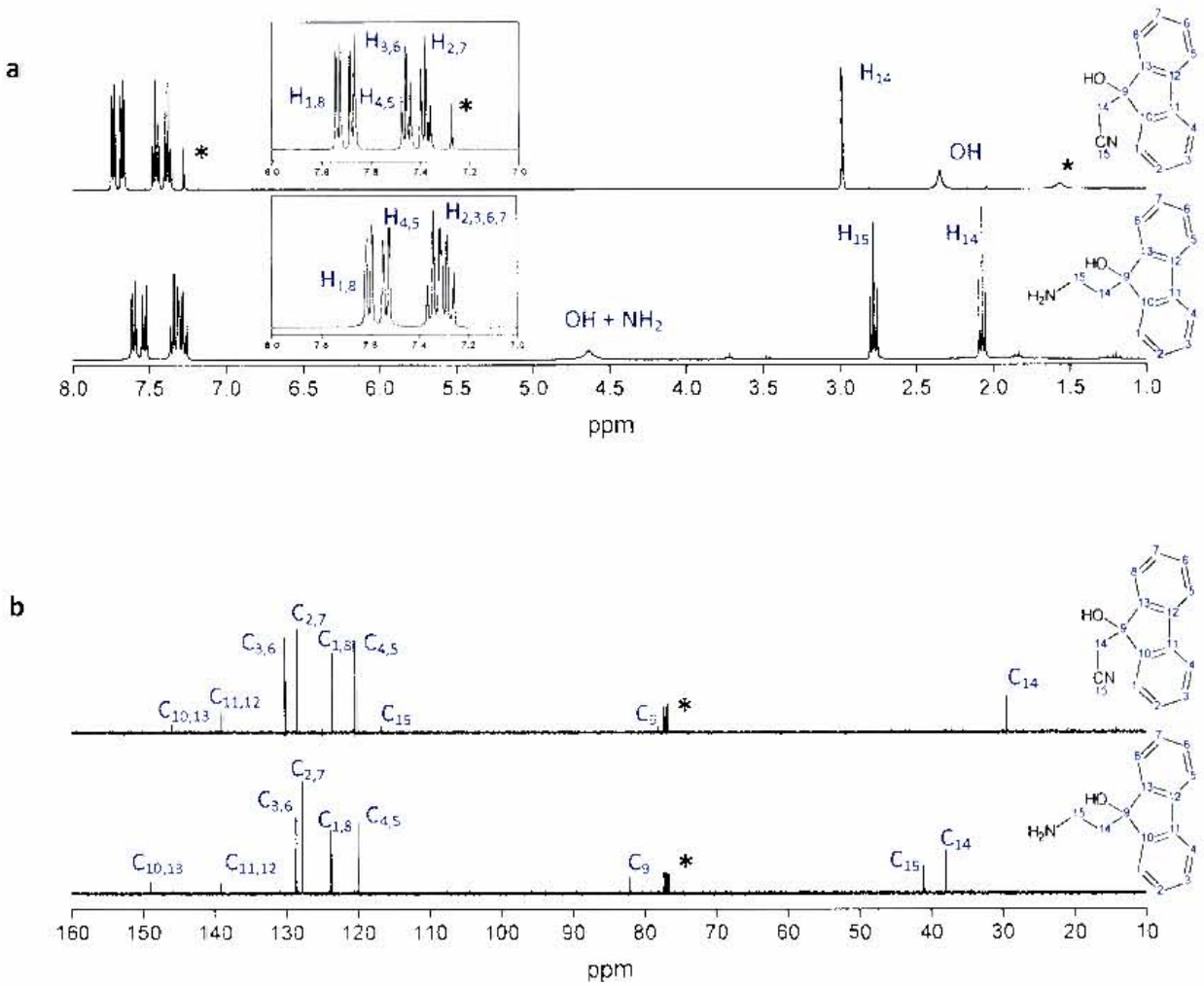

Figure 4.3: (a) ^{1}H NMR spectra of compound **25** (top) and compound **A** (bottom) comparing changes in methylene and shifts in aromatic peaks. **Insets.** Expanded aromatic region. (b) ^{13}C NMR spectra of compound **25** (top) and compound **A** (bottom) showing shifts and appearances of methylene peaks. Asterisk denotes $CDCl_3$ and water solvent peaks. Baseline impurities in compound **B** are ascribed to minor solvent contamination from the isolation process.

4.3 Synthesis of 1-[2-(9-hydroxy-fluoren-9-yl)ethyl]guanidine, B

The retrosynthetic pathway developed for the synthesis of the guanidine derivative, **B**, is shown in scheme 4.4.

Scheme 4.4

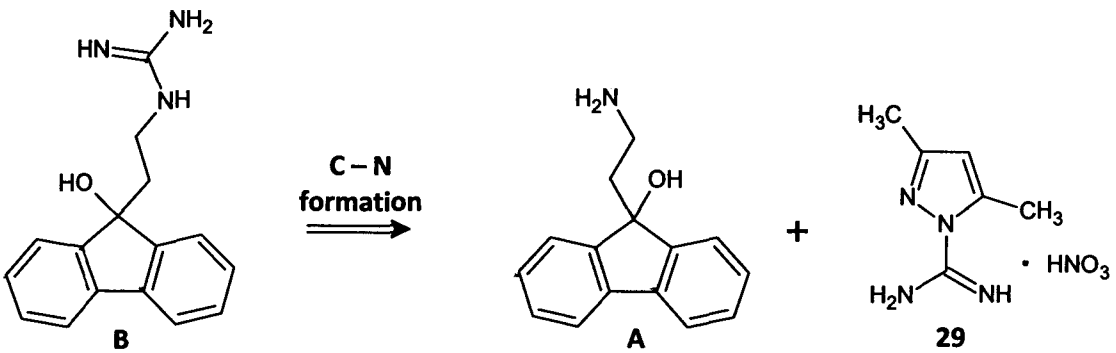

The envisaged synthesis of compound **B** required the guanylation of compound **A** utilising a suitable guanylating agent. The commonly used guanylating agent 3,5-dimethylpyrazole-1-carboxamidine nitrate (DPCN), **29**, was chosen which would undergo nucleophilic attack from the primary amine of compound **A** resulting in the formation of target product, compound **B**, and release 3,5-dimethylpyrazole as a by-product (see scheme 4.5 for proposed mechanism).

Scheme 4.5:

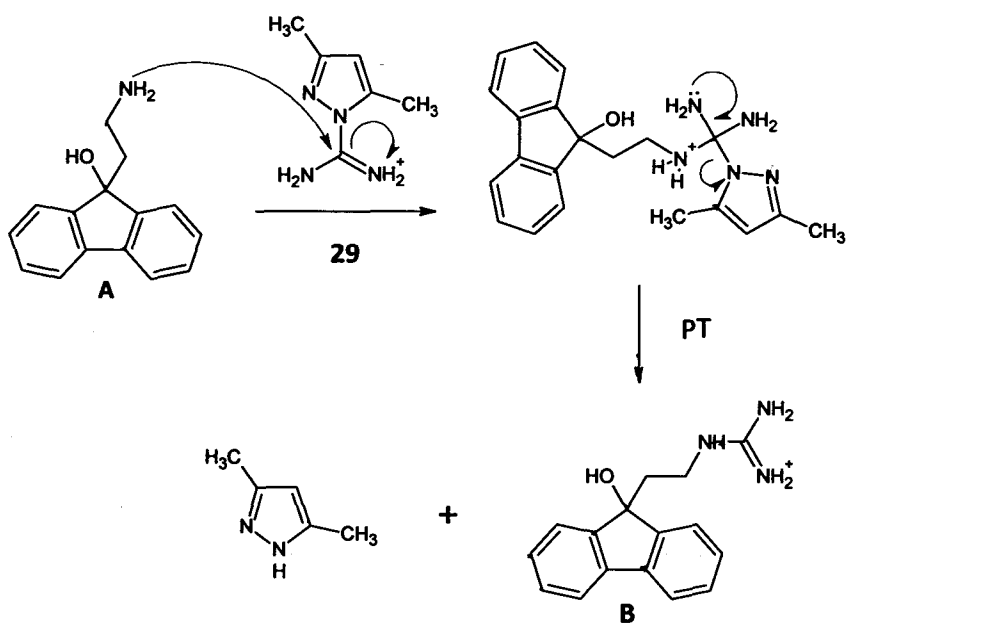

The synthesis of the guanidine derivative, **B**, was successfully performed, according to a general procedure reported by Yedavalli *et al.*[118], by reacting the guanylating agent DPCN and primary amine, **A**, under relatively mild conditions, detailed in scheme 4.6, to give the corresponding guanidine as a nitrate salt.

Scheme 4.6:

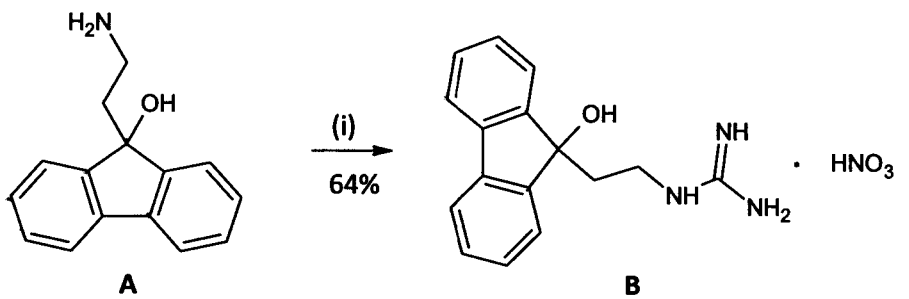

A **B**

(i) DPCN, MeOH, reflux, 14 h.

While the reaction proceeded with relative ease to give the required product, isolation and purification was somewhat challenging. Owing to the tendency of guanidines to tail on silica columns, some impurities from the reaction co-eluted with the required product after purification by column chromatography. Unfortunately, the use of bases such as triethylamine (TEA) and ammonium hydroxide in the eluent system did nothing to limit this effect and in order to obtain the product in high purity, the compound was subjected to numerous rounds of purification by column chromatography (see chapter 7 for details). The target product was eventually isolated in a moderate yield (64%) and identified as compound **B** by IR, NMR and mass spectroscopy. Methylene peak shifts in the ^{1}H and ^{13}C NMR spectra (see figure 4.4) indicated the product was significantly different from the starting material, **A**. Confirmation of the required guanidine formation was obtained from the IR spectrum of the product. Comparing this IR spectrum to that of guanidine hydrochloride and starting material, **A**, (see figure 4.5), a peak indicative of a guanidine moiety was observed at 1665 cm^{-1} in compound **B** but was not present in compound **A**.

With the successful synthesis of compound **B**, preparation of compound **C** was then attempted.

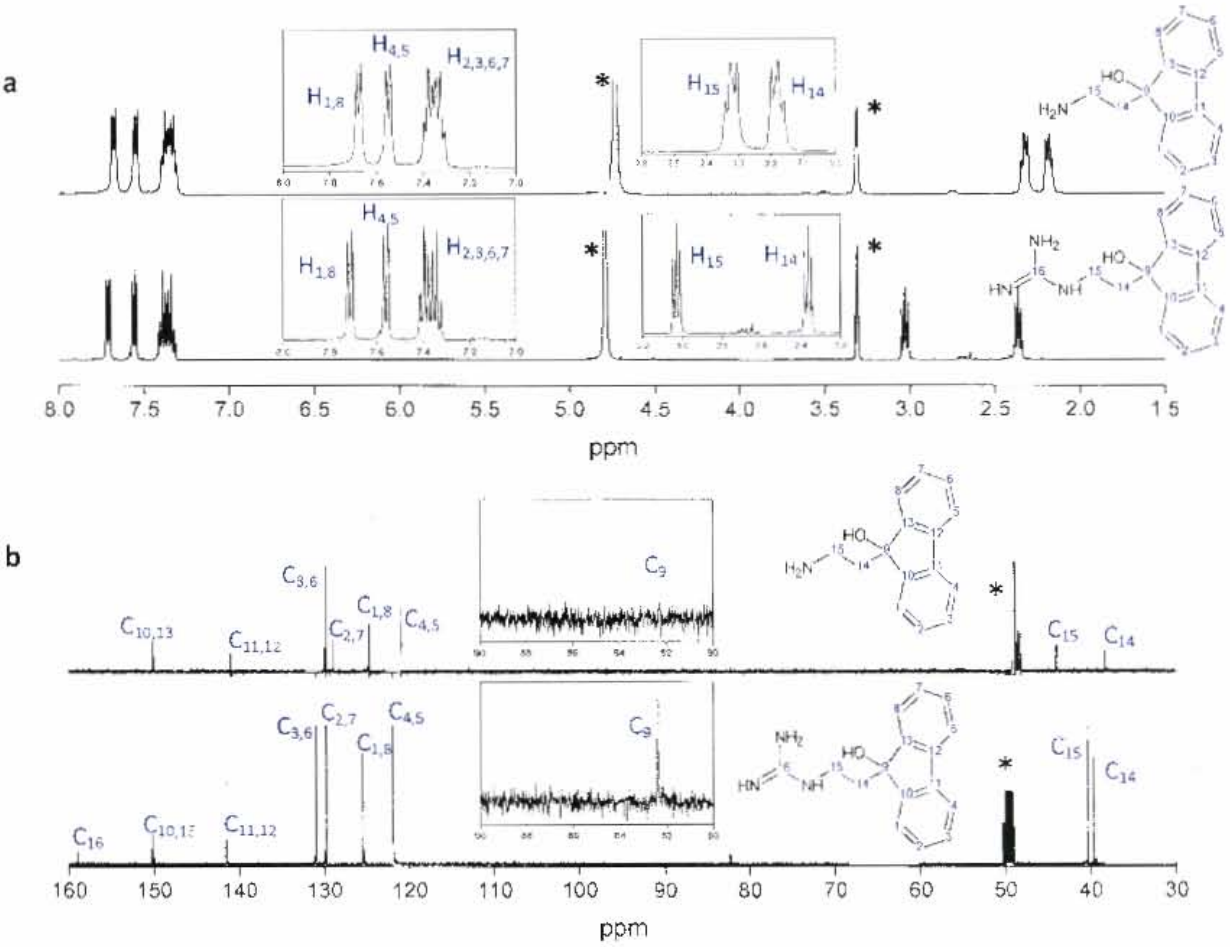

Figure 4.4: (**a**) ^{1}H NMR spectra of compound **A** (top) and compound **B** (bottom) comparing shifts in methylene peaks. **Insets.** Expanded aromatic and aliphatic regions. (**b**) ^{13}C NMR spectra of compound **A** (top) and compound **B** (bottom) showing shifts of methylene peaks. **Insets.** Expanded region showing quaternary carbon 9. Asterisks denote d_4-CD_3OD solvent and water peaks.

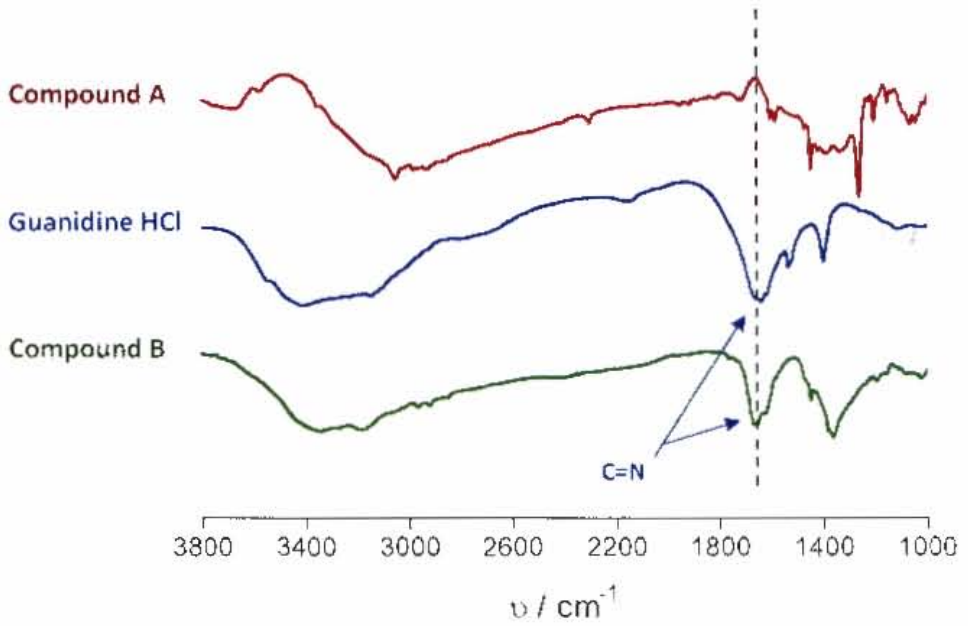

Figure 4.5: Infrared spectra of starting material **A**, guanidine HCl and product **B**, indicating the presence of guanidine peak at 1665 cm^{-1} in compound **B**.

4.4 Synthesis of 9-(aminomethyl)-fluoren-9-ol, C

The synthesis of compound **C** was investigated using two different routes, as the first route failed to produce the required product. A second route was then developed which led to the successful synthesis of compound **C**. Both routes have been described, below.

Route 1:

Scheme 4.7:

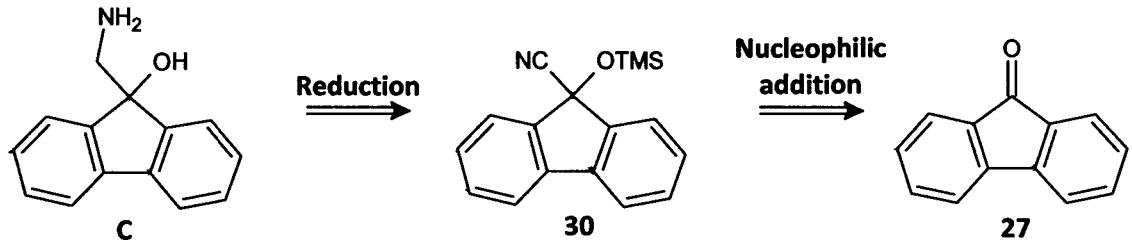

The retrosynthetic analysis of compound **C** (see scheme 4.7) was initially envisaged to follow a similar pathway as the one developed for compound **A** (see section 4.1), where the required primary amine would be obtained through the reduction of nitrile group. The synthesis of the required nitrile, **30**, had been previously been reported in the literature[119, 120] where the use of nucleophilic attack by trimethylsilyl cyanide (TMSCN) on the carbonyl of fluorenone, **27**, resulted in the target product being obtained. Reduction of the nitrile would result in the simultaneous deprotection of compound **30**.

While compound **30** was synthesised under the conditions described in scheme 4.8, unfortunately, reduction of the nitrile group to form the primary amine moiety failed to occur. The details of this are described in section 4.4.1.

Scheme 4.8:

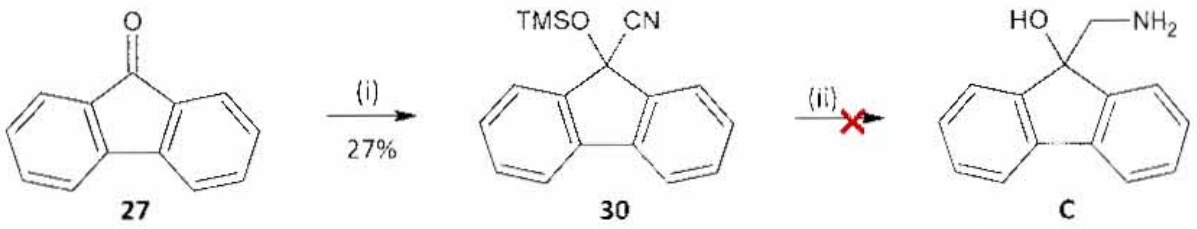

(i) TMSCN, I_2, DCM, N_2 atm, RT, 2h. (ii) LAH, THF, N_2 atm, 0 °C to RT, 24 h.

4.4.1 Synthesis of 9-[(trimethylsilyl)oxy]-fluorene-9-carbonitrile, ***30****.*

As mentioned above, the synthesis of compound **30** had been well described in the literature.[119, 120] The mechanism of formation involved the use of a Lewis acid in order to activate the carbonyl group of compound **27** toward nucleophilic attack of the nitrile. The reagent used in the synthesis of the title compound was TMSCN, which has both a Lewis acid (TMS) and nucleophilic (CN) moiety that provide for an efficient method of nucleophilic addition. While the reaction proceeded under fairly mild conditions with a relatively short reaction time to produce compound **30** in high purity, unfortunately low yields were obtained (27%). The appearance of an additional quaternary carbon peak at 120.2 ppm in the ^{13}C NMR spectrum indicated the product obtained was different from the starting material, **27**. The appearance of a nitrile peak at 2238 cm^{-1} in the infrared spectrum (see figure 4.6) that confirmed the formation of compound **30**.

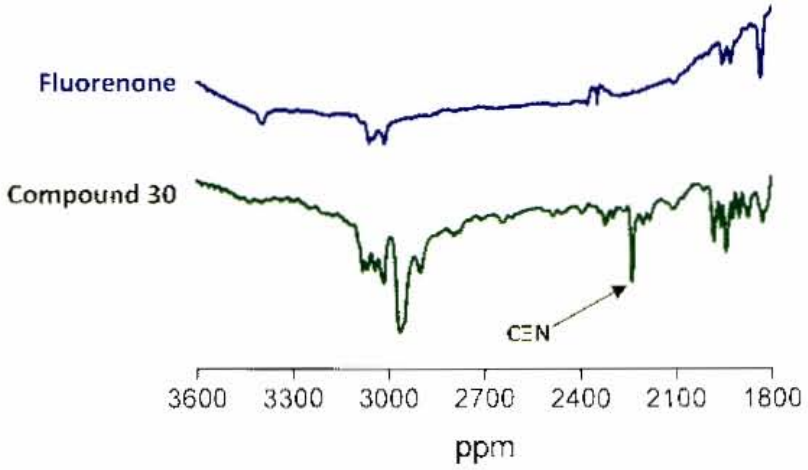

Figure 4.6: IR spectrum of fluorenone, **27**, and compound **30** indicating the appearance in the product of a characteristic nitrile peak at 2238 cm^{-1}.

The following step in which the amine, **C**, would be obtained from the nitrile required the reduction of compound **30** with lithium aluminium hydride (LAH), which would both reduce the nitrile to the amine as well as remove the trimethylsilyl, TMS, group from the alcohol. It was at this point that the synthetic route failed, and the target product was not obtained. At the time, it was thought that the harsh reducing conditions of this reaction led to the formation of a variety of side products instead of the required product. It was later discovered that the LAH reagent used was not active and thus did not reduce the nitrile as it should have. Because of this apparent non-reactivity and fragile nature of the β-amino alcohol, **C**, coupled with the low yields obtained, route 2 was devised in an attempt to circumvent these problems. This approach incorporated seemingly milder reducing conditions to obtain the amine and the use of compound **26** as an intermediate which was already well established from previous reactions (see section 4.2.1).

Route 2:

Scheme 4.9:

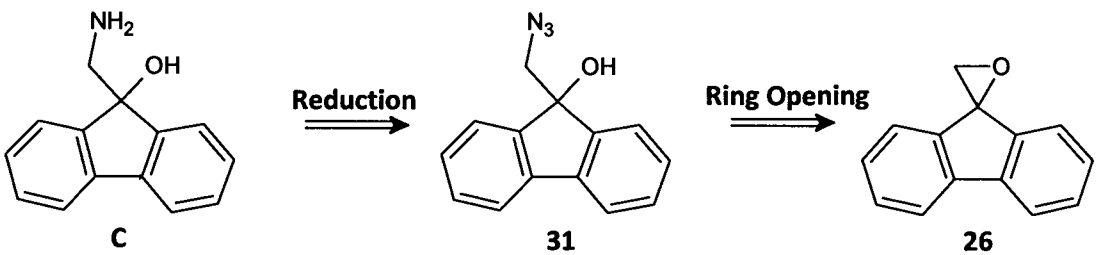

C **31** **26**

The retrosynthetic pathway of route 2, shown in scheme 4.9, was developed in an attempt to bypass some of the problems experienced in route 1 (detailed above). The reduction method chosen for its milder reaction conditions was that of the Staudinger reaction[121], whereby azide **31** (formed through ring opening of compound **26**) would be converted to the target primary amine **C**. Details of these reactions are shown in scheme 4.10.

Scheme 4.10:

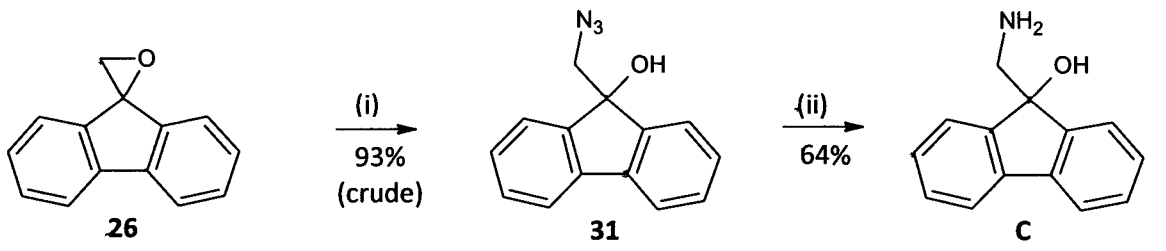

26 **31** **C**

(i) NaN_3, NH_4Cl, $MeOH/H_2O$ (8:1), RT, 16h. (ii) PPh_3, $MeCN/H_2O$ (7:1), RT, 14h.

4.4.2 Synthesis of 9-(azidomethyl)-fluoren-9-ol, ***31****.*

Compound **31** was obtained through a ring opening reaction where the azide group of sodium azide was delivered to the less sterically hindered carbon of the epoxide ring. The reaction proceeded under the mild conditions reported by Benedetti *et al.*[122] to produce compound **31** in high yields (93%) which was characterised using IR and NMR spectrometry. The IR spectrum of the product identified characteristic peaks corresponding to the azide and alcohol moieties (2106 and 3392 cm^{-1} respectively). While the ^1H NMR spectrum (see figure 4.7) showed a small shift in the methylene peaks from 3.70 ppm in the starting material to 3.85 ppm in the product. Shifts in the ^{13}C spectrum were more convincing of product formation, where the methylene carbon peaks shifted from 54.9 to 68.0 ppm.

It was initially thought that the tertiary alcohol of compound **31** needed to be protected before the Staudinger reduction step with triphenylphosphine, PPh_3, was attempted. Unfortunately, all attempts at protecting the alcohol with benzyl bromide failed. The rationale behind the inability to protect the alcohol was that the protecting group was too bulky for the reaction to take place. This meant that it was even more unlikely that the bulkier PPh_3 reagent would be able to react with this alcohol moiety and so the Staudinger reduction was performed on an impure sample of compound **31**.

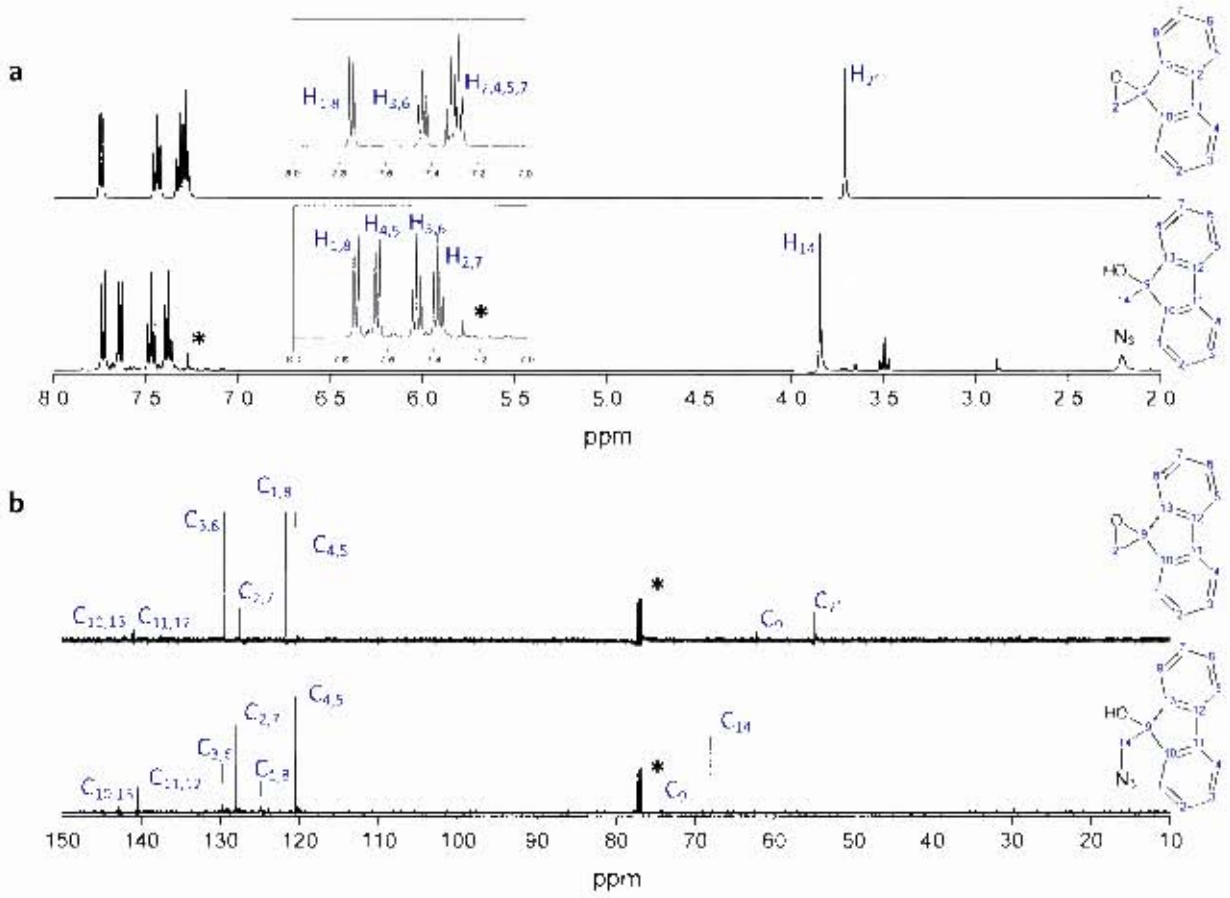

Figure 4.7: (**a**) ^{1}H NMR spectra of compound **26** (top) and compound **31** (bottom) comparing shifts in methylene and aromatic peaks. **Insets.** Expanded aromatic region. (**b**) ^{13}C NMR spectra of compound **26** (top) and compound **31** (bottom) showing shifts in methylene peaks. Asterisk denotes $CDCl_3$ solvent peaks.

*4.4.3 Synthesis of 9-(aminomethyl)-fluoren-9-ol, **C**.*

Compound **C** was synthesised from the azide, **31**, via a Staudinger reaction following literature procedures where PPh_3 was added to an azide in the presence of a tertiary alcohol. The mechanism of this reaction was investigated by Tian and Wang[123] and is described in scheme 4.11.

Scheme 4.11:

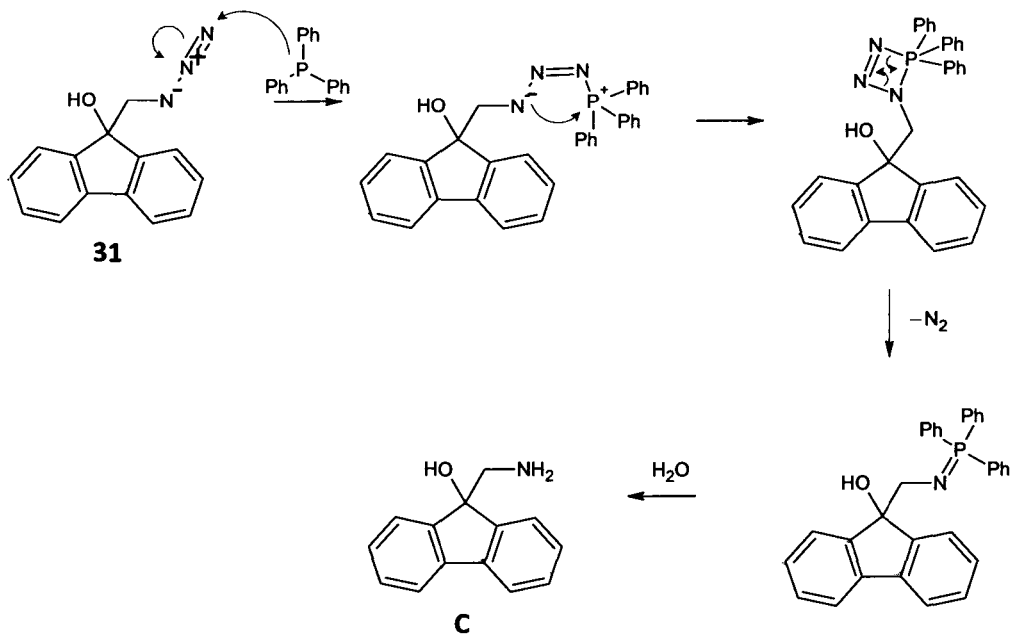

The phosphorus of PPh_3 attacks the nitrogen of the azide to form the phosphazide intermediate. Nitrogen gas is then released to form the iminophosphorane intermediate which is then hydrolysed by water to produce the target amine as well as triphenylphosphine oxide as a by-product.

The reaction proceeded under mild conditions to give compound **C** in a moderate yield (64%), with the absence of azide peak at 2106 cm^{-1} in the IR spectrum of the product supporting the formation of the required compound. ^{1}H and ^{13}C NMR spectra (shown in figure 4.8) showed slight shifts in the methylene groups of the product (3.70 and 69.2 ppm respectively) as compared to the starting material (3.85 and 68.0 ppm respectively) and mass spectrometry also confirmed product formation.

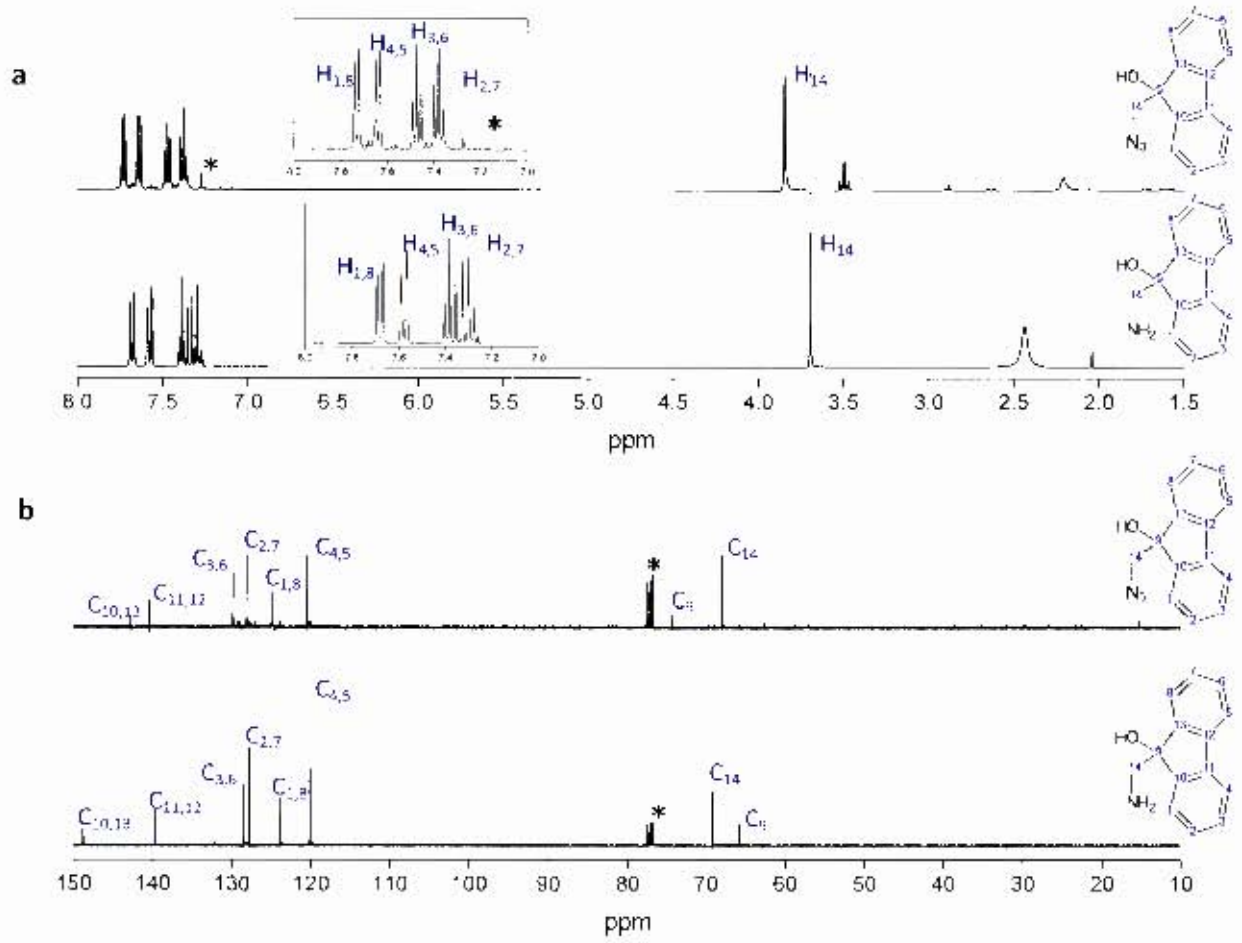

Figure 4.7: (a) ^{1}H NMR spectra of compound **31** (top) and compound **C** (bottom) comparing shifts in methylene and aromatic peaks. **Insets.** Expanded aromatic region. (b) ^{13}C NMR spectra of compound **31** (top) and compound **A** (bottom) showing shifts in methylene peaks. Asterisk denotes $CDCl_3$ solvent peaks.

With the required primary amine, **C**, successfully obtained, synthesis of the corresponding guanidine target, **D**, was then attempted.

4.5 Attempted synthesis of 1-[(9-hydroxy-fluoren-9-yl)methyl]guanidine, D

The synthesis of the guanidine **D** required the guanylation of the primary amine of compound **C** and because of various reasons, detailed further on, three different guanylating agents (**29**, **32** and **33** in scheme 4.12) were used in the attempted synthesis of compound **D**. While the formation of compound **D** was confirmed by mass spectrometry, unfortunately this compound could not be isolated.

Scheme 4.12:

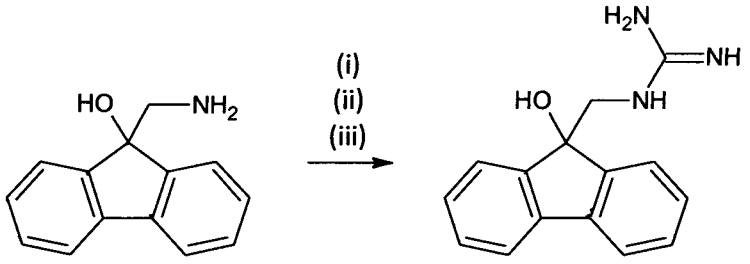

C D

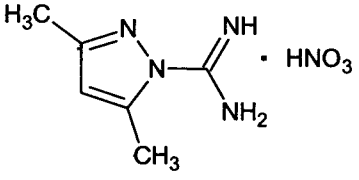

29

32

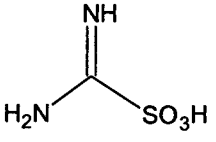

33

(i) **29**, Tea, EtOH or DMF/H_2O (1:1). (ii) **32**, MeOH or EtOH. (iii) **33**, TEA, MeOH or EtOH.

3,5-Dimethylpyrazole-1-carboxamidine nitrate (DPCN), 29.

As with the formation of compound **B**, the commonly used guanylating agent, DPCN, was initially employed in the attempted formation of compound **D**. Initially the reaction was carried out under the same conditions as those employed in the synthesis of guanidine, **B**. Thin layer chromatography (TLC) indicated that the reaction was not successful. In an attempt to promote the formation of the required product, reaction conditions were varied and the base TEA introduced to aid dissolution of compound **A** in the solvent system as well as neutralise the salt of the product formed. The reaction temperature was also increased from 40 °C to 80 °C and the mixture left for 5 days to react. Even after this, TLC still indicated no product formation had occurred and so the solvent system was changed to DMF/H_2O (1:1) to gauge whether solvent interaction may play a significant role in the reaction. Unfortunately, this still resulted in no product formation. Reaction mixtures were then subjected to microwave irradiation (150 W at 40 °C, 80 °C and 100 °C for 10 minutes per irradiation) in an attempt to provide a more effective method of heating, but product formation was not observed by TLC methods.

It was reasoned at this point that perhaps there may be steric hindrance experienced by the short chain primary amine and thus nucleophilic attack at the sp^2 centre of the carboxamidine of DPCN would be difficult to attain. The smaller guanylating agent, cyanamide, was then substituted for DPCN as this was less likely to encounter these presumed steric hindrances.

Cyanamide, 32.

Compound **C** was reacted with cyanamide under the conditions detailed in scheme 4.13, but product formation was still not observed. Since the smaller cyanamide was unable to produce the required guanidine, it was then suspected that steric hindrance may not be the sole reason behind the failure of this reaction. A second possible explanation was then postulated as being the existence of an intramolecular hydrogen bond between the primary amine and tertiary alcohol moieties of compound **C**. Assuming this to be the case, the lone pair of the primary amine nitrogen atom of compound **C** would then be involved with the hydrogen bond and thus have reduced nucleophilicity. In addition, the predicted pK_a of the compound was calculated as 5.97 ± 0.40[112] which is significantly lower than expected for a primary amine moiety. The low nucleophilicity and possible presence of an intramolecular bond is a likely explanation for the lack of reactivity of this compound.

A literature search for alternate guanylating agents was then undertaken and a paper by Wityak *et al.*[124] was found, in which similar problems with intramolecular interactions were experienced where guanidine formation using DPCN and cyanamide was prevented. The paper described the use of formamidinesulfonic acid (FSA), **33**, as an alternate reagent which was more reactive and resulted in the formation of their required guanidine. With this success in mind, the use of FSA was then attempted in the synthesis of compound **D**.

Formamidinesulfonic acid (FSA), 33.

FSA is not a commercially available compound and thus had to be synthesised. Literature[125] reports indicated that this reagent was easily obtained by the oxidation of the commercially available starting material, formamidinesulfinic acid, **34**, using peracetic acid. Reaction conditions used are detailed in scheme 4.13.

Scheme 4.13:

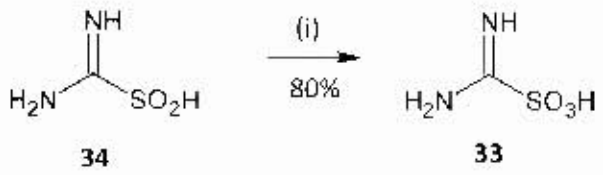

34 **33**

(i) CH_3CO_3H, CH_3CO_2H, 10-20 °C, 3h.

IR spectroscopy was used to confirm the formation of the required sulfonic acid with characteristic peaks for this moiety appearing at 1227 and 1054 cm^{-1}. Comparison of the spectrum of starting material, **34**, to product **33** (see figure 4.9) revealed no peaks corresponding to the sulfinic acid (1435 and 999 cm^{-1}). Mass spectrometry also confirmed product formation.

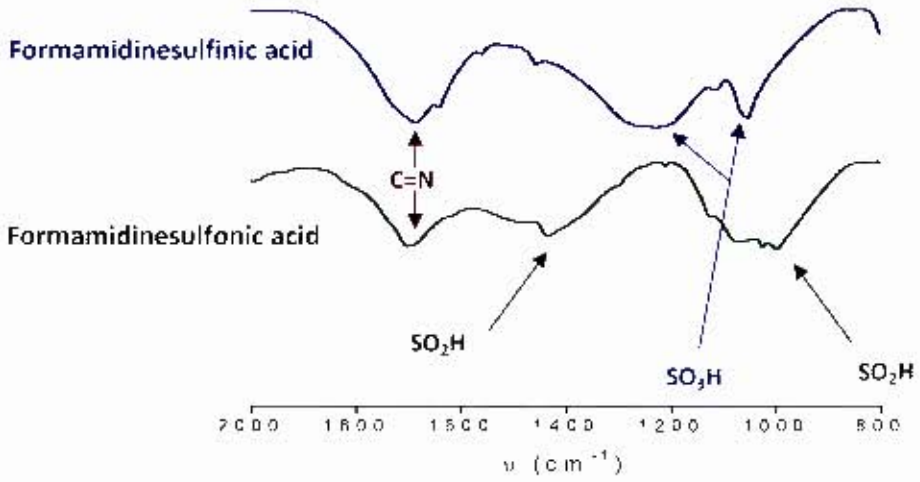

Figure 4.9: IR spectra of starting material, formamidinesulfinic acid (**34**, blue), and product, formamidinesulfonic acid (**33**, green) which identify characteristic peaks indicating the conversion of starting material to product.

With the formation of formamidinesulfonic acid successful, guanylation of compound **C** was then attempted, whereby the guanylating reagent, TEA and primary amine, **C**, were left to reflux in methanol. After 45 hours, no product formation was observed. The reaction mixture was then subjected to microwave irradiation (150 W) at 80 °C and 100 °C for 10 minutes each, but still produced no identifiable product by TLC analysis.

As TLC is not always a reliable method of product identification, the proton NMR spectrum of all reaction mixtures was taken. No discernable shift in the methylene peak was observed. Mass spectrometry was then used to identify the possibility of product formation by investigating whether a mass peak corresponding to the product was present. The mass spectra of the reaction mixtures were taken and all were found to have a peak corresponding to the target product (254 *m/z*) as well as the starting material (212 *m/z*). This indicated that the reactions had proceeded albeit to a far lesser degree with yields that would not practically afford the desired product.

In an attempt to isolate any compound **D** formed, separation of impurities and starting material, using column chromatography, was undertaken. Unfortunately, owing to the large amount of by-products and unreacted starting material in the reaction mixture, compound **D** could not be isolated as it was presumably present in minute quantities compared to by-products. Because of this difficulty in isolation, apparent low yield and time constraints, the synthesis of this compound was abandoned in favour of the synthesis of the final proposed compound **E**.

While the isolation of compound **D** remained elusive, mass spectrometry indicated the synthesis of this compound was indeed possible. With more time to vary reaction conditions in order to improve presumably low yields, as well as access to equipment such as preparative HPLC, the possibility remains that this compound could yet be isolated and tested for β-haematin inhibition in the future.

4.6 Attempted synthesis of 9-(7-methyl-1,3,5-triaza-adamantanyl)-fluoren-9-ol, E

The retrosynthetic pathway developed for the synthesis of the title azaadamantane derivative is shown in Scheme 4.14.

Scheme 4.14:

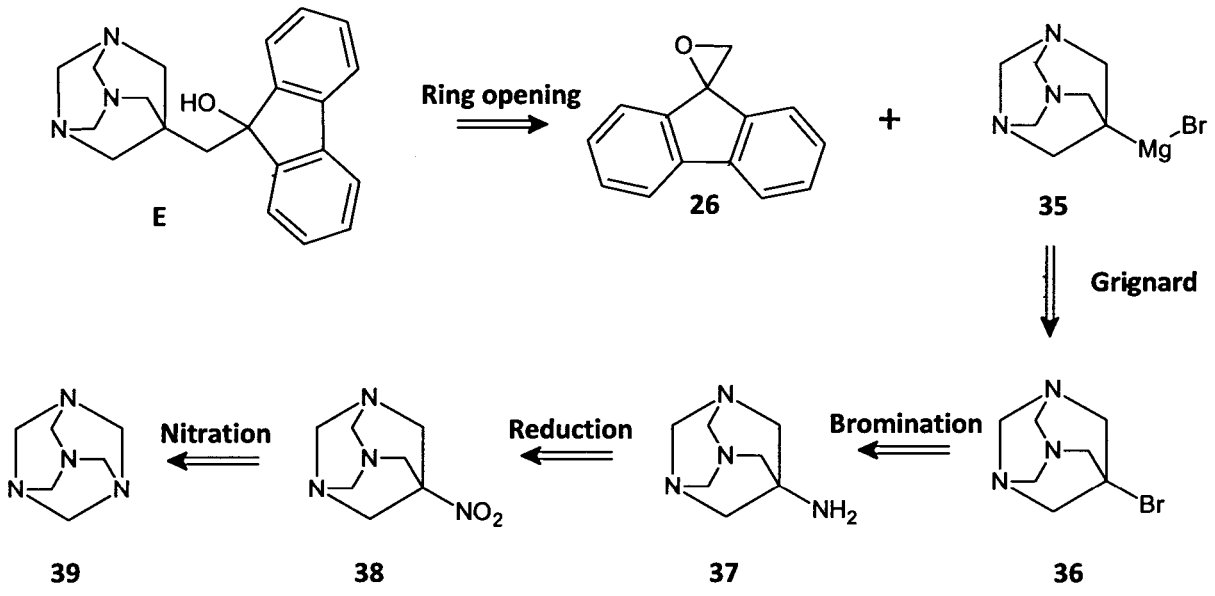

The first retrosynthetic step in the formation of compound **E**, required nucleophilic attack of the Grignard reagent, **35**, formed from 7-bromo-1,3,5-triazaadamantane, **36**, at the least substituted carbon of the spiro epoxide, **26**. Because of the steric bulk of compound **26**, the regioisomer, [9-(1,3,5-azaadamant-7-yl)-fluoren-9-yl]methanol, was deemed unlikely to form as this would require the nucleophilic attack to occur at the more unfavourable, quaternary carbon of the epoxide of compound **26**.

While formation of the above mentioned Grignard reagent had never previously been reported, the synthesis of the required bromo intermediate **36** from the commercially available starting material hexamethylenetatramine, **39**, has been claimed in a patent by Wiezer.[126] Hexamethylenetatramine underwent nitration to form the nitro intermediate, **38**, which was then reduced to the corresponding primary amine intermediate, **37**. The final step involved the bromination of compound **37**, to give 7-bromo-1,3,5-triazaadamantane, **36**. The synthesis of the required spiro epoxide, **26**, was already well established and is detailed in section 4.2.1.

Synthesis of the required azaadamantane intermediates was accomplished under relatively mild conditions with moderate yields obtained (see scheme 4.15). Unfortunately, the final coupling step involving nucleophilic attack by the Grignard reagent on epoxide, **26**, failed to produce the target compound **E**. Details of the synthesis of the azaadamantane intermediates and attempted synthesis of compound E are provided further on.

Scheme 4.15:

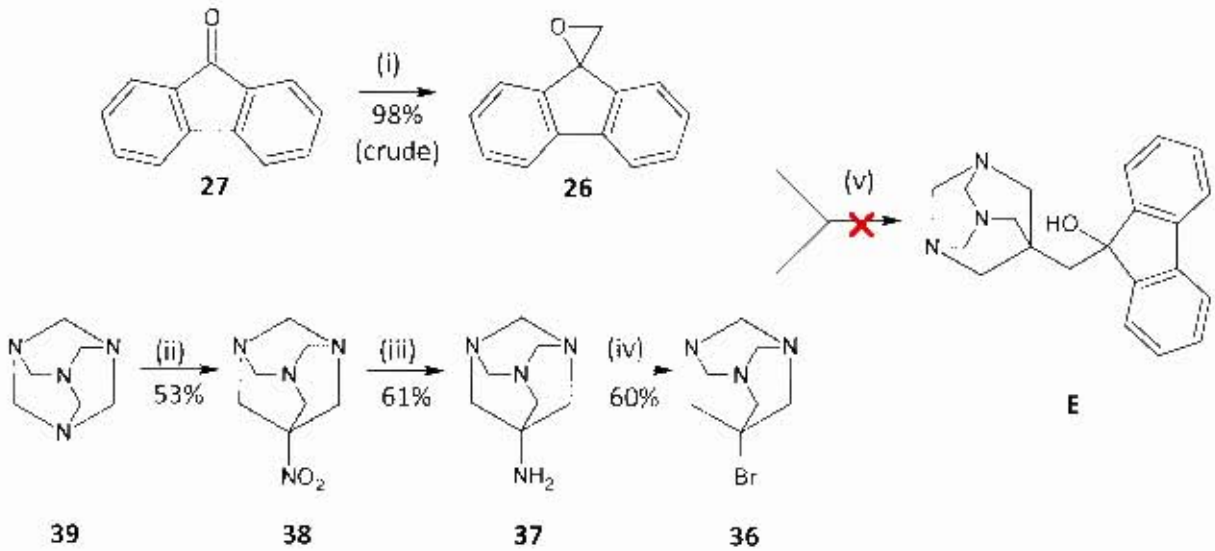

(i) *1.* NaH, TMSOI, DMSO, N_2 atm, 25 °C, 30 min. *2.* 9-Fluorenone, 25 °C, 1.5 h. **(ii)** $MeNO_2$, CH_3COOH, reflux 95 °C, 6 h. **(iii)** RaNi, H_2NNH_2, H_2O/*i*-PrOH (14:1), RT, 4h. **(iv)** $NaNO_2$, HBr (45%), 0 °C – RT, 3 h. **(v)** Mg, Et_2O or THF, N_2 atm, -30 °C to reflux, 24 h.

*4.6.1 Synthesis of 7-nitro-1,3,5-triazaadamantane, **38**.*

The synthesis of compound **38** had been described for industrial use in a patent by Wiezer[126], which involved the reaction between hexamethylenetatramine, **39**, and nitromethane. The mechanism of formation of **38** was proposed by Kuznetsov *et al.*[127] and is described in scheme 4.16, below. This mechanism was based on a modification of the Mannich reaction, where hexamethylenetatramine serves as both the ammonium and methylene element, while nitromethane acts as the C-H element.[127]

Scheme 4.16:

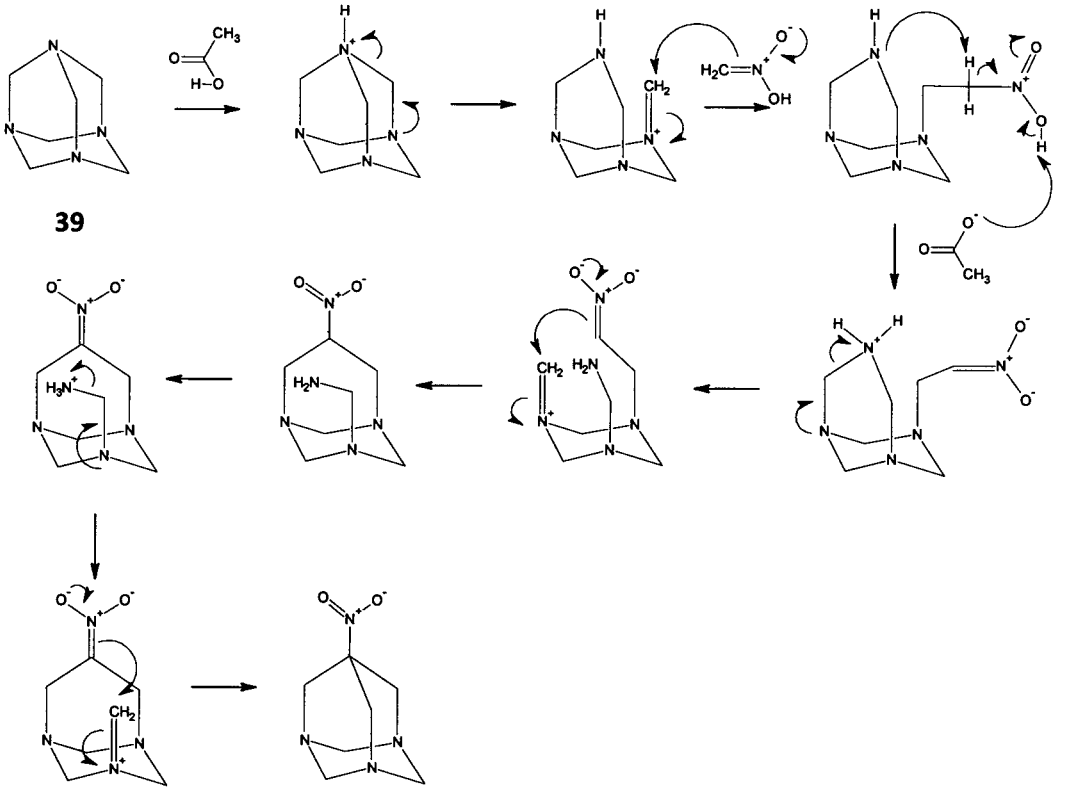

39

38

The patent by Wiezer[126] provided a number of varying conditions for the formation of compound **38**, which could be essentially divided into two categories: (a) using a primary alcohol, where C = 1 to 4, as a solvent or (b) using the acid component as a solvent. The patent also clearly stated that water contamination needs to be kept to a minimum, preferably not more than 4_{wt}%, in order to prevent the formation of by-products that are nearly impossible to remove.

Owing to the hygroscopic nature of the acid component, glacial acetic acid, it was initially decided to use category (a), with butanol as the solvent, in order to keep the amount of acetic acid and water contamination to a minimum. Upon completion of the reaction, a dark black syrup was obtained, indicating that a large amount of by-product had formed. Eventually, through copious washings and a recrystalisation from water, a cream coloured precipitate was obtained in a low yield (12%), which was identified as product **38** through NMR and mass spectrometry.

Because of its symmetry, the starting material hexamethylenetatramine, **39**, only has a single peak in both the ^{1}H and ^{13}C NMR spectra. Breaking the symmetry of **39** by the removal of one tertiary amine and insertion of the nitromethylene group in **38** resulted in the appearance of three peaks in both ^{1}H and ^{13}C NMR. In the proton spectrum (see figure 4.10), the singlet obtained integrated for six protons and the two doublets accounted for three protons each. The six protons described by the singlet are all in the same chemical environment (assigned as H_1 in figure 4.2). Because of the fused chair nature of the molecule, the remaining six protons are not all in the same environment. Each doublet accounts for three protons that are in the equatorial or axial position (assigned as H_2 in figure 4.10). The three peaks in the ^{13}C spectrum were assigned as the two sets of methylene carbons (assigned as position 1 and 2 in figure 4.10) and the quaternary carbon of the inserted nitromethylene group.

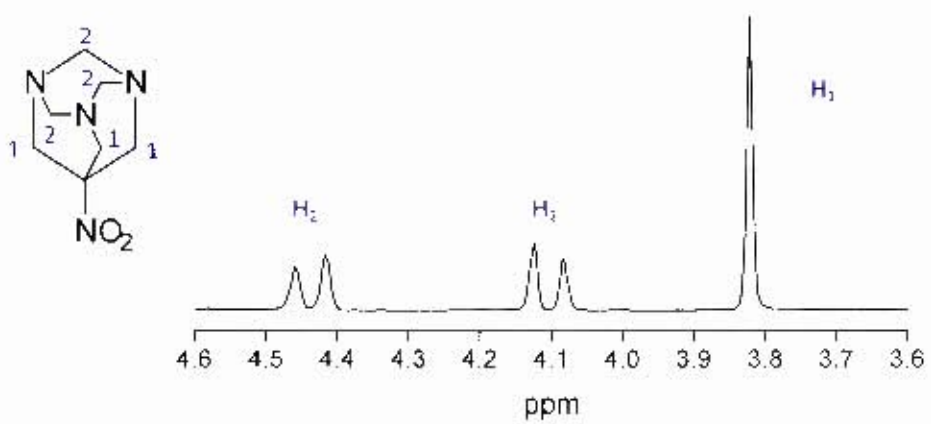

Figure 4.10: ^{1}H NMR spectrum (in D_2O) of compound **38**. For clarity, azaadamantane structure has not been numbered according to IUPAC nomenclature.

The melting point obtained for this compound was found to be 183 – 185 °C, and could not be directly compared to literature values because of the large discrepancies in melting point between the various authors. These reported values ranged between 260 °C and 310 °C. [128-130] It was concluded from NMR and mass spectrometry that the correct product had indeed been obtained.

While this method did produce the required compound, yields obtained were low and isolation was difficult. Thus formation of compound **38** was then attempted using conditions of category (b) described in the patent by Wiezer[126]. Using acetic acid as both solvent and acid component resulted in the successful synthesis of compound **38** in a moderate yield (53%) which required no further purification for use in the subsequent reduction reaction.

4.6.2 Synthesis of 7-amino-1,3,5-triazaadamantane, ***37****.*

The synthesis of amine **37** required the reduction of the nitro moiety of compound **38**. Kuznetsov *et al.*[127] had previously reported this reaction using Raney Nickel as a catalyst and hydrazine as a hydrogen source under fairly mild conditions. Following this procedure, the reduction of compound **38** to compound **37** was achieved in moderate yields (61%). Product formation was confirmed by the ^{13}C NMR spectrum (see figure 4.11), where shifts in the quaternary carbon peak (assigned as C_1 in figure 4.11) from 57.4 ppm in compound **38** to 38.4 ppm in compound **37** were observed. Mass spectrometry also indicated formation of the desired product.

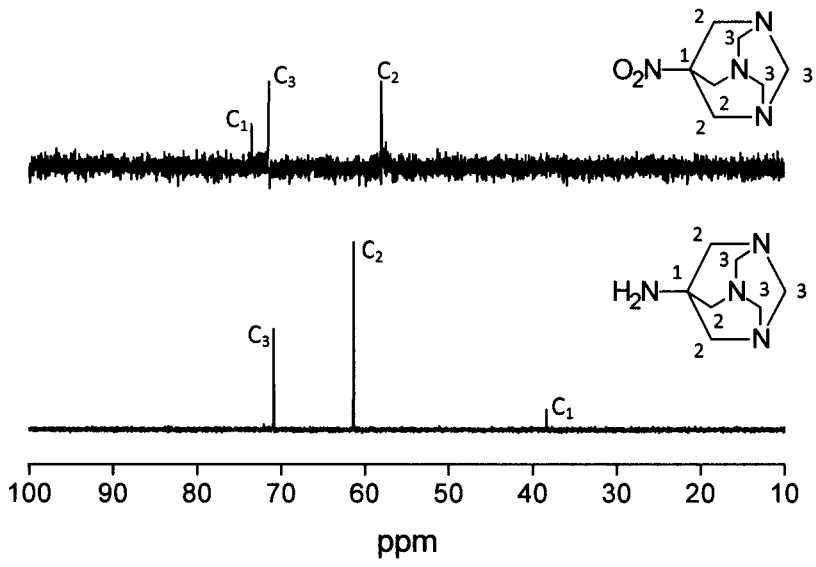

Figure 4.11: ^{13}C NMR spectra (in D_2O) showing quaternary carbon peak shifts of starting material, compound **38** (top) and isolated product **37** (bottom).

Since the report of this reaction in 1985, there had been no further mention of alternative methods of nitro reduction for this specific compound. A brief survey of alternative reduction methods was then undertaken, in which Raney Nickel was substituted for the more commonly used palladium over activated carbon (Pd/C) catalyst and altering the hydrogen source according to various references[131, 132].

A paper by Ram and Ehrenkaufer[131] reported the use of ammonium formate and Pd/C in the reduction of aliphatic nitro groups to corresponding amine groups. The synthetic conditions of the reported procedure required the reactants to be dissolved in methanol and left to stir at 25 °C. Reported reaction times did not exceed 120 minutes. When compound **38** was subjected to these conditions, no product formation was observed even after 24 hours reaction time.

An additional method then employed was the more commonly used reduction technique of catalytic hydrogenation utilising hydrogen gas under pressurised conditions. Compound **38** was dissolved in a small amount of acetic acid and added to Pd/C in methanol.[132] The container was charged with hydrogen gas to 3 atm and left to run for 4 hours. Unfortunately, upon workup of the reaction, it was discovered that only a small amount of product had formed, leaving most of the starting material unreacted. This indicated that the original Raney Nickel procedure was the most favourable. Since the second alternative reduction procedure was able to produce the required product, albeit in low yields, this may provide a suitable alternative should Raney Nickel not be available. Reaction conditions, such as reaction time and temperature, would need further optimisation in order to produce potentially higher yields and thus provide a more suitable alternative reduction method.

*4.6.3 Synthesis of 7-bromo-1,3,5-triazaadamantane, **36**.*

The bromination of amine **37** to form compound **36** was reported in the same Kuznetsov paper[127] as mentioned in section 4.6.1, above, and the proposed mechanism of this reaction is shown in scheme 4.17.

Scheme 4.17:

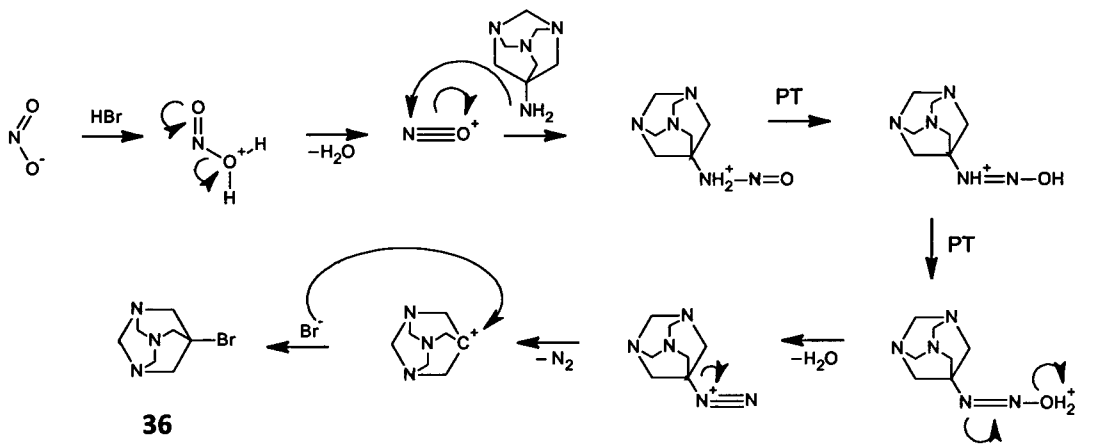

Hydrogen bromide was used to generate the key nitrosonium ion intermediate which facilitated the conversion of the primary amine to the diazonium species. Presumably the diazonium moiety was released as nitrogen gas in an S_N1 type fashion, to give a stable tertiary carbocation intermediate. This carbocation was then subjected to the nucleophilic attack of the bromide anion, which was generated *in situ*, to form product **36**.

Compound **36** was prepared according to the reported procedure[127], deviating only in purification of the crude product by washing it with small quantities of diethyl ether. The resulting product was obtained in a moderate yield (60%), comparable to reported yields of 50%.[127] Shifts in the ^{13}C NMR spectrum (see figure 4.12) indicated the product obtained was different from the starting material, **37**, and mass spectrometry confirmed the formation of the required product which was pure enough to be used in the final coupling reaction.

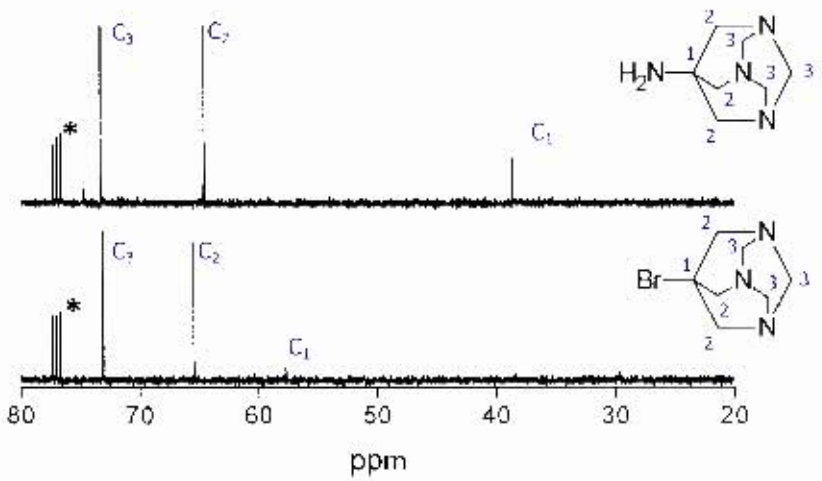

Figure 4.12: ^{13}C NMR spectra showing quaternary carbon peak shifts of starting material, compound **37** (top) and isolated product **36** (bottom). Asterisks denote $CDCl_3$ solvent peaks.

4.6.4 Attempted Grignard reaction between 7-bromo-1,3,5-triazaadamantane, ***36****, and spiro[fluorene-9,2'-oxirane],* ***26****.*

The final coupling step between compound **26** and **36** to form the proposed compound **E** required the formation of a Grignard reagent from compound **36**. The formation of this reagent had not been reported in the literature, but the formation of a Grignard reagent from 7-bromo-adamantane had been described.[133-135] The literature preparation described an interesting departure from conventional Grignard reaction conditions, demanding no mechanical stirring for the successful formation of the Grignard reagent. When stirring was employed, the exclusive formation of by-products was observed.[135]

While use of this unusual reaction condition in the formation of the adamantyl Grignard reagent is well documented, the reasons as to why mechanical stirring has such a pronounced effect are not fully understood. Molle *et al.*[135] have undertaken exhaustive investigation into this unusual occurrence and from the results obtained have been able provide a possible explanation.

They propose that the Grignard reaction follows the mechanism detailed in scheme 4.13, in which the first step involves the adsorption of 1-bromo-adamantane (Ad–Br) to the magnesium metal and a transient species (Ad··MgBr) is formed. The subsequent formation of the Grignard reagent via route ii typically requires the transient species to stay adsorbed to the metal surface, while formation of the by-products in routes iii and iv occur upon desorption. In route iii, the desorbed transient species reacts with another Ad–Br molecule in solution to produce the bi-adamantane (Ad–Ad) side product and in route 4 the transient species reacts with solvent molecules (SH) to give side products Ad–H and Ad–S. It was found that mechanical stirring of the reaction mixture gave a 70% yield of by-products from route iv and 30% yield of by-products from route iii, while with no stirring a yield of 56% of the organomagnesium Grignard product was obtained.

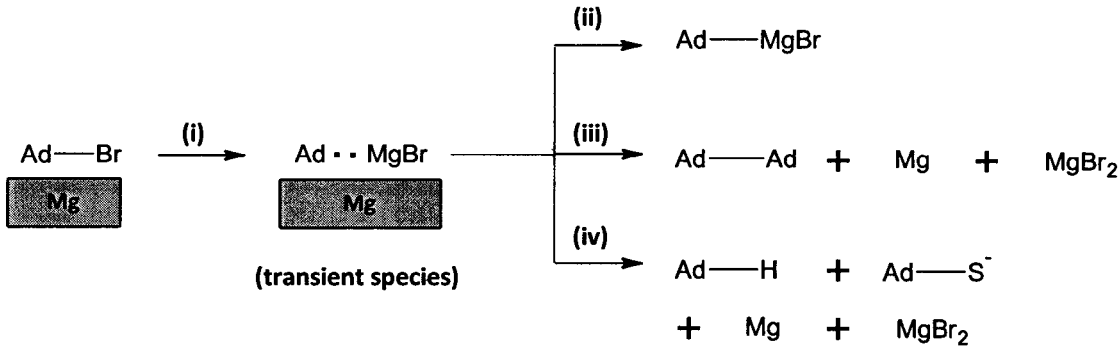

Figure 4.13: Proposed mechanism by Molle *et al.*[135] for the Grignard reaction of 1-bromo-adamantane (Ad–Br). Three possible product routes can occur, with route ii leading to the Grignard reagent and routes iii and iv leading to by-product formation. Figure adapted from reference 135.

Molle *et al.*[135] concluded that competition between the three possible routes (ii, iii and iv in figure 4.13) was dependant on the degree of adsorption of the transient species at the metal surface. Because of the large steric volume of the adamantyl molecule, it was assumed that the inherent ability of this compound to stay adsorbed to the metal surface was less than other haloalkyl compounds. Thus when mechanical stirring was employed, the absorption of the transient species formed was further decreased by shearing forces which would release the intermediate into the solution. Once in solution, by-products from routes iii and iv would begin to form, with the bi-adamantane precipitating from solution and coating the metal surface, further shielding adsorption of Ad–Br.

With this in mind, initial reaction conditions for the formation of the Grignard reagent from compound **36** were undertaken with no mechanical stirring. Activated dry magnesium turnings (activated by acid wash, followed by water and acetone wash) were added to compound **36** in dry diethyl ether, the reaction was gently refluxed and monitored over 19 hours. Samples taken from the reaction periodically were added to water and the pH tested. Should a Grignard reagent have been present, removal of a hydrogen atom by the Grignard from water would have left hydroxide ions in solution resulting in a high pH being obtained. No such pH was obtained from the reaction samples, indicating no reaction had occurred. It was then reasoned that owing to the insolubility of compound **36** in diethyl ether, a change in solvent system may result in the formation of the required Grignard reagent. Dry tetrahydrofuran (THF) was then substituted for diethyl ether and the reaction once more attempted to no avail.

In order to ascertain whether the Grignard reagent was formed only in small amounts, both reaction conditions were repeated with mechanical stirring employed. The rational behind this approach was that if the reaction indeed produced the Grignard reagent in small amounts, stirring would result in the formation of the by-products detailed in scheme 4.13. Alternatively, since this compound had never been reported, there was the possibility that stirring was required to form the product. Unfortunately, NMR spectra taken of the reaction mixture showed only starting material with no shifts in the proton or carbon spectra, indicating neither formation of the by-product nor the Grignard reagent had occurred.

It was thus concluded that the formation of the proposed target compound **E** could not be achieved from this synthetic route and the lack of Grignard reagent formation was attributed to its insolubility even in the more polar solvent, THF. Perhaps the use of a more polar solvent such as dioxane could be used to replace THF. Given the complexity with regard to Grignard reagent formation of these types of compounds, it was decided, to abandon the synthesis of this proposed compound.

4.7 Conclusions

Three of the five proposed compounds (**A**, **B** and **C**) were successfully synthesised and isolated. Mass spectrometry indentified the formation of the fourth proposed compound, **D**, and isolation via column chromatography was attempted. Unfortunately owing presumably to low yields of the target and large quantities of by-product formation, purification was not successful. The fifth proposed compound, **E**, could not be prepared, seemingly because of solubility issues experienced in the final Grignard reaction step. No formation of the required Grignard reagent was observed.

Association constants with haematin and ability to inhibit β-haematin formation were determined for the three successfully synthesised compounds, the details of which follow in chapter 5.

CHAPTER 5.

INVESTIGATION OF β-HAEMATIN INHIBITION ACTIVITY BY SYNTHESISED COMPOUNDS

5.1 Introduction

The ability to measure β-haematin (synthetic haemozoin) inhibition has been previously investigated utilising a HTS colorimetric assay, developed by Ncokazi and Egan.[44] In this assay, pyridine added to the reaction mixture selectively coordinates to unreacted Fe(III)PPIX but not β-haematin. The former species is present when a compound successfully inhibits β-haematin formation. A bis-pyridyl Fe(III)PPIX complex is formed in the assay that has an absorbance maximum at 405 nm. Using UV-vis spectroscopy, the relative quantity of bis-pyridyl Fe(III)PPIX can then be determined and from this an IC_{50} for β-haematin inhibition can be calculated. While the conditions employed in this assay are not biological in nature, the ability to screen compounds using this technique can identify compounds that have the potential for antimalarial activity.

5.2 β-Haematin inhibition

Compounds **A**, **B**, **C** as well as the template compound, 9-hydroxyfluorene, (see figure 5.1) were tested for β-haematin inhibition, according to the modified method of Ncokazi and Egan.[44] Over the scale of 0 to 10 equivalents of compound relative to Fe(III)PPIX, the range used for the detection of strong β-haematin inhibitors, no activity by any of the compounds was observed. Equivalents were increased to 200 (70 in the case of compound **A**, because of lack of solubility) in order to ascertain whether there was any weak inhibiting ability which could perhaps be further improved through the modification of aromatic substituents. Unfortunately, no inhibition was observed, even at these higher concentrations.

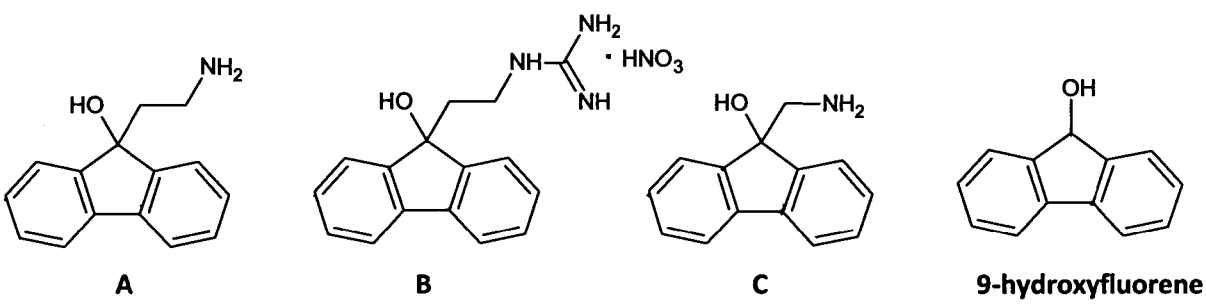

Figure 5.1. Compounds tested for β-haematin inhibition.

While the lack of inhibition was unexpected with compound **B**, which was initially thought to possess the required features for inhibiting ability, the inability to inhibit β-haematin formation by the 9-hydroxyfluorene, compound **A** and negative control, compound **C**, was expected. In the case of 9-hydroxyfluorene, it was hypothesised that the lack of a hydrogen bonding group would result in a lack of inhibitory activity and this was confirmed even up to a 200 equivalent scale. Modelling showed the hydrogen bonding group of compound **A** adopted a conformation in which it was directed away from the propionate side chain, and thus accounts for its inactivity. The negative control, compound **C**, was through computational modelling, also hypothesised to have no activity because of the short one carbon linker which does not provide a favourable distance for the primary amine to hydrogen bond to the propionate side chain of Fe(III)PPIX (see section 3.5).

While the inactivity of compounds **A**, **C** and the template molecule had been predicted, the inability of compound **B** to prevent formation of β-haematin was not immediately understood. It was reasoned that perhaps the lack of pre-organisation of the hydrogen bonding group, as seen in the computational modelling, played a large role in the lack of activity. In order to obtain better insight into the interactions of these compounds with Fe(III)PPIX, association constants for compounds **A** to **C** were determined with Fe(III)PPIX

5.3 Fe(III)PPIX association

Association constants (log K_{obs}) for compounds **A** to **C** with Fe(III)PPIX were determined and compared to that of 9-hydroxyfluorene (see table 5.1). It was observed that all the synthesised compounds displayed a markedly lower association constant than the template molecule, indicating that introduction of the linker chain bearing the hydrogen bond donor at position 9 of the fluorene ring system caused a decreased association interaction with Fe(III)PPIX. In order to gain some further understanding of the interactions, pK_a values for compounds **A** to **C** were determined using the MOKA[113] software and incorporated into prediction equation 8 (see section 2.4) in order to obtain the predicted association constants (log K_{calc}). Values are summarised in table 5.1.

Table 5.1. Predicted pK_a values and association constants (observed and predicted) for synthesised compounds **A** to **C** and 9-hydroxyfluorene.

Compound	pK_a [a]	Log K_{obs}	Log K_{calc} [b]
9-Hydroxyfluorene	14.33 ± 0.52	3.64 ± 0.09	3.33 ± 0.25
A	15.13 ± 0.52	3.03 ± 0.09	2.98 ± 0.25
B	15.18 ± 0.52	2.80 ± 0.03	2.97 ± 0.25
C	14.07 ± 0.52	2.93 ± 0.02	3.30 ± 0.25

[a] Predicted using MOKA (reference 113).
[b] Calculated using equation 8 (section 2.4)

Owing to the large errors in predicted pK_a values, predicted association constants (log K_{calc}) are not particularly accurate, nevertheless, the trend observed in the calculated pK_a values uncovered a possible explanation for the lower than expected haematin association constants.

Comparing the pK_a value of 9-hydroxyfluorene to synthesised compounds **A** and **B**, it was observed that introduction of an alkyl substituent at the 9-position of the fluorene ring system caused an increase in pK_a of the hydroxyl moiety. This increase in pK_a has a detrimental effect on Fe(III)PPIX coordination and hence overall association constant under the experimental aqueous conditions (pH 7.4) in which association constants are measured, leaving little deprotonated species in solution to coordinate to Fe(III)PPIX owing to proton competition. This is somewhat confirmed by the fact that the predicted association constants, which take proton competition into account, are similar in value to the experimentally obtained association constants.

In the case of compound **C**, a lower pK_a value than 9-hydroxyfluorene was predicted which should have resulted in a greater association constant. In fact, the observed association constant was as low as compounds **A** and **B**, indicating that compound **C** probably has a similar lack of coordinating ability with Fe(III)PPIX. The possible explanation of this lower than expected association constant for compound **C** was attributed to a hypothesised intramolecular hydrogen bond between the primary amine and hydroxyl moieties (see section 4.5). The hydrogen of the hydroxyl moiety is thus less available for deprotonation and this would result in a lower affinity for coordination.

5.4 Conclusions

From these results, it can be concluded that a substituent at the 9-position of the 9-hydroxyfluorene template is not suitable for designing potential β-haematin inhibition compounds, as introducing the linker bearing the hydrogen bonding moiety at this position causes an increase in pK_a values of the coordinating hydroxyl group, resulting in a loss of coordinating ability in aqueous solution. This results in a lower association with Fe(III)PPIX which seemingly does not have a strong enough interaction with Fe(III)PPIX to anchor the compound and allow for favourable hydrogen bonding interactions, thus resulting in an inability to cause β-haematin inhibition.

CHAPTER 6.

CONCLUSIONS AND FUTURE WORK

6.1 Conclusions

The aims of this project were to investigate coordination and π-stacking interactions with the target compound Fe(III)PPIX in order to optimise these underlying interactions together with hydrogen bonding in order to propose potential novel β-haematin formation inhibitors. These proposed compounds were then to be synthesised and activity against β-haematin formation tested to provide evidence for a hypothesised mechanism of action.

Investigation of coordination and π-stacking with Fe(III)PPIX provided useful insight into such interactions. Coordination is simply determined by basicity of the donor atom, while π-stacking is largely determined by the number of π-electrons in the aromatic ring. The results obtained from these investigations provided a general LFER equation which can be used to predict moderately accurate association constants of many small compounds with Fe(III)PPIX. This has provided a platform for the identification of novel scaffold molecules that can be further developed into β-haematin inhibitors.

Unfortunately, while identification of moderately strong Fe(III)PPIX associating molecules is seemingly a fairly trivial exercise, developing these scaffolds into β-haematin inhibitors, through incorporation of hydrogen bonding moieties, remains a challenge. This was observed in the current study where none of the three successfully synthesised compounds proposed as β-haematin inhibitors (compounds **A**, **B** and **C**) were in fact unable to inhibit β-haematin formation. Fortunately, a possible reason behind the inactivity of the compounds could be proposed, namely that of increased pK_a of the hydroxyl group upon substitution at the 9 position of the scaffold 9-hydroxyfluorene ring system which decreases the coordinating ability to the iron centre of Fe(III)PPIX. While the synthesised compounds are unable to inhibit β-haematin formation, the findings of this study suggest that the effect of substitutions on the pK_a of the coordinating group will need to be taken into account when designing further β-haematin inhibitors in the future.

6.2 Future work

Understanding interactions with Fe(III)PPIX is paramount for the rational design of β-haematin inhibitors and while this study has uncovered some information about two interactions, coordination and π-stacking, there remain areas that require further investigations. Firstly, a study on the effects of differing aromatic substituents and positions on π-stacking interactions with Fe(III)PPIX would prove an informative endeavour, as substituents that provide for favourable interactions could be incorporated into the template ring system. This would result in stronger interactions with Fe(III)PPIX which would provide for a more suitable anchor moiety onto which hydrogen bonding groups can be attached to interact with the propionate side chain and hence potentially inhibit β-haematin formation. Substituted benzoic acids, benzyl alcohols and pyridines are just some of the commercially available compounds that could be tested with Fe(III)PPIX in a similar study to that reported here, so as to provide insight into these effects. Secondly, a more detailed investigation into the enhanced associating ability of 4-aminoquinolines with Fe(III)PPIX is required, focusing primarily on charge-charge and cation-π interactions. By having a better understanding of these interactions, compounds can be proposed with a greater potential for inhibiting β-haematin formation.

While none of the three proposed compounds in this study which were successfully synthesised and isolated (**A**, **B** and **C**) were able to inhibit β-haematin formation, the scaffold molecule, 9-hydroxyflourene, remains of interest owing to its relatively strong association with Fe(III)PPIX. The findings of this work suggest that incorporation of the linker containing the hydrogen bonding group at the 9-position of the ring system is detrimental to coordination interactions. This could be possibly be alleviated by substitution of this moiety on the fluorene aromatic ring system instead. As an alternative to aromatic methanols, thought should be given to amine moieties as potential iron coordinators. As seen from this study, primary amines that can both coordinate and π-stack are not suitable as scaffold molecules probably because the preferred conformations results in only one of these interactions with Fe(III)PPIX occurring, nevertheless, by substituting bulky groups on the carbon adjacent to the amine, the conformation could possibly be locked to provide the geometry necessary for simultaneous coordination and π-stacking interactions with Fe(III)PPIX.

CHAPTER 7.

EXPERIMENTAL METHODOLOGIES

7.1 Physicochemical methods

7.1.1 General.

Unless otherwise stated, all compounds were purchased from Sigma-Aldrich and were of analytical grade. With the exception of imidazole and quinoline, they were used without further purification. Imidazole was recrystalised from toluene, while quinoline was vacuum distilled at 125 °C. Haemin was obtained from Fluka and used as received. Spectrophotometric titrations were recorded on Varian Cary 100 UV-vis spectrophotometer (manufacturer specifications report linearity up to 3 aufs) with quartz cuvettes of 1 cm pathlength. Temperature was maintained at 25.0 ± 0.2 °C throughout by means of a thermostatted water bath. Aliquots of ligand solutions were delivered into cuvettes using a Hamilton syringe, except in the case of 5-methylphenanthroline where Gilson pipettes were used as complexation to free metal in the Hamilton syringe was observed. Cuvettes were scrupulously washed with 0.2 M NaOH, followed by rinsing with water, then addition of 1 M HNO_3 and a final water rinsing, as previously described by Asher *et al.*[104], to avoid a buildup of adsorbed Fe(III)PPIX and PPIX.

7.1.2 Beers law studies.

Haematin (2 x 10^{-4} M, 20% (v/v) DMSO in methanol) and PPIX (1 x 10^{-4} M in DMSO) were titrated into the solvent systems of interest. Final composition of DMSO added in 40% (v/v) aqueous DMSO solvent system was 41.6%.

7.1.3 Spectrophotometric titrations.

Titrations with Fe(III)PPIX under aqueous DMSO conditions were carried out as detailed previously,[75, 84] deviating only in the use of a 1 x 10^{-5} M Fe(III)PPIX working solution. Titrations under organic conditions (20% DMSO in methanol) were carried out by preparing a stock solution of haematin (1 x 10^{-3} M in DMSO) which was then diluted to give 1 x 10^{-5} M in a 20% DMSO in methanol solution. Titrations with PPIX under aqueous conditions were carried out as for aqueous Fe(III)PPIX titrations but a stock solution of PPIX (6 x 10^{-4} M in DMSO) was used and diluted to give a working solution concentration of 3 x 10^{-6} M in 40% (v/v) aqueous DMSO. All stock solutions were stored in the dark and working solutions made up just before use.

Solutions of compounds tested were made up and pH corrected to 7.4, with concentrations ranging from 5 x 10^{-3} M to 2 M, depending on the strength of association with Fe(III)PPIX or PPIX and its solubility. Data obtained were corrected for dilution and analysed using non-linear least squares fitting methods at A_{max} (400 and 402 nm for Fe(III)PPIX and PPIX, respectively). Equations 2, 3 and 4 were considered in each case and the best fit was chosen. Titrations were performed in triplicate to give an average association constant and are reported with the standard error of the mean (SEM).

1:1
$$A = \frac{A_0 + A_\infty K[L]}{1 + K[L]} \quad (2)$$

2:1 stepwise
$$A = \frac{A_0 + A_1 K_1[L] + A_\infty K_1 K_2 [L]^2}{1 + K_1[L] + K_1 K_2 [L]^2} \quad (3)$$

2:1 cooperative
$$A = \frac{A_0 + A_\infty K[L]^2}{1 + K[L]^2} \quad (4)$$

Where K is the association constant, [L] is the free ligand concentration which in the case of weak association is approximately the concentration of ligand added, A is the observed absorbance, A_0 the initial absorbance, A_1 the absorbance of the intermediate (in the case of 2:1 stepwise complex) and A_∞ is the absorbance of the final complex formed in the presence of a very large excess of ligand.

7.1.4 pK_a determination.

A 9-aminofluorene hydrochloride solution (1 mM in water) was titrated with a 0.1 M NaOH solution and the pH measured after each addition using a glass electrode on a Crison MicropH 2000 pH meter. Data were analysed by a non-linear regression to give a measured pK_a. Experiments were repeated in triplicate to produce an average with SEM.

7.1.5 Molecular mechanics and dynamics (with simulated annealing) modelling.

Modelling of compounds bound to the iron centre of Fe(III)PPIX was performed using HYPERCHEM[136]. The force field employed was based on that of Allinger[137] as modified by Marques and co-workers[138, 139] for metalloporphyrins and further parameterised for metalloporphyrin-alkoxide interactions.[76] Proposed compounds were built in HYPERCHEM containing a protonated terminal hydrogen bond donor and Fe(III)PPIX was built with both propionate side chains deprotonated. Proposed compounds were then bonded to the iron centre of Fe(III)PPIX through the alkoxide group and geometry optimisation performed using molecular mechanics. In order to obtain the lowest energy conformation of the complex, molecular dynamics were then preformed with simulated annealing. Trajectories were calculated at a run time of 100 ps at 1000 K. For each complex, 1000 snapshots were recorded and simulated annealing (from 1000 to 0 K over 20 ps) of every 10^{th} snapshot was performed. The snapshot with the lowest energy conformation was then identified, and an intramolecular hydrogen bonded conformation between the hydrogen bond donor and propionate group was constrained using a dummy bond with a force constant of 100 000 mdyne/Å. Molecular mechanics were performed on this complex, after which the dummy bond was removed and further mechanics performed to optimise geometry. The single point energy of this conformation was compared to that of the lowest energy conformation. An energy surface map of compound **E** bound to Fe(III)PPIX was determined using the method reported by de Villiers *et al.*[76] The conformational strain energy as the complex was rotated (in 30 °C increments) around bonds, N2-Fe(III)-O(87)-C(74) and C(76)-C(24)-C(88)-C(89), defined as ϕ and ψ respectively, was measured. Plotting ϕ vs ψ produced the energy surface for the complex.

7.1.6 β-Haematin inhibition.

β-Haematin inhibition tests were carried out by modifying the pyridine colorimetric assay developed by Ncokazi and Egan.[44] The original procedure required the use of a 12.9 M acetate buffer (pH 4.8) but because of difficulties solubilising acetate, the concentration was lowered to 9.7 M (pH 4.8) and volumes of reagents adjusted accordingly. This less concentrated buffer was made by adding sodium acetate (47.5 g) to acetic acid (35.5 ml) and diluted to 100 ml with water with pre-incubation for 1 hour at 60 °C required for complete dissolution.

Serial dilutions of compounds in a 96 well plate were made by placing 20 µl of a stock solution (0.168 M) in the first well and 10 µl of solvent in the remaining wells. Removal of 10 µl from the first well and mixing into the second well provide a 1 in 2 dilution, and this was then repeated down the plate to give compound:Fe(III)PPIX rations of 10, 5, 2.5, 1.25, 0.625, 0.313 and 0.156 mole equivalents as well as a control with no compound added. To this, 83.6 µl of haematin (2.03×10^{-3} M in 0.1 M NaOH), 8.4 µl HCl (1 M) and 78 µl acetate buffer (9.7 M) were added to each well and mixed. The plate was incubated for 60 minutes at 60 °C after which the wells were quenched by addition of 80 µl of 30% (v/v) aqueous pyridine solution (2×10^{-2} M HEPES, pH 7.5) and allowed to settle. Once settled, 38 µl of the supernatant was removed and placed in another 96 well plate. These were diluted with 250 µl of the aqueous pyridine solution, absorbances read at 405 nm and the data obtained fitted to a sigmoidal dose response model.

7.2 Synthesis

7.2.1 General.

All chemicals and solvents were purchased from Sigma-Aldrich and, unless otherwise stated, used as received. Tetrahydrofuran and diethyl ether were distilled under a nitrogen atmosphere and dried over sodium wire with benzophenone. Dichloromethane was distilled under nitrogen atmosphere and dried over phosphorous pentoxide. Reactions were monitored by thin-layer chromatography (TLC) using pre-coated silica-gel 60 F_{254} (0.2 mm) mounted on aluminium-backed plates, commercially available from Merck. Compounds were detected using UV absorption (254 nm) and spray reagents anisaldehyde and ninhydrin, prepared according to literature.[140] Column chromatography was conducted using Merck Kieselgel 60 silica gel. Flash chromatography was performed using a Suplco VersaFlush.

Nuclear magnetic resonance spectra were recorded on either a Varian Unity 400 (at 399.95 MHz for ^{1}H and 100.58 MHz of ^{13}C) or Varian VXR-300 (at 300.08 MHz for ^{1}H and 75.5 MHz for ^{13}C). Solvents used were d-$CDCl_3$, d_6-DMSO, d_4-CD_3OD and D_2O with residual peaks occurring at 7.26, 2.50, 3.31 and 7.79 ppm in ^{1}H NMR and 77.16, 39.52 and 49.00 ppm in ^{13}C NMR, respectively.[141] All chemical shifts are reported in ppm and coupling constants in Hz.

Infrared (IR) spectra were recorded on a Perkin-Elmer Paragon 1000 FT-IR spectrophotometer, using potassium bromide plates. Elemental analysis (EA) was performed using a Fisons EA 1108 CHN elemental analyser. Melting points were determined using a Reichert Jung Thermovar hot-stage microscope. Electron ionisation (EI) mass spectrometry was recorded on a JEOL GCmate II at the Department of Chemistry, University of Cape Town and high resolution mass spectrometry (HRMS) was recorded on an API Q-TOF Ultima machine at The School of Chemistry, University of Stellenbosch.

7.2.2 4-Quinonline methanol, **22.**

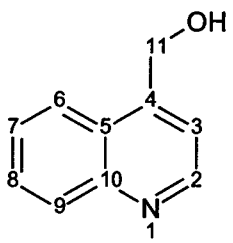

To a solution of 4-quinoline carboxaldehyde (0.158 g, 1.00 mmol) in ethanol (15 ml), sodium borohydride (0.077 g, 2.04 mmol) was added slowly at room temperature. The reaction was left stirring for 1.5 hours after which TLC (MeOH/DCM, 5:95, R_f = 0.29) indicated no starting material remained. Et_2O (25 ml) was then added, followed by washing with water (2 x 25 ml). Aqueous washings were combined and extracted with Et_2O (2 x 50 ml). All organic fractions were then pooled, dried over magnesium sulfate, filtered and the filtrate evapourated under reduced pressure. The resulting brown crystals obtained were recrystalised using Hex/EtOAc to give white crystals identified as compound **22** (0.037 g, 67%) by NMR spectrometry. m.p. 91-93 °C (Lit:[114] 99-100 °C). ^{1}H NMR (400 MHz, d-$CDCl_3$): δ_H 5.24 (2H, s, H-11), 7.55 (2H, m, H-3 and -7), 7.72 (1H, t, J = 7.1 Hz, H-8), 7.96 (1H, d, J = 8.3 Hz, H-9), 8.13 (1H, d, J = 8.4 Hz, H-6), 8.84 (1H, d, J = 4.4 Hz, H-2); ^{13}C NMR (100 MHz, d-$CDCl_3$): δ_C 61.4 (C-11), 118.2 (C-3), 122.9 (C-6), 125.9 (C-4), 126.7 (C-7), 129.3 (C-9), 129.9 (C-8), 146.5 (C-5), 147.7 (C-10), 150.3 (C-2). MS (EI): Found 158.9435 ($[M]^+$). $C_{10}H_9NO$ requires 159.1846 ([M]).

7.2.3 *Spiro[fluorene-9,2'-oxirane]*, **26**.

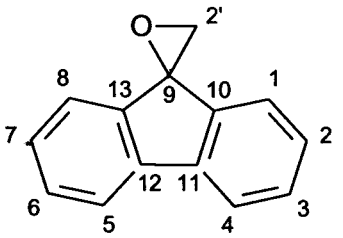

To sodium hydride (60% oil immersion, 0.266 g, 6.65 mmol) in dry DMSO (5 ml), trimethylsulfoxonium iodide (1.47 g, 6.72 mmol) was slowly added and the mixture left to stir at room temperature for 30 minutes. 9-Fluorenone (0.989 g, 5.49 mmol) was then slowly added and the reaction mixture left to stir for a further 1.5 hours, after which TLC (EtOAc/Hex, 5:95, R_f = 0.45) indicated no starting material remained. Ice water (10 ml) was added to quench the reaction and an extraction with Et_2O (2 x 15 ml) followed. Organic layers were washed with cold water (2 x 30 ml), dried over $MgSO_4$, filtered and the filtrate reduced under vacuum at 25 °C. The resulting yellow/white solid obtained was identified as the epoxide **26** (0.672 g, 98% crude) and was used in its impure form in subsequent reactions. m.p. 56-58 °C (Lit:[142] 108-110 °C). ^{1}H NMR (300 MHz, d-$CDCl_3$): δ_H 3.71 (2H, s, H-2'), 7.27 (4H, m, H-2, -4, -5 and -7), 7.43 (2H, t, *J* = 7.0 Hz, H-3 and -6), 7.73 (2H, d, *J* = 7.5 Hz, H-1 and -8); ^{13}C NMR (100 MHz, d-$CDCl_3$): δ_C 54.9 (C-2'), 62.3 (C-9), 120.4 (C-4 and -5), 121.7 (C-1 and -8), 127.6 (C-2 and -7), 129.4 (C-3 and -6), 140.9 (C-11 and -12), 141.1 (C-10 and -13). MS (EI): Found 193.9588 ($[M]^+$). $C_{14}H_{10}O$ requires 194.2286 ([M]).

7.2.4 9-Hydroxy-fluorene-9-acetonitrile, 25.

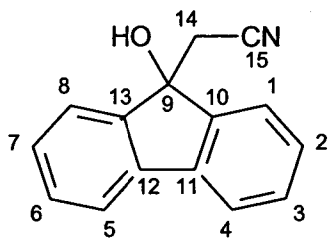

To crude spiro[fluorene-9,2'-oxirane] (2.50 g, 12.5 mmol) in methanol (32 ml), sodium cyanide (3.15 g, 64.3 mmol), ammonium chloride (2.08 g, 38.8 mmol) and water (4 ml) were added at room temperature. The mixture was left to stir overnight (14 hours) at 25 °C, after which TLC (EtOAc/Hex, 20:80, R_f = 0.26) indicated no starting material remained. The mixture was then diluted with water (24 ml), extracted with Et_2O (3 x 50 ml), washed with water (2 x 100 ml) and the organic layers dried over $MgSO_4$. After filtration, the filtrate was reduced under vacuum and the resulting orange oil purified using column chromatography (SiO_2, EtOAc/Hex, 10:90 to 20:80) to give the compound **25** as a white solid (1.58 g, 65% over 2 steps). m. p. 93-95 °C (Lit:[143] 97.5-98.5 °C). ν_{max} /cm^{-1} (KBr): 3340b (O-H), 3066w + 3044w (C-H, aromatic), 2957m + 2928m (C-H, aliphatic), 2257m (CN, nitrile), 1607m (C=C, aromatic); ^{1}H NMR (400 MHz, d-$CDCl_3$): δ_H 2.34 (1H, bs, OH), 2.98 (2H, s, H-14), 7.38 (2H, t, *J* = 7.3 Hz, H-2 and -7), 7.46 (2H, t, *J* = 7.4 Hz, H-3 and -6), 7.67 (2H, d, *J* = 7.4 Hz, H-4 and -5), 7.73 (2H, d, *J* = 7.2 Hz, H-1 and -8); ^{13}C NMR (400 MHz, d-$CDCl_3$): δ_C 29.4 (C-14), 78.1 (C-9), 116.7 (C-15), 120.4 (C-4 and -5), 123.6 (C-1 and -8), 128.5 (C-2 and -7), 130.1 (C-3 and -6), 139.0 (C-11 and -12), 145.9 (C-10 and -13). MS (EI): Found 220.5823 ([M]$^+$). $C_{15}H_{11}NO$ requires 221.2539 ([M]).

7.2.5 9-(2-Aminoethyl)-fluoren-9-ol, A.

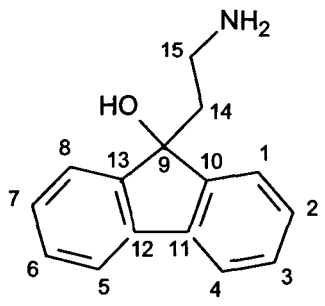

To (9-hydroxy-9H-fluoren-9-yl)acetonitrile (0.73 g, 3.32 mmol) in dry Et_2O (20 ml) at 0 °C, lithium aluminium hydride (0.25 g, 6.64 mmol) was slowly added. The reaction mixture was then left to warm to a temperature of roughly 10 °C over 2 hours, after which, the temperature was increased to 25 °C and the reaction mixture left for 22 hours. TLC (EtOH/DCM, 10:90, R_f = baseline) indicated no starting material remained and so NaOH (2 M, 10 ml) was slowly added at 0 °C. The organic layer was separated and an extraction of the aqueous layer with DCM (3 x 20 ml) followed. All organic fractions were combined, washed with water (1 x 40 ml), dried over $MgSO_4$ and filtered. The filtrate was then reduced under vacuum to give a yellow oil. This was purified using flash chromatography (MeOH/DCM, 0:100 to 15:85) and the tan coloured oil obtained washed with Et_2O to give a white solid identified as the *amine* (0.51 g, 68%). m. p. 105-107 °C. ν_{max} /cm^{-1} (KBr): 3340b (OH), 3054w (C-H, aromatic), 2985m + 2931m (C-H, aliphatic), 1265s (C-N, amine); ^{1}H NMR (300 MHz, d-$CDCl_3$): δ_H 2.03 (2H, t, J = 7.3 Hz, H-14), 2.68 (2H, t, J = 7.4 Hz, H-15), 7.19 – 7.32 (4H, m, H-2, -3, -6 and -7), 7.45 (2H, d, J = 7.4 Hz, H-4 and -5), 7.54 (2H, d, J = 7.3 Hz, H-1 and -8); ^{13}C NMR (100 MHz, d-$CDCl_3$): δ_C 38.0 (C-14), 44.0 (C-15), 82.1 (C-9), 119.9 (C-4 and -5), 123.8 (C-1 and -8), 127.8 (C-2 and -7), 128.7 (C-3 and -6), 139.1 (C-11 and -12), 149.0 (C-10 and -13). HRMS (ESI): Found 226.1248 ([M+H]$^+$). $C_{15}H_{15}NO$ requires 225.2857 ([M]).

7.2.6 1-[2-(9-Hydroxy-fluoren-9-yl)ethyl]guanidinium nitrate, B.

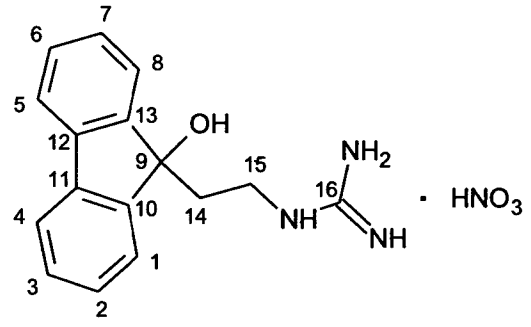

To 9-(2-aminoethyl)-9H-fluoren-9-ol (0.22 g, 0.99 mmol) in methanol (8 ml), 3,5-dimethyl-pyrazole-1-carboximidamidium nitrate (0.20 g, 0.99 mmol) was added and the mixture left to reflux for 14 hours. TLC (MeOH/DCM, 10:90, R_f = 0.16) showed product formation and no starting material remaining. The reaction mixture was concentrated under reduced pressure and the resulting tan oil was subjected to flash chromatography (SiO_2, EtOH/MeOH/DCM, 5:0:95 to 0:10:90). The clear oil obtained still contained impurities and so was subjected to further column chromatography (SiO_2, MeOH/DCM, 0:100 to 5:95 and then EtOH/DCM, 0:100 to 15:85) resulting in the isolation of the pure *guanidine* product in the form of a white solid (0.21 g, 64%). m. p. 150-153 °C. ν_{max} /cm^{-1} (KBr): 3342b (OH), 2964m + 2920m (C-H, aliphatic), 1665s (C=N, guanidine). ^{1}H NMR (400 MHz, d_4-CD_3OD): δ_H 2.36 (2H, t, J = 7.2 Hz, H-14), 3.02 (2H, t, J = 7.8 Hz, H-15), 7.34 (2H, t, J = 7.2 Hz, H-2 and -7), 7.39 (2H, t, J = 7.3 Hz, H-3 and -6), 7.55 (2H, d, J = 6.9 Hz, H-4 and -5), 7.71 (2H, d, J = 7.6 Hz, H-1 and -8); ^{13}C NMR (100 MHz, d_4-CD_3OD): δ_C 39.7 (C-14), 40.4 (C-15), 82.4 (C-9), 121.9 (C-4 and -5), 125.4 (C-1 and -8), 129.8 (C-2 and -7), 130.9 (C-3 and -6), 141.5 (C-11 and -12), 150.2 (C-10 and -13), 159.0 (C-16). HRMS (ESI): Found 268.1443 ([M+H]$^+$). $C_{16}H_{17}N_3O$ requires 267.327 ([M]). Anal. Calcd for $C_{16}H_{18}N_4O_4 \cdot 0.4H_2O$: C, 55.89; H, 5.72; N, 16.29. Found: C, 55.89; H, 5.53; N, 17.32.

7.2.7 9-[(Trimethylsilyl)oxy]-fluorene-9-carbonitrile, 30.

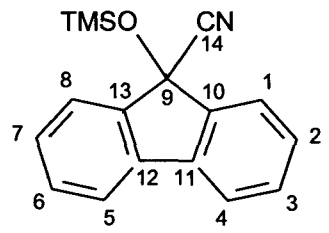

To a mixture of fluorenone (1.98 g, 11.0 mmol) and iodine (0.14 g, 0.6 mmol) in dry DCM (50 ml) under nitrogen atmosphere, trimethylsilyl cyanide (2 ml, 14.9 mmol) was slowly added at 0 °C. The reaction was then left to stir at room temperature for 2 hours, after which TLC (EtOAc/Hex, 10:90, R_f = 0.54) indicated no starting material remained. The reaction mixture was then quenched with water (50 ml) and extracted with DCM (2 x 50 ml). Organic layers were pooled, washed with 15% sodium thiosulfate (100 ml) and dried over sodium sulfate. This was then filtered and the filtrate removed under reduced pressure to give yellow/white crystals. These were washed with hexane to give product **30** (0.836 g, 27%) as white crystals in high purity. m.p. 91-93 °C (Lit:[120] 98-100 °C). ν_{max} /cm^{-1} (KBr): 3080m to 3012m (C-H, aromatic), 2964s + 2902m (C-H, aliphatic), 2238s (CN, nitrile); ^{1}H NMR (300 MHz, d-$CDCl_3$): δ_H 7.39 (2H, t, J = 7.5 Hz, H-2 and -7), 7.47 (2H, t, J = 7.5 Hz, H-3 and -6), 7.65 (2H, d, J = 7.4 Hz, H-4 and -5), 7.73 (2H, d, J = 7.5 Hz, H-1 and -8); ^{13}C NMR (100 MHz, d-$CDCl_3$): δ_C 1.3 (TMSO), 53.4 (C-9), 120.2 (C-14), 120.6 (C-4 and -5), 125.5 (C-1 and -8), 128.8 (C-2 and-7), 131.0 (C-3 and -6), 139.6 (C-11 and -12), 143.1 (C-10 and -13).

7.2.8 9-*(Azidomethyl)-fluoren-9-ol*, 31.

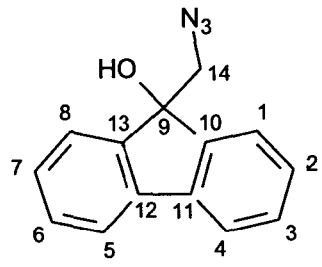

To a mixture of spiro[fluorene-9,2'-oxirane] (2.03 g, 10.4 mmol) and ammonium chloride (1.50 g, 28.1 mmol) in MeOH/H_2O (8:1, 27 ml), sodium azide (3.09 g, 47.5 mmol) was added and the mixture left to stir at room temperature for 16 hours. TLC (EtOAc/Hex, 20:80, R_f = 0.29) indicated no starting material remained, so water (23 ml) was added to the reaction mixture and an extraction with Et_2O (2 x 50 ml) followed. Organic layers were washed with water (2 x 100 ml) and dried over $MgSO_4$. After filtration, the filtrate was reduced under vacuum to give a pale yellow oil identified as the *azide* **14** (2.43 g, 98%) which was pure enough to be used in subsequent reactions. ν_{max} /cm^{-1} (Thin layer): 3392b (O-H), 3058w (C-H, aromatic), 2924w (C-H, aliphatic), 2106s (N_3, azide), 1607w (C=C, aromatic); ^{1}H NMR (400 MHz, d-$CDCl_3$): δ_H 3.85 (2H, s, H-14), 7.38 (2H, t, *J* = 7.5 Hz, H-2 and -7), 7.47 (2H, t, *J* = 7.5 Hz, H-3 and -6), 7.64 (2H, d, *J* = 7.5 Hz, H-4 and -5), 7.73 (2H, d, *J* = 7.5 Hz, H-1 and -8); ^{13}C NMR (100 MHz, d-$CDCl_3$): δ_C 65.8 (C-9), 68.0 (C-14), 120.4 (C-4 and -5), 124.7 (C-1 and -8), 128.1 (C-2 and -7), 129.8 (C-3 and -6), 140.4 (C-11 and -12), 142.7 (C-10 and -13). MS (EI): Found 237.0096 ($[M]^+$). $C_{14}H_{11}N_3O$ requires 237.2566 ([M]).

7.2.9 9-(Aminomethyl)-fluoren-9-ol, C

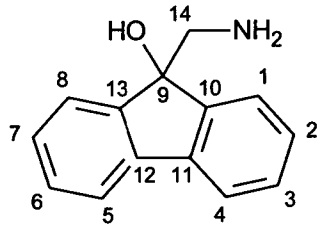

To 9-(azidomethyl)-fluoren-9-ol (0.37 g, 1.56 mmol) in a MeCN/H_2O (16 ml, 7:1) solution, triphenylphosphine (0.49 g, 1.88 mmol) was added and the mixture left to stir at room temperature for 14 hours. TLC (MeOH/DCM, 5:95, R_f = 0.41) indicated no starting material remained and so the reaction mixture was concentrated under reduced pressure and the resulting dark brown oil purified using column chromatography (SiO_2, MeOH/DCM, 1:99 to 5:95). To the yellow oil obtained, Et_2O was slowly added which caused precipitation of a white solid. The solid was filtered, washed with Et_2O and kept aside. Washings were reduced under vacuum and the procedure repeated again to give more white precipitate. All solid was pooled and identified as the amine **C** (0.21 g, 64%). m.p. 117-118 °C (Lit:[144] 134-135 °C). ^{1}H NMR (300 MHz, d-$CDCl_3$): δ_H 2.43 (3H, bs, -OH and -NH_2), 3.70 (2H, s, H-14), 7.30 (2H, t, *J* = 7.4 Hz, H-2 and -7), 7.38 (2H, t, *J* = 7.4 Hz, H-3 and -6), 7.58 (2H, d, *J* = 7.7 Hz, H-4 and -5), 7.68 (2H, d, *J* = 7.5 Hz, H-1 and -8); ^{13}C NMR (100 MHz, d-$CDCl_3$): δ_C 65.8 (C-9), 69.2 (C-14), 120.1 (C-4 and -5), 123.8 (C-1 and -8), 127.7 (C-2 and -5), 128.6 (C-3 and -6), 139.6 (C-11 and -12), 148.8 (C-10 and -13). MS (EI): Found 210.9317 ([M]$^+$). $C_{14}H_{13}NO$ requires 211.2591 ([M]).

7.2.10 Formamidinesulfonic acid, **33.**

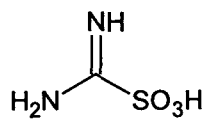

Formamidinesulfinic acid (2.00 g, 18.5 mmol) in acetic acid (6 ml), was chilled to roughly 10 °C and peracetic acid (4.8 ml, 25.4 mmol) slowly added so as to maintain the temperature under 20 °C. After addition, the reaction was left to stir at roughly 15 °C for 1 hour and room temperature for 2 hours. The precipitate formed was filtered and washed with ethanol to give formamidinesulfonic acid as a white solid (1.84 g, 80%). ν_{max} /cm^{-1} (KBr): 3353b and 3129b (N-H), 1688s (C=N), 1228s and 1054m (SO_3H). MS (EI): Found 125.5359 ([M+H]$^+$). $CH_4N_2O_3S$ requires 124.1191 ([M]).

7.2.11* 7-*Nitro*-1,3,5-*azaadamantane,* 38*: Method a.

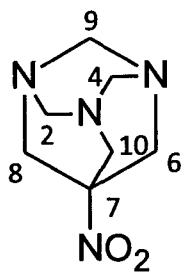

To a solution of hexamethylenetatramine (14.02 g, 0.10 mol) and glacial acetic acid (6.25 ml, 0.12 mol) in *n*-butanol (15 ml), nitromethane (6.5 ml, 0.12 mol) was slowly added at room temperature. The mixture was left to reflux at 109 °C for 4 hours after which TLC (MeOH/DCM, 10:90, R_f = 0.50) indicated no starting material remained and the resulting precipitate was filtered. A recrystalisation from water produced a dark brown solid which floated on the surface of the water and a tan colour solid which lay on the bottom of the recrystalisation vessel. The tan coloured crystals were collected and identified as compound **38** (2.21 g, 12%) by NMR and mass spectrometry (see 7.2.12 for details). m.p. 166-168 °C (Lit:[130] 260-310 °C).

7.2.12 7-*Nitro*-1,3,5-*azaadamantane*, **38**: *Method b*.

To a solution of hexamethylenetatramine (10.00 g, 71.3 mmol) in glacial acetic acid (10 ml, 184.0 mmol), nitromethane (4.25 ml, 79.1 mmol) was slowly added at room temperature. The mixture was left to reflux at 95 °C for 6 hours, after which the resulting precipitate was filtered and washed with copious amounts of water. The precipitate was collected and dried under vacuum to give tan crystals of product **7** (13.1 g, 53%) which were deemed pure enough for subsequent reactions. m.p. 183-185 °C (Lit:[130] 260-310 °C). ^{1}H NMR (300 MHz, D_2O): δ_H 3.82 (6H, s, H-6, -8, -10), 4.10 (3H, d, J = 6.0 Hz), 4.43 (3H, d, J = 12.9 Hz); ^{13}C NMR (100 MHz, D_2O): δ_C 57.4 (C-6, -8, -10), 70.9 (C-2, -4, -9), 72.8 (C-7). MS (EI): Found 184.0449 ($[M]^+$). $C_7H_{12}N_4O_2$ requires 184.1958 ([M]).

7.2.13 7-*Amino*-1,3,5-*azaadamantane*, **37**.

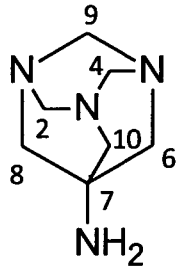

To 7-nitro-1,3,5-azaadamantane (23.17 g, 126.0 mmol) and Raney Nickel (50% in water, 3.59 g) in a water/isopropanol (14:1, 34 ml) solution, hydrazine monohydrate (0.6 ml, 12.37 mmol) was slowly added in portions over a 1 hour period. Upon completion of addition, the reaction mixture was left to stir at room temperature for an hour after which another portion of Raney Nickel (1.01 g) in a water/isopropanol mixture (14:1, 2 ml) was added. The reaction left to stir for a further 2 hours after which TLC (MeOH/DCM, 10:90, baseline) indicated no starting material remained. The mixture was then filtered to remove Raney Nickel, washed with isopropanol and the filtrate reduced under vacuum to give the hygroscopic tan coloured solid **37** (11.83 g, 61%). m. p. 139-144 °C (dec.). (Lit:[127] 295-297 °C) ^{1}H NMR (400 MHz, D_2O): δ_H 3.15 (6H, s, H-6, -8, -10), 3.98 (3H, d, J = 12.1 Hz), 4.33 (3H, d, J = 12.5 Hz); ^{13}C NMR (400 MHz, D_2O): δ_C 38.4 (C-7), 61.4 (C-6, -8, -10), 70.9 (C-2, -4, -9). MS (EI): Found 154.0955 ($[M]^+$). $C_7H_{14}N_4$ requires 154.2129 ([M]).

7.2.14 7-Bromo-1,3,5-azaadamantane, **36.**

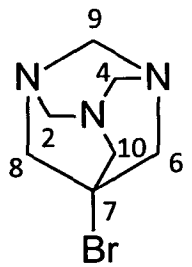

To 7-amino-1,3,5-azaadamantane (0.99 g, 6.45 mmol) suspended in aqueous hydrogen bromide (48%, 4.6 ml) at 0 °C, sodium nitrite (0.55 g, 7.93 mmol) was slowly added over 30 minutes. Once addition was completed, the reaction was allowed to gradually reach room temperature and was left to stir for 3 hours. Potassium carbonate was then added to the reaction mixture until effervescence ceased (*ca.* pH 8) and an extraction with DCM (3 x 40 ml) followed. The organic layers (top layers) were pooled, dried with $MgSO_4$, filtered and the filtrate reduced under vacuum. The resulting yellow solid obtained was then washed with Et_2O, filtered and kept aside. The filtrate was collected, reduced and washing repeated twice more. All solid material obtained was combined to give the bromide **36** (0.84 g. 60%). m. p. > 295 °C (Lit:[127] 217-219 °C). ^{1}H NMR (300 MHz, D_2O): δ_H 3.79 (6H, s, H-6, -8, -10), 4.26 (3H, d, J = 11.6 Hz), 4.51 (3H, d, J = 12.8 Hz); ^{13}C NMR (100 MHz, D_2O): δ_C 57.7 (C-7), 65.5 (C-6, -8, -10), 73.1 (C-2, -4, -9). MS (EI): Found 218.7651 ($[M]^+$). $C_7H_{12}BrN_3$ requires 218.0942 ([M]).

CHAPTER 8.

REFERENCES

REFERENCES

(1) J. N. Hays, in *Epidemics and Pandemics: Their Impacts on Human History*, ABC CLIO, Santa Barbra, 2005, pp 457-464.

(2) L. M. Prescott, J. P. Harley and D. A. Klein, in *Microbiology*, McGraw-Hill, New York, sixth edition, 2005, pp 929-931.

(3) E. Korenromp, J. Miller, B. Nahlen, T. Wardlaw and M. Young, *World Malaria Report 2005*, WHO Global Malaria Programme, WHO Library Cataloguing-in-Publication Data, Geneva, 2005.

(4) K. J. Arrow and C. B. Panosian, in *Saving Lives, Buying Time: Economics of Malaria Drugs in an Age of Resistance*, ed. H. Gelband, The National Academies Press, Washington, 2004, pp 23-26, 136-140.

(5) http://www.nathnac.org/includes/contents/documents/malariamap.gif, accessed 30 November 2009.

(6) N. A. Campbell and J. B. Reece, in *Biology*, Banjamin Cummings, San Francisco, sixth edition, 2002, pp 557-558.

(7) G. Jiang, M. Shi, S. Conteh, N. Richie, G. Banania, H. Geneshan, A. Valencia, P. Singh, J. Aguiar, K. Limbach, K. I. Kamrud, J. Rayner, J. Smith, J. T. Bruder, C. R. King, T. Tsuboi, S. Takeo, Y. Endo, D. L. Doolan, T. L. Richie and W. R. Weiss, *PLOS one*, 2009, **4**, e6659.

(8) P. H. Raven, G. B. Johnson, in *Biology*, Times Mirror/Mosby College Publishing, St. Louis, second edition, 1989, pp. 625-266.

(9) M. Aregawi, R. Cibulskis, M. Otten, R. Williams and C. Dye, *World Malaria Report 2008*, WHO Global Malaria Programme, WHO Library Cataloguing-in-Publication Data, Geneva, 2008.

(10) P. Olliaro, *Pharmacol. Therapeut.*, 2001, **89**, 207-219.

(11) G. Padmanaban, V. A. Nagaraj and P. N. Rangarajan, *Curr. Sci.*, 2007, **92**, 1545-1555.

(12) H. J. Painter, J. M. Morrisey, M. W. Mather and A. B. Vaidya, *Nature*, 2007, **446**, 88-91.

(13) U. Eckstein-Ludwig, R. J. Webb, I. D. A. van Goethem, J. M. East, A. G. Lee,M. Kimura, P.M. O'Neill, P. G. Bray, S. A. Ward and S. Krishna, *Nature*, 2003, **424**, 957-961.

(14) A. C. Chou, R. Chevli and C. D. Fitch, *Biochemistry*, 1980, **19**, 1543-1549.

(15) Y. Sugioka, M. Suzuki, K. Sugioka and M. Nakano, *FEBS Lett.*, 1987, **223**, 251-254.

(16) M. Mungthin, P. G. Bray, R. G. Ridley and S. A Ward, *Antimicrob. Agents Chemother.*, 1998, **42**, 2973-2977.

(17) J. Ziegler, R. Linck and D.W. Wright, *Curr. Med. Chem.*, 2001, **8**, 171-189.

(18) R. C. San George, R. L. Nagel and M. E. Fabry, *Biochim. Biophys. Acta*, 1984, **803**, 174-181.

(19) M. Foley and L. Tilley, *Int. J. Parasitol.*, 1997, **27**, 231-240.

(20) T. J. Egan, *S. Afr. J. Sci.*, 2002, **98**, 411-412.

(21) D. A. Elliott, M. T. McIntosh, H. D. Hosgood III, S. Chen, G. Zhang, P. Baevova and K. A. Joiner, *Proc. Natl. Acad. Sci. USA.*, 2008, **105**, 2463-2468.

(22) T. J. Egan, J. M. Combrink, J. Egan, G. R. Hearne, H. M. Marques, S. Nteteni, B. T. Sewell, P. J. Smith, D. Taylor, D. A. van Schalkwyk and J. C. Walden, *Biochem. J.*, 2002, **365**, 343-347.

(23) C. Slomianny, *Blood Cells*, 1990, **16**, 369-378.

(24) E. Hempelmann, C. Motta, R. Hughes, S. A. Ward and P. G. Bray, *Trends Parasitol.*, 2003, **19**, 23-26.

(25) R. Hayward, K. J. Saliba and K. Kirk, *J. Cell Sci.* 2006, **119**, 1016-1025.

(26) D. J. Krogstad, P. H. Schlesinger and I. Y. Gluzman, *J. Cell Biol.*, 1985, **101**, 2302-2309.

(27) R. Banerjee, J. Liu, W. Beatty, L. Pelosof, M. Klemba and D. E. Goldberg, *Proc. Natl. Acad. Sci. USA*, 2002, **99**, 990-995.

(28) P.J. Rosenthal, P.S. Sijwali, A. Singh and B.R. Shenai, *Curr. Pharm. Des.*, 2002, **8**, 1659-1672.

(29) K. K. Eggleson, K. L. Duffin and D. E. Goldberg, *J. Biol. Chem.*, 1999, **274**, 32411-32417.

(30) D. E. Goldberg, *Semin. Cell Biol.*, 1993, **4**, 355-361.

(31) T. J. Egan, *Targets*, 2003, **2**, 115-124.

(32) T. J. Egan, *Mol. Biochem. Parasitol.* 2008, **157**, 127-136.

(33) H. Ladan, Y. Nitzan and Z. Malik, *FEMS Microbiol. Lett.*, 1993, **112**, 173-177.

(34) S. Pagola, P. W. Stephens, D. S. Bohle, A. D. Kosar, and S. K. Madsen, *Nature*, 2000, **404**, 307-310.

(35) D. J. Sullivan, I. Y. Gluzman and D. E. Goldberg, *Science*, 1996, **271**, 219-222.

(36) A. Dorn, R. Stoffel, H. Matile, A. Bubendorf and R. G. Ridley, *Nature*, 1995, **374**, 269-271.

(37) K. Bendrat, B. J. Berger and A. Cerami, *Nature*, 1995, **378**, 138-139.

(38) I. Coppens and O. Vielemayer, *Int. J. Parasitol.*, 2005, **35**, 597-615.

(39) J. M. Pisciotta, I. Coppens, A. K. Tripathi, P. F Scholl, J. Shuman, S. Bajad, V. Shulaev, and D. J. Sullivan, *Biochem. J.*, 2007, ***402***, 197-204.

(40) J. B. R. Corrêa Soares, C. M. Maya-Monterio, P. R. B. Bittencourt-Cunha, G. C. Atella, F. A. Lara, J. C. P. d'Avila, D. Menezes, M. A. Vannier-Santos, P. L. Oliveira, T. J. Egan and M. F. Oliveira, *FEBS Lett.*, 2007, **581**, 1742-1750.

(41) T. J. Egan, J. Y-J. Chen, K. A. de Villiers, T. E. Mabotha, K. J. Naidoo, K. K. Ncokazi, S. J. Langford, D. McNaughton, S. Pandiancherri and B. R. Wood, *FEBS Lett*, 2006, **580**, 5105-5110.

(42) K. A. de Villiers, C. H. Kaschula, T. J. Egan and H. M. Marques, *J. Biol. Inorg. Chem.* 2007, **12**, 101-117.

(43) S. R. Hawley, P. G. Bray, M. Mungthin, J. D. Atkinson, P. M. O'Neill and S. A. Ward, *Antimicrob. Agents Chemother.*, 1998, **42**, 682-686.

(44) K. K. Ncokazi and T. J. Egan, *Anal. Biochem.*, 2005, **338**, 306-319.

(45) J. E. Hyde, *FEBS J.*, 2007, **274**, 4688-4698.

(46) M. Adjuik, A. Babiker, P. Garner, P. Olliaro, W. Taylor and N. White, *Lancet*, 2004, **363**, 9-17.

(47) A. Ogbonna and C. J. Uneke, *T. Roy. Soc. Trop. Med. H.*, 2008, **102**, 621-627.

(48) B. Greenwood and T. Mutabingwa, *Nature*, 2002, **415**, 670-672.

(49) D. Menard, M. D. Matsika-Claquin, D, Djalle, F. Yapou, A. Manirakiza, V. Dolmazon, J. Sarda and A. Talarmin, *Am. J. Trop. Med. Hyg.*, 2005, **73**, 616-621.

(50) C. Sisowath, J. Stromberg, A. Martensson, M. Msellem, C. Obondo, A. Bjorkman and J. P. Gil, *J Infect. Dis.*, 2005, **191**, 1014-1017.

(51) C. Dokomajilar, S. L. Nsobya, B. Greenhouse, P. J. Rosenthal and G. Dorsey, *Antimicrob. Agents Chemother.*, 2006, **50**, 1893-1895.

(52) C. D. Fitch, *Science*, 1970, **169**, 289-290.

(53) D. J. Krogstad and P. H. Schlesinger, *N. Engl. J. Med.*, 1987, **317**, 542-549.

(54) C. A. Homewood, D. C. Warhurst, N. Peters and C. Baggaley, *Nature*, 1972, **235**, 50-52.

(55) D. J. Krogstad, I. Y. Gluzman, D. E. Kyle, A. M. Oduola, S. K. Martin, W. K. Milhous and P. H. Schlesinger, *Science*, 1987, **238**, 1283-1285.

(56) D. C. Warhurst, *Curr. Sci. India*, 2007, **92**, 1556-1560.

(57) S. K. Martin, A. M. Oduola and W. K. Milhous, *Science*, 1987, **235**, 899-901.

(58) R. E. Martin, R. V. Marchetti, A. I. Cowan, S. M. Howitt, S. Bröer and K. Kirk, *Science*, 2009, **325**, 1680-1682.

(59) V. Lakshmanan, P. G. Bray, D. Verdier-Pinard, D. J. Johnson, P. Horrocks, R. A Muhle, G. E. Alakpa, R. H. Hughes, S. A. Ward, D. J. Krogstad, A. B. S. Sidhu and D. A Fidock, *EMBO J.*, 2005, **24**, 2294-2305.

(60) D. C. Warhurst, J. C. Craig and I. S. Adagu, *Lancet*, 2002, **360**, 1527-1529.

(61) C. M. Wilson, A. Serrano, A. Wasley, M. P. Bogenschutz, A. H. Shankar and D. F. Wirth, *Science*, 1989, **244**, 1184-1186.

(62) S. A. Peel, P. Brigh, B. Yount, J. Handy and R. S. Baric, *Am. J. Trop.Med. Hyg.*, 1994, **51**, 648-658.

(63) D. Barnes, S. Foote, D. Galatis, D. Kemp and A. F. Cowman, *EMBO J.*, 1992, **11**, 3067-3075.

(64) S. C. Chaiyaroj, A. Buranakiti, P. Angkasekwinai, S. Looressuwan and A. F. Cowman, *Am. J. Trop. Med. Hyg.*, 1999, **61**, 780-783.

(65) M. G. Zalis, L. Pang, M. S. Silveira, W. K. Milhous and D. F. Wirth, *Am. J. Trop. Med. Hyg.*, 1998, **58**, 630-637.

(66) M. T. Duraisingh and P. Refour, *Mol. Microbiol.*, 2005, **57**, 874–877.

(67) R. A. Cooper, K. D. Lane, B. Deng, J. Mu, J. J. Patel, T. E. Wellems, X. Su, M. T. Ferdig, *Mol. Microbiol.*, 2007, **63**, 270-282.

(68) P. L. Olliaro and Y. Yuthavong, *Pharmacol. Ther.*, 1999, **81**, 91-110.

(69) R. Buller, M. L. Peterson, Ö. Almarsson and L. Leiserowitz, *Cryst. Growth Des.*, 2002, **2**, 553-562.

(70) S. Moreau, B. Perly, C. Chachaty and C. Deleuze, *Biochimie.*, 1982, **64**, 1015-1025.

(71) P. M. O'Neill, D. J. Willock, S. R. Hawley, P. G. Bray, R. C. Storr, S. A. Ward and B. K. Park, *J. Med. Chem.*, 1997, **40**, 437-448.

(72) D. C. Warhurst, *Biochem. Pharmacol.*, 1981, **30**, 3323-3327.

(73) D. V. Behere and H. M. Goff, *J. Am. Chem. Soc.*, 1984, **106**, 4945-4950.

(74) H. M. Marques, K. Voster and T. J. Egan, *J. Inorg. Biochem.*, 1996, **64**, 7-23.

(75) T. J. Egan and K. K. Ncokazi, *J. Inorg. Biochem.*, 2004, **98**, 144-152.

(76) K. A. de Villiers, H. M. Marques and T. J. Egan, *J. Inorg. Biochem.*, 2008, **102**, 1660-1667.

(77) D. A. Erlanson, R. S. McDowell and T. O'Brien, *J. Med. Chem.*, 2004, **47**, 3463-3482.

(78) R. A. E. Carr, M. Congreve, C. W. Murray and D. C. Rees, *Drug Discov. Today*, 2005, **10**, 987-992.

(79) P. Gribbon and S. Andreas, *Drug Discov. Today*, 2005, **10**, 17-22.

(80) D. Fattori, A. Squarcia and S. Bartoli, *Drugs R&D*, 2008, **9**, 217-227.

(81) A.F.G. Slater and A. Cerami, *Nature*, 1992, **355**, 167-169.

(82) S. Parapini, N. Basilico, E. Pasini, T.J. Egan, P. Olliaro, D. Taramelli and D. Monti, *Exp. Parasitol.*, 2000, **96**, 249-256.

(83) M. Kalkanidis, N. Klonis, L. Tilley and L.W. Deady, *Biochem. Pharmacol.*, 2002, **63**, 833-842.

(84) T. J. Egan, *J. Inorg. Biochem.*, 2006, **100**, 916-926.

(85) H. M. Marques, M. P. Byfield and J. M. Pratt, *J. Chem. Soc. Dalton Trans.*, 1993, 1633-1639.

(86) M. P. Byfield, M. S. A. Hamza and J. M. Pratt, *J. Chem. Soc. Dalton Trans.*, 1993, 1641-1645.

(87) M. S. A. Hamza and J. M. Pratt, *J. Chem. Soc. Dalton Trans.*, 1993, 1647-1650.

(88) M. S. A. Hamza and J. M. Pratt, *J. Chem. Soc. Dalton Trans.*, 1994, 1367-1371.

(89) H. M. Marques, O. Q. Munro, T. Munro, M. de Wet and P. R. Vashi, *Inorg. Chem.*, 1999, **38**, 2312-2319.

(90) E. Bayer and P. Schretzmann, *Struct. Bonding*, 1967, **2**, 181-250.

(91) C. A. Hunter and J. K. M. Sanders, *J. Am. Chem. Soc.*, 1990, **112**, 5525-5534.

(92) C. A. Hunter, *Chem. Soc. Rev.*, 1994, **23**, 101-109.

(93) C. Janiak, *J. Chem. Soc. Dalton Trans.*, 2000, 3885-3896.

(94) H.-J. Schneider and M. Wang, *J. Org. Chem.*, 1994, **59**, 7464-7472.

(95) T. Liu and H.-J. Schneider, *Angew. Chem. Int. Ed.*, 2002, **41**, 1368-1370.

(96) E. Kim, S. Paliwal and C. S. Wilcox, *J. Am. Chem. Soc.*, 1998, **120**, 11192-11193.

(97) T. Steiner, *Angew. Chem. Int. Ed.*, 2002, **41**, 48-76.

(98) H.-J. Schneider, *Angew. Chem. Int. Ed.*, 2009, **48**, 3924-3977.

(99) R. J. Fitzmaurice, G. M. Kyne, D. Douheret and J. D. Kilburn, *J. Chem. Soc. Perkin Trans. 1*, 2002, 841-864.

(100) E. Kimura, A. Sakonaka, T. Yatsunami and M. Kodama, *J. Am. Chem. Soc.*, 1981, **103**, 3041-3045.

(101) M. Barboiu, C. T. Supuran, A. Scozzafava, F. Briganti, C. Luca, G. Popescu, L. Cot and N. Hovnanian, *Liebigs Ann. Chem.*, 1997, 1853-1859.

(102) C. Schmuck, *Chem. Commun.*, 1999, 843-844.

(103) A. Mayence, J. J. van den Eynde, F. M. Krogstad, D. J. Krogstad, M. T. Cushion and T. L. Huang, *J. Med. Chem.*, 2004, **47**, 2700-2705.

(104) C. Asher, K. A. de Villiers and T. J. Egan, *Inorg. Chem.*, 2009, **48**, 7994-8005.

(105) W. Scheler, *Biochem. Z.*, 1960, **332**, 542-549.

(106) T. H. Davies, *Biochim. Biophys. Acta*, 1973, **329**, 108-117.

(107) W. L. Hinze and J. H. Fendler, *J. Chem. Soc. Dalton Trans.*, 1976, 1469-1475.

(108) P. A. Adams, D. A. Baldwin, C. E. Hepner and J. M. Pratt, *Bioinorg. Chem.*, 1978, **9**, 479-494.

(109) T. Uno, K. Hatano, T. Nawa, K. Nakamura, Y. Nishimura and Y. Arata, *Inorg. Chem.*, 1991, **30**, 4322-4327.

(110) H. M. Marques, O. Q. Munro and M. L. Crawcour, *Inorg. Chim. Acta*, 1992, **196**, 221-229.

(111) A. E. Martell and R. M. Smith, in *Critical Stability Constants*, Plenum Press, New York, 1974, vol. 1-6.

(112) E. A. Castro, M. Aliaga, and J. G. Santos, *J. Org. Chem.*, 2004, **69**, 6711-6714.

(113) F. Milletti, L. Storchi, G. Sforna and G. Cruciani, *J. Chem. Inf. Model.*, 2007, **47**, 2172-2181.

(114) S. R. Hörtner, T. Ritschel, B. Stengl, C. Kramer, W. B. Schweizer, B. Wagner, M. Kansy, G. Klebe and F. Diederich, *Angew. Chem. Int. Ed.*, 2007, **46**, 8266-8266.

(115) E. J. Corey, and M. J. Chaykovsky, *J. Am. Chem. Soc.*, 1962, **84**, 867-868.

(116) J. M. Holland, M. Lewis and A. Nelsen, *J. Org. Chem.*, 2003, **68**, 747-753.

(117) M. Chini, P. Crotti, L. Favero and F. Macchia, *Tetrahedron Lett.*, 1991, **32**, 4775-4778.

(118) V. S. R. K. Yedavalli, N. Zhang, H. Cai, P. Zhang, M. F. Starost, R. S. Hosmane and K.-T. Jeang, *J. Med. Chem.*, 2008, **51**, 5043-5051.

(119) J. S. Yadav, B. V. S. Reddy, M. Sridhar Reddy and A. R. Prasad, *Tetrahedron Lett.*, 2002, **43**, 9703-9706.

(120) P. G. Gassman and J. J. Talley, *Org. Synth.*, 1981, **60**, 14-18.

(121) H. Staudinger and J. Meyer, *Helv. Chim. Acta*, 1919, **2**, 635-646.

(122) F. Benedetti, S. Miertus, S. Norbedo, A. Tossi and Pavel Zlatoidzky, *J. Org. Chem.*, 1997, **62**, 9348-9353.

(123) W. Q. Tian and Y. A. Wang, *J. Org. Chem.*, 2004, **69**, 4299-4308.

(124) J. Wityak, R. A. Earl, M. M. Abelman, Y. B. Bethel, B. N. Fisher, G. S. Kauffman, C. A. Kettner, P. Ma, J. L. McMillan Lawrence, J. Mersinger, J. Pesti, M. E. Pierce, F. W. Rankin, R. J. Chorvat and P. N. Confalone, *J. Org. Chem.*, 1995, **60**, 3717-3722.

(125) S. V. Makarov, C. Mundoma, J. H. Penn, J. L. Petersen, S. A. Svarovsky and R. H. Simoyi, *Inorg. Chim. Acta*, 1999, **286**, 149-154.

(126) *West Ger. Pat.*, 4267322, 1981.

(127) A. I. Kutznetsov, V. A. Kosmakov and B. V. Unkovskii, *Chem. Heterocyc. Compd.*, 1985, 21, 697-700.

(128) A. F. Farminer and G. A. Webb, *J. Chem. Soc. Perkin I*, 1976, 940-942.

(129) A. T. Nielsen, *J. Heterocyclic Chem.*, 1975, **12**, 161-164.

(130) E. B. Hodge, *J. Org. Chem.*, 1972, **37**, 320-321.

(131) S. Ram and R. E. Ehrenkaufer, *Tetrahedron Lett.*, 1984, **25**, 3415-3418.

(132) K. Fahey and F. Aldabbagh, *Tetrahedron Lett.*, 2008, **49**, 5235-5237.

(133) D. R. Rayner, A. J. Gordon and K. Mislow, *J. Am. Chem. Soc.*, 1968, **90**, 4854-4860.

(134) A. Aranyos, D. W. Old, A. Kiyomori, J. P. Wolfe, J. P. Sadighi and S. L. Buchwald, *J. Am. Chem. Soc.*, 1999, **121**, 4369-4378.

(135) G. Molle, P. Bauer and J. E. Dubois, *J. Org. Chem.*, 1982, **47**, 4120-4128.

(136) HYPERCHEM, 7.0 ed., Hypercube inc., Gainesville, Fl.

(137) N. L. Allinger, *J. Am. Chem. Soc.*, 1977, **99**, 8127-8134.

(138) H. M. Marques, O. Q. Munro, N. E. Grimmer, D. C. Levendis, F. Marsicano, G. Pattrick, T. Markoulides, *J. Chem. Soc. Faraday Trans.*, 1995, **91**, 1741-1749.

(139) O. Q. Munro, J. C. Bradley, R. D. Hancock, H. M. Marques, F. Marsicano, P. W. Wade, *J. Am. Chem. Soc.*, 1992, **114**, 7218-7230.

(140) E. Merck, in *Dyeing reagents for Thin Layer and Paper Chromatography*, Darmstadt, 1980, pp 6, 61.

(141) H. E. Gottlieb, V. Kotlyar and A. Nudelman, *J. Org. Chem.*, 1997, **62**, 7512-7515.

(142) R. S. Tewari, *Z. Naturforsch. B*, 1977, **32**, 1165-1167.

(143) E. M. Kaiser and C. Hause, J. Org. Chem., 1968, **33**, 3402-3404.

(144) O. Tsuge, S. Kanemasa, A. Hatada and K. Matsuda, *Bull. Chem. Soc. Jpn.*, 1986, **59**, 2537-2545.